Measuring Seed Velocity and Seed Counting in a Pneumatic Conveying System using Electrostatic Sensors

A Thesis Submitted

to the College of Graduate and Postdoctoral Studies

in Partial Fulfillment of the Requirements

for the Degree of Master of Science

in the Department of Electrical and Computer Engineering

University of Saskatchewan

by

Yuzhe (Solomon) Ouyang

Saskatoon, Saskatchewan, Canada

Permission to Use

Abstract

The trend towards precision agriculture has led to the advent of a new generation of modern equipment for agriculture. Pneumatic conveying systems are widely used for seeding operations in modern agriculture. This thesis considers the problem of seed velocity measurement and counting seed number in the pneumatic conveying process.

For the flowing seed velocity measurement, the experimental object was wheat seed. Tests were performed with air velocities of 12, 15, 20, 25, and 30 m/s in a 57.3 mm acrylic pipe while the seed mass flow rate was increased from 1 kg/min to 6 kg/min in 1 kg/min increments. All measurements were taken 10 meters downstream of the feed point of the rotary feeder into the air steam. The proposed method of velocity measurement is based on the cross-correlation algorithm. Two different active start points of the cross-correlation have been developed, one is the fixed time window, and the other is the threshold detection. The horizontal velocity of the seeds and the slip ratio were calculated from the results. Beside some clumping-seed testing groups, the slip ratio between the total seeds velocity and the air velocity was relatively constant at approximately 0.63.

For counting the number of seeds, the experimental objects were wheat and canola, and the tests were taken in the secondary pipeline of the seed drill system. One contribution of this part is signal denoising using compressive sensing. Compressive sensing provides a feasible method based on the sparsity of the seed signal. The other contribution of this part is utilizing pattern recognition technique for counting number. Features were extracted from the seed signal, which are *Threshold Detection, Full Width Half Maximum, Cluster Width, Peak and Valley Detection, Number of Turns, and Energy Comparison.* Four of them was selected to be applied in the experiments. Multiple classifier approach was also developed in the classification task of the pattern recognition. The counting accuracy for all of the wheat groups were higher than 92% and for the canola groups were higher than 96%.

Acknowledgments

I would like to express my greatest gratitude to my dear supervisor, Prof. Francis Bui for his invaluable suggestions, support and encouragement throughout my graduate experience at University of Saskatchewan. Also, thanks Prof. Scott Noble, my co-supervisor, for his incalculable help in mechanical engineering and instrument knowledge. I appreciate their support throughout my Master's degree program. Without their encouragements and continuous guidance, this thesis would never have been possible.

I must acknowledge the other members of my thesis committee for examining this thesis and for their insightful comments.

I would also like to thank my family and my Canadian mother, Therese Janzen, for their unwavering love, constant support and encouragement throughout my life. Without the inspiration, drive, and support that they have given me, I might not be the person I am today.

Finally, I truly appreciate the help from everyone involved in this research study. Thank all of you for everything.

Table of Contents

List of Tables

List of Figures

List of Abbreviations

CCr	Correct Classification Rate
DAQ	Data Acquisition Device
ECT	Electrical Capacitance Tomography
ESG	Electrostatic Graphic
FWHM	Full Width Half Maximum
IDIs	Inter-Discharge Intervals
LASSO	Least Absolute Shrinkage and Selection Operator
LDV	Laser Doppler Velocimetry
MU	Motor Units
MUPTs	Motor Unit Potential Trains
PEW	Persistent Empirical Wiener
PTV	Particle Tracking Velocimetry
SD	Standard Deviation

1. Introduction

Grain is indispensable for human society. As the population base continues to expand, food is becoming more precious. In order to maximize the benefits of planting grain, each seed is very valuable for growing grain. With the development of human society, the area of available arable land is shrinking. To meet the development of modern society and human needs, precision agriculture has gradually attracted people's attention [1, 2]. Seed spacing and planting density are important factors in grain yield [3]. In thousands of years of farming, humans have paid little attention to maximizing the production from a single seed. Early, when farmers sowed, they walked from the head of the field to the other end, while throwing a handful of seed. However, this so-called "sowing" method was unreliable. Many seeds fall at the same place, while the rest of the seeds fell sparsely. In this process, many seeds were wasted. Due to uneven planting, the utilization rate of arable land is very low [4]. Even when large-scale agricultural equipment emancipates a lot of labor, there are many unknown variables in the sowing process. These variables are worth measuring and can help people understand seed states is from sowing to harvesting.

In modern agriculture, pneumatic transport is widely used in large-scale seeders [5–7]. Pneumatic transport is using air as a medium to promote the movement of objects. It requires a source of gas, a material feed device, and a conveying pipe [8]. High pressure or low pressure can be used to transfer these materials [9]. In the agricultural equipment, the seeds are transported at a high speed and in a low pressure environment, which is considered as a two-phase flow with the solid particle in a gas flow [10, 11].

The project was concerned with measuring the movement velocity and the number of the seeds flowing in the pipeline during the sowing process based on an electrostatic sensor previously developed at the University of Saskatchewan [12, 13]. In agricultural cultivation activities, the seed velocity is rarely known as it enters and travels through the air stream. Knowing the seed velocity can help to study the minimum requirement of air velocity, which is useful to learn the maximum efficiency and minimum power consumption of the pneumatic conveying system without the seeds settling in the distribution pipeline. Multiple seeds if planted together can result in the growing crops without enough space or nutrients. Conversely, some of the arable land is not sown, the arable land is wasted. Analyzing the number of seeds can help farmers control the uniform distribution of seed density sowed into the land, which can improve the utilization of arable land.

1.1 Challenges

Due to the demanding operating conditions and fundamental environmental resource constraints in the seed sowing process, many traditional velocity measurement or counting solutions are inappropriate.

Even though there have been many methods to measure particles in a gas flow [14], the one key point is that these particles pass though the test points in an orderly manner. However, in the real sowing process, the large quantity of seeds moving though the large-scale seed drill pipeline results in the seeds clumping together along the bottom of the pipe, making the signal induced by seed segmentation difficult.

In modern agriculture the seed drill has been used for a long time. Adding the measurement device should minimize the change of the equipment. It is best that the device adapt to the seeder, which can reduce the cost and improve its applicability and popularity.

Environmental factors have to be considered. The seed drill is working in the outside, and the working environment may be poor. In order to maintain high accuracy results, many advanced devices should be kept in a clean environment. During the sowing process, the measurement device is in movement and there would be some bumps and vibration during its working process, so the device should have a certain anti-interference capability.

The application scenarios pose other challenges. The measurement device can measure different type seeds, like canola, wheat, and so on. For different seeds, their properties are not the same. Extensive adaptability must be taken into account in this project.

Another challenge is that the seeds should be always kept safe for future growth. The seeds in the seed drill are used to be cultivated into crops and then processed into food for human needs, which means it is not allowed to add markers, like isotopes, to label or identify seed for the seed measurements.

Furthermore, signal denoising must be taken into account during the signal process, especially in the seed counting task. Due to the different condition of seed conveying operation and the different number of seed through the sensor in a certain period of time, a standard denoising filter cannot be directly used for denoising. A feasible method for signal denoising is needed to be developed.

1.2 Problem Statement

Accurate detection of seed is among the most vexing issue in the measurement process during the sowing process. The seed detection sensor device must be easy to be fixed on the sowing machine, and have a certain anti-interference ability for the seed drill shaking. The impurities in the transported seed leaves the pipeline prone to become dirty, which cause the sensor to lose the detection ability if a direct-contact or optical sensor is used. A reliable seed sensor needs to be adapted to detect the flowing seed in an air seeder system.

Specifically, in an air seeder system, there are two parts of the pipeline. One is the primary pipeline, which is responsible for the transport of seeds. Measuring seed velocity is important to control the air seeder system for seed conveying in the primary pipeline. The other part is the secondary pipeline, which can split seeds into the different lines for the uniform seed distribution density. Knowing the number of seeds should be the task in the secondary pipeline.

For seed velocity measurement, the key point is to find out the time difference between a seed passing though two seed sensor nodes. However, at a high density of seed flow, it is challenging to identify each seed and obtain the time of each seed passing the next sensor node. A velocity measurement method should be developed to solve the problem in the pneumatic conveying system.

For the seed counting, traditional counting methods, like peak detection or pulse detection [15, 16], cannot provide reliable information about the number of seeds. To address this concern, a novel method of seed counting should be investigated for the moving seed in a pneumatic conveying system.

Also, signal denoising is one of the most important parts of the signal process. Due to the environment noise and seed signal overlapping or seed pumping, many popular types of filters could not be used or directly applied. A denoising method based on compressive sensing has a potential to remove the noise in seed signal.

Motivated by these problems, this thesis is dedicated to the design and development of velocity measurement and counting number for the flowing seed in a pipeline of air seeder with a realistic sowing process setting.

1.3 Objectives of the Thesis

The purpose of this study is to propose solutions for measuring seed velocity and seed counting based on the existing electrostatic sensors. In the following, the objectives of this thesis will be described and discussed briefly.

- To adapt a two-electrode electrostatic sensor that was developed for the secondary pipeline to the primary pipeline. The sensor device should be easily installed and stable in a real seed drill,
- To investigate a velocimetry algorithm for the detected seed electrostatic graphic (ESG) signal, and evaluate the performance with a reference result from the PTV technique,
- To examine the impact of system parameters, such as the air velocity and the seed mass flow rate, on the electrostatic velocimetry device,

- To investigate the signal waveform templates induced by seed from single seeds and seed groups, and to develop enough features from these templates,

- To exploit an effective signal denoising method to fit different seeds and operation conditions, and evaluate the denoising performance,

- To train a classifier based on the known seed groups and specify the template feature reference set, and apply the reference set to the classifier for the testing group.

- To select useful and highly reliable features for classification task, and make the combined classifier decision for the testing seed groups.

- To examine the counting number results by different experiment settings for multi-classification pattern recognition.

1.4 Assumptions

The assumptions made in this project were as follows:

- The seed types used in experiments were canola and wheat. The distance from the electrostatic sensor electrode to the seed was much greater than the seed size, so each seed was treated as a point charge.

- Although each seed had slight differences in shape and weight, the assumption was made that each kind seeds were uniform.

- In the experimental lab, it was assumed that the air temperature, humidity and barometric pressure had little effect on the testing experiment output because they remained relatively consistent throughout testing. Note that all tests for a particular experiment were done at approximately the same time. The changing of the environment factor was not considered in this work.

- The velocity measurement assumes that there is zero acceleration when a particle moves from the first electrostatic sensor electrode to the second, for the two electrodes are very close.

1.5 Scope and Limitations

Like any other research studies, this study also includes some scope and limitations. Even though the developed velocity measurement method and seed number counting method were tested and assessed under some experiments in the lab environment, empirical measurements were not practiced in a cultivated field, which can be considered beyond the scope of this study. However, the main task of this project is to establish an analytical framework to apply to various generalized scenarios. Through comparison with reference results, the performance of methods were evaluated.

During the experiments, the environment factors were in a relatively stable state. If the sensor is applied out of the laboratory, environmental factors, particularly relative humidity might affect the signal acquisition. A larger or smaller pipeline size would also change the strength of the induced ESG signal, so the limitations and restrictions of the system need to be understood.

In the whole process, the size of the seed particle was not taken into consideration. In the signal process, the size constraint of the seed needs to be considered.

1.6 Application Areas

Initial applications of the seed velocity measurement and counting are in the seed sowing process, in particular for continuous monitoring the moving seed information in the pipeline. It is expected to be adopted into every seed drill device, meaning that farmer can effectively improve the seed state from the measured information to maximize the value of each seed in the sowing process and reach to the goal of precision agriculture.

The velocity measurement and couting results can offer the seed flowing data in the pipeline. If the seeds are clogged in the pipeline, it can alert the operator during the sowing process, which can avoid the loss of grain due to sowing system problems in the seeder machine. Also, planting operators can set a suitable air velocity based on the seed velocity and counting data to control uniform sowing into the ground.

In addition to enabling inexpensive and continuous sowing seeds monitoring, the seed velocity and counting measurement system has a wide variety of applications, such as harvest, transport and storage of crops. Extending the technology to new areas could also assist other two-phase flow transport systems by collecting data from the electrostatic induction signal.

1.7 Thesis Organization

This thesis is organized as follows. Chapter 2 contains relevant literature survey of particle velocity measurement, counting the number of seeds, the principle of electrostatic sensor and its applications. Chapter 3 provides the description of the lab-scale air seeder system, the electrostatic sensor and the signal collection software. Chapter 4 discusses the measurement of seed particle velocity in the primary pipeline of a pneumatic conveying system by using electrostatic sensors. In Chapter 5, flowing seed counting in the secondary pipeline using electrostatic sensors based on pattern recognition is discussed. Finally, Chapter 6 presents a conclusion with some remarks and possible future improvement or application direction.

2. Literature Review

In this chapter, some velocity measurement methods and particle counting methods for the solid-gas flow are reviewed, and the concept and principles of cross-correlation and pattern recognition concerning the seeds to estimate seed moving velocity and the number of seeds are covered. Also, the development of the electrostatic sensor in terms of both hardware and its application are discussed.

2.1 Particle Velocity Sensing Methods

Velocity measurement systems for particles in trained in a flow has been developed for decades. This research can date back to the high-speed photography method [17] or a double-flash exposure technique [18], which is a kind of direct visual techniques. These classical and famous methods tend to be accurate and non-intrusive. There are some advanced visual techniques. For example, particle tracking velocimetry (PTV) [19,20] uses a light sheet from laser to detect and illuminate particles in the flow. Digital cameras take pictures of the flow at a preset time interval. To analyze the images, the particles in the flow can be detected, as well as the particle velocity and direction. Because the process needs to deal with images, the process of velocity calculation is time-consuming and it needs a clean environment for a photograph, which are not suitable for seed drilling operation. Also, the PTV equipment is expensive and not easy to be applied into the real seed drill machine.

Laser Doppler velocimetry (LDV) [21–24] can be used for the simultaneous measurement of the gas and particle velocities in a gas-solid, two-phase flow. When two beams of monochromatic coherent electromagnetic radiation cross at an angle, interference fringes will be formed. If a particle then passes through the region of the beam intersection, it will reflect pulses of light. The frequency of these pulses is termed the Doppler frequency, and is a function of the velocity of the particle. Such measurements have the same problems as PTV.

Dual-plane Electrical Capacitance Tomography (ECT) [25] is an alternative technique to estimate the velocity in case of multi-phase flow. ECT can generate sequences of 2D tomographic reconstructed images, and using the cross-correlation of the signals from the two planes enables the velocity of the gas–solid flow to be calculated.

For the technique of optic probes [26, 27], the light-emitting and light-receiving optic probes are employed to detect the reflected light from the nearby particles. The intensity of the reflected light shows the concentration, size and material properties of the particles. If there are two receiving fibers aligned in the direction of the flow, the signals received from a given particle or group of particles will have a time delay between them. The time delay is related to the cross-correlation coefficiency of the pair of signals, which is the key for the velocity analysis.

2.2 Velocity Measurement Method based on Cross-Correlation

To obtain the velocity distribution of the moving seed in a pipeline, several different techniques have been proposed. By using the ESG signal, one of the most effective methods is to obtain the local correlation of two ESG signals having a short distance and time interval between them. By computing the quotient of the small distance and the maximum correlation, the velocity of the moving seed can be identified.

One application of the cross-correlation algorithm on the velocity measurement is to estimate the blood velocity for the clinical diagnosis of vascular disease [28]. The indispensable noninvasive tool for the velocity measurement is ultrasound. The time delay can be found by searching for the maximum correlation coefficient between the successive received echoes, and then the blood velocity can be obtained.

An image-to-image cross-correlation software has been developed to apply pairs of digital satellite images to map the velocity field of moving ice [29]. By searching a subsequent image for matching areas using a cross-correlation algorithm, the peak correlation value allows the displacement between two images to be measured with sub-pixel accuracy, resulting in the precise velocity measurement. Keane et al. [30] indicated that cross-correlation methods of interrogation of successive single-exposure frames can be used to measure the separation of pairs of particle images between successive frames and the instantaneous velocity fields.

Volk et al. [31,32] utilized the cross-correlation of ambient seismic noise signals to analyze the apparent changes in the noise sources and velocity changes in a medium. Thses changes can be used to image the subsurface or for monitoring geological settings where the seismic velocity changes, like volcanoes or reservoirs.

Liu et al. [33,34] measured the local velocity of passing solids by using a cross-correlation method. The time-lag between pairs of two light-receiving signals allows the effective distance between receiving ends of the probe to be determined. The effective distance and time lag determined from cross-correlation of experimental data give the velocity of particles passing the fibers.

2.3 Particle Counting Sensing Methods

Particle counting research can date back to the ultrasonic sensor [35] and the photoelectric seed counting detector [36], which are essential to ensure that only one seed crosses the slit between tubes at any one time.

Mussadiq *et al.* [37] considered the problem of the seed counting can be solved by the digital image processing. Four open-source image analysis programs, which are ImageJ, CellProfiler, P-TRAP and SmartGrain, was evaluated by eight sample seeds groups. For each testing group, all seeds are spreaded on a black background without overlap, and the picture of the seeds is applied the four open-source image analysis algorithms to obtain the number of the seeds in the picture.

Another example of the digital image processing for seed counting is that Liu *et al.* [38] developed a novel method with the grain and shadow images. Under the four direction light source, the seeds produce four-way shadows. After applying a binary classification algorithm, the shadow-based method not only can count the seed number, but also can distinguish the unfilled grain and filled grain, which has a higher speed than X-ray spectroscopy. The advantages of the image processing method are cheap and time-saving, but the experiment requires a relative stable and clean environment.

Liu *et al.* [39] investigated the problem of seed counting by weight is an efficient method. According to the known weight of each seed, and applying a normal distribution with production variation, the number of the sample bag of seeds can be calculated. Because of wear and tear and different types or amounts of foreign materials in seeds, the expression of the seed number function should contain the lower confidence bound for calibration. The key structure of the problem is the statistical model estimated from a calibration data set, and how to apply it for the testing group.

2.4 Signal Denoising by Compressive Sensing

Denoising is one of the most significant part in the signal processing. Lots of work has been done regarding signal denoising. Techniques such as classic filter denoising, Fourier transform denoising or wavelet transform denoising are limited to particular transform distribution [40, 41]. If the signal parameter changes, those methods would be greatly affected. In this study, the compressed sensing denoising method is a better choice. Signal sparsity is the prerequisite of compressive sensing, and compressive sensing denoising just makes use of the close connection between compressive sensing and signal sparsity [42]. Compressive sensing denoising can overcome the shortages of those classic filter denoising methods [43,44].

For the basic principle of compressed sensing [42–47], a sparse signal X in some transform domain Ψ with sparse Θ, then the signal X can be presented as:

$$X = \Psi\Theta. \tag{2.1}$$

The transform coefficients $\Theta = \Psi^T X$. Then an observation matrix Φ is designed to measure X. The matrix Φ should be unrelated to the matrix Ψ and can be replaced by a random matrix. A observation vector Y can be represented as:

$$Y = \Phi\Theta = \Phi\Psi^T X = AX, \tag{2.2}$$

where $A = \Phi\Psi^T$ known as information operator. For the compressive sensing recovery process, the simplest way is using l_0 optimization:

$$X' = min||\Psi^T X||_0 \ \ \text{subject to} \ \ Y = \Phi\Psi^T X. \tag{2.3}$$

An alternative to the l_0 norm used in Equation 2.3 is to use the l_1 norm, with the resulting adaptation defined as

$$X' = min||\Psi^T X||_1 \ \ \text{subject to} \ Y = \Phi\Psi^T X. \tag{2.4}$$

If the signal X is combined with a noise Z, the mixed signal $(X + Z)$ is no longer sparse in transform domain Ψ. After the compressed sensing on the mixed signal, we can get $A(X + Z) = AX + AZ = Y + Y_Z$, which means the measured signal Y is affected by Y_Z. Due to the information in Z is removed by the process of compressed sensing, the rest of the information in Y_Z has only a limited influence. Also if the power of the signal X is much stronger than the noise Z, the influence of Y_Z can be ignored [43]. Figure 2.1 proposes the principle model of compressed sensing denoising.

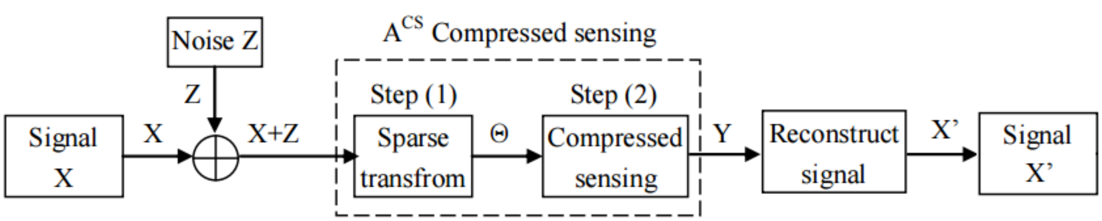

Figure 2.1: Principle model of compressive sensing denoising [43].

2.5 Pattern Recognition for Particle Counting

Pattern recognition is defined as a process by which external signals arriving at the sensors are converted into meaningful perceptual experiences [48]. Its main task is the classification of items into major taxonomic groups were based on discriminant analysis of features [49]. Many applications about pattern recognition have been developed, such as language recognition, voice recognition, character recognition, and so on [50, 51].

General pattern recognition units and corresponding tasks have been defined. The first step is pattern acquisition. It can have different forms like data acquisition or collection. Secondly, the feature extraction should be applied. Then in most situations, the signal cannot be fed into classifier directly, and needs the pre-processing module to standardize the features. Next, the kernel unit of the pattern recognition is the classification, regression or description. The final step, if other operations are needed, is the post-processing module. Pattern recognition with its main functional units is shown in Figure 2.2.

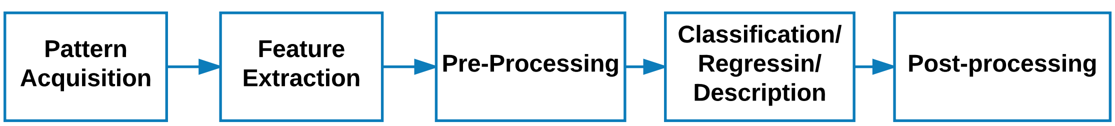

Figure 2.2: Pattern recognition with main functional units [52].

The performance of a pattern recognition scheme can be evaluated by training and testing. The training groups can offer variables for the classifier, then the "learned" features can be applied into the testing groups in the pattern recognition [52]. For example, Tkach et al. [53] utilized the training data set to analyze the features of electromyographic signals, and apply the features into the testing groups, which is to learn the electromyographic pattern recognition.

2.6 Electrostatic Sensor Principles and Applications

In the process of the seed flowing, the triboelectric charging [54, 55] can make the seed carry a certain mount of charges. An electrostatic sensor is a relatively simple device that measures the changing electric field produced by a moving charge.

There are two classes of electrostatic sensors, the charge transfer type and the the charge induction type, which are based on the different types of the interaction modes between the sensor and charging particles [56]. For the charge transfer type sensor, the charge passes the electrode of the sensor directly by the charged particle colliding with the sensor. For the charge induction type, the charge in the electrode is generated by electrostatic induction [57, 58]. The particle does not contact the electrode, but only passes though the electrode of the electrostatic sensor.

In order to avoid the sensor affecting the transmission of seeds into the pipeline, the charge induction type sensor was employed in this project. When one charged particle passes the electrode, the electrons in the electrode are redistributed to balance the changing electric field. This produces a current flow in the electrode and the current can be measured by a signal collection device [59]. Figure 2.3 shows the process of the production of the induced current in the electrode.

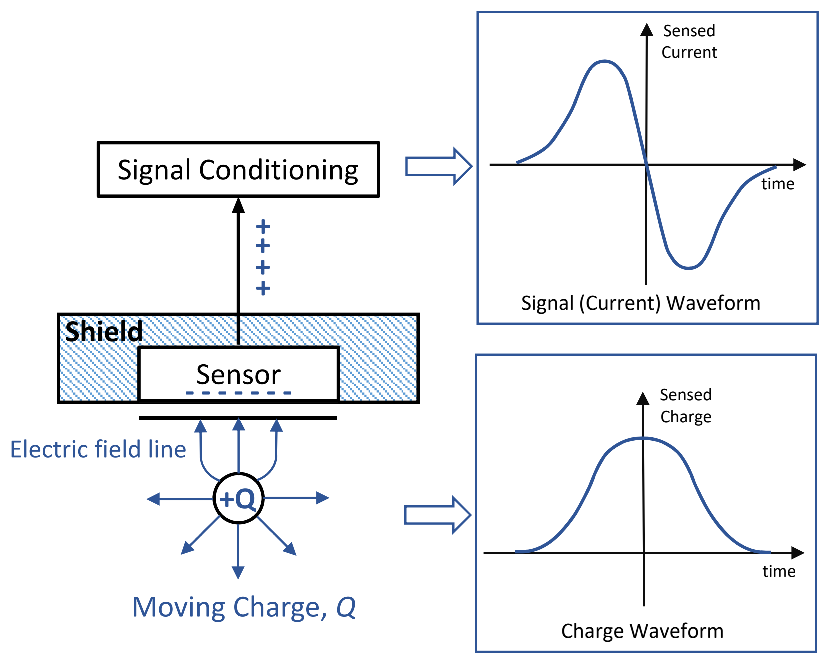

Figure 2.3: The process of the production of the induced current in the electrode [59].

According to the electrostatic induction principle, the electric field formed by a point charge [60] can be described by the following Poisson equation and Dirichlet boundary conditions in Equation 2.5 [59, 61],

$$\begin{cases} \varepsilon\nabla^2\varphi(x,y,z) & = & -\rho(x,y,z) \\ \varphi(x,y,z)|_{(x,y,z)\in\Gamma_F} & = & 0 \\ \varphi(x,y,z)|_{(x,y,z)\in\Gamma_E} & = & 0 \\ \varphi(x,y,z)|_{(x,y,z)\in\Gamma_N} & = & C \end{cases} \tag{2.5}$$

where ∇^2 is the Laplacian operator, $\varphi(x,y,z)$ is the electrostatic potential; $\rho(x,y,z)$ is the charge volume density; ε is the dielectric permitirity, Γ_F, Γ_E, Γ_N are the boundaries of the pipe wall, sensor shield cover, and sensor electrode, and C means the electrode is an equipotential body.

There are several different shapes of the electrode for electrostatic sensors. Figure 2.4 indicates three different shapes of the sensor electrode.

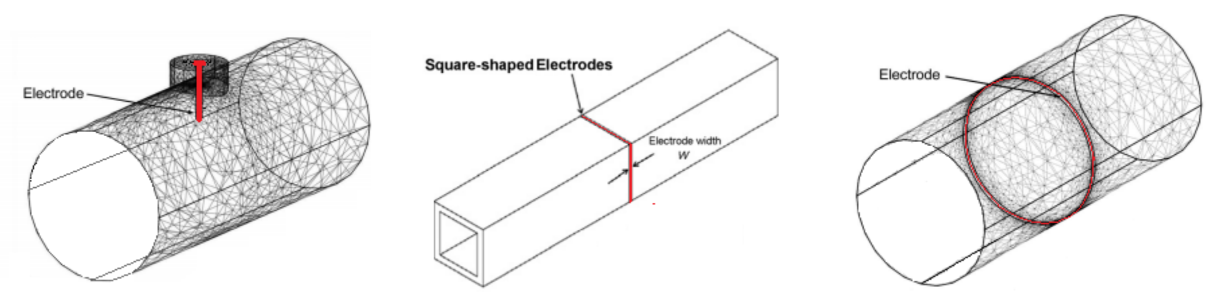

(a) Rod (b) Square-shaped (c) Circular

Figure 2.4: Physical construction of the electrostatic sensor electrode [61, 62].

One alternative to the non-intrusive design is to use a metal rod, as Figure 2.4 (a) shows, as an electrostatic probe, which requires a suitable hole drilled in the pipeline to fit the rod electrode and can reveal flow information by several points around the pipeline [58, 61]. Also, there are some researches on the square-shaped electrode, shown in Figure 2.4 (b), for pneumatic conveying applications [62]. The shape of the sensor electrode used in this study is circular type, as Figure 2.4 (c) shows, which can avoid the electrode wear problem and is matched with the pipeline shape. Equation 2.6 represents the magnitude of charge induced on the surface of the circular electrode for one point charge [59, 61] ,

$$q^{'} = q \cdot \sum_{n=1}^{\infty} \frac{2}{x_n} f(\frac{c}{a}, \frac{z_0}{c}, x_n) \frac{J_0(x_n[\frac{r_0}{a}])}{J_1(x_n)}. \tag{2.6}$$

Here,

$$f = \begin{cases} 1 - exp(-x_n \frac{c}{a}) cosh(x_n \frac{c}{a} \frac{z_0}{c}) & for \ \frac{z_0}{c} \leq 1 \\ exp(-x_n \frac{c}{a} \frac{z_0}{c}) sinh(x_n \frac{c}{a}) & for \ \frac{z_0}{c} \leq 1 \end{cases}. \tag{2.7}$$

Where,

q	=	value of the point charge;
$q^{'}$	=	charge that was induced on the circular electrode;
a	=	radius of the cylinder;
c	=	one half of the length of the cylindrical sensor element;
r, z	=	radial and axial coordinates, respectively, for a cylindrical coordinate system, with its origin placed at the center of the cylindrical segment;
r_0, z_0	=	coordinates of the point charge;
J_s	=	Bessel function of order s;
x_n	=	nth zero of J_0.

The electrostatic sensor has many applications. One application is to utilize the electrostatic sensor to measure the operating deflection shape of a moving belt [63]. The sensing characteristics of a strip-shaped electrode can detect the sensing signal, which can be determined by the transverse velocity.

An electrostatic sensor can also be used to monitor the glue wear in oil-lubricated contacts [64]. The tribocharging, surface charge variation, exo-emissions, and debris generation can be detected by the electrostatic sensor. The investigation of the contribution of wear debris based on the electrostatic charge sensing technology also has been described in [65, 66].

An electrostatic sensor combined with signal processing algorithms also has ability to conduct on-line and continuous measurements of the mass-median size of particles in a dilute-phase pneumatic suspension [67]. It also can be used to achieve solid particles mass flow rate and concentration profile [68].

An array of three identical arc-shaped electrostatic electrodes housed in a sensing head has been used to derive particle flow signals on the pulverized coal on a full-scale power plant [69, 70], which enable operators to balance fuel distribution between fuel feeding pipes and ultimately achieve higher combustion efficiency and lower greenhouse gas emissions [56].

2.7 Conclusion

According to the literature review an electrostatic sensor is a relatively simple and reliable device that measures the ESG signal produced by a moving seed. It has several different shapes of the electrode for the different application. In this study, the shape of the sensor electrode used is circular type to match with the pipeline shape. In order to adapt to the primary and secondary pipelines, only the radius of the sensor electrode needs to be adjusted.

The cross-correlation algorithm would be the most appropriate method for identifying the moving seed velocity based on the seed ESG signal. The compressed sensing denoising method was chosen to remove the noise in the ESG signal. Furthermore, pattern recognition was selected to be studied and developed as a seed counting method for the pneumatic conveying system.

As a consequence, this study would specifically establish and implement novel methods for measuring the flowing seed velocity in the primary pipeline and seed counting in the secondary pipeline in a pneumatic conveying system, which would be based on the use of electrostatic sensors.

3. Materials and Methods

This chapter introduces the hardware for the ESG signal acquisition consisted of two main pieces from the Air Handling Lab at the University of Saskatchewan. The air seeder was previously developed to simulate the process of seed transport in the seeder, and it allows the operator to measure and test the characteristics of the flowing seeds. The electrostatic sensor has been built to allow for detecting of the flowing seeds in the pipeline, through the use of a circular electrode and a data acquisition device with a transducer. Also, the design of signal collection software is described.

3.1 Lab-scale Air Seeder

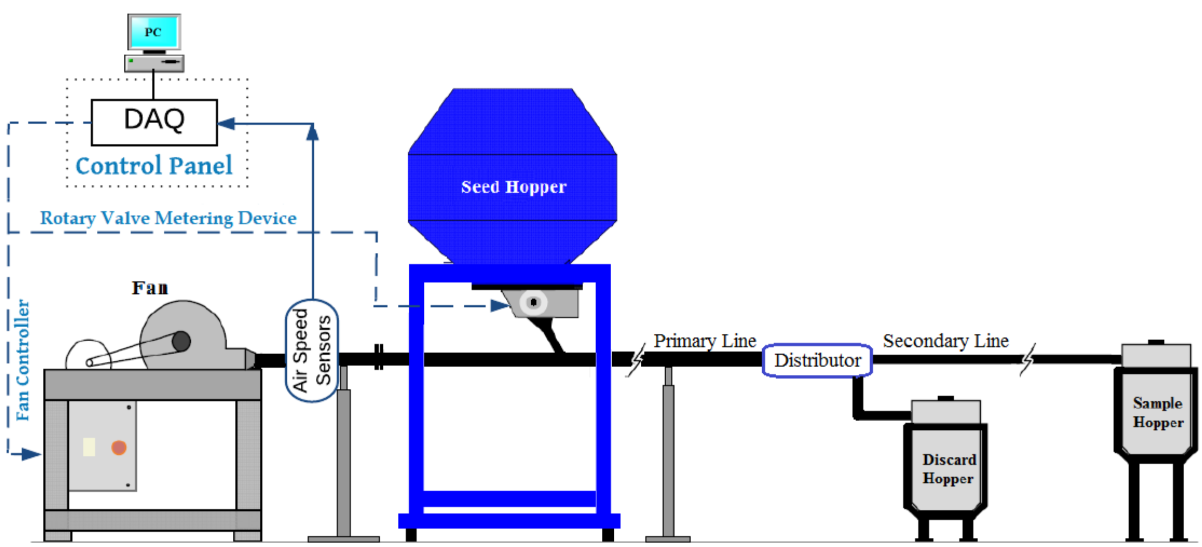

Figure 3.1: Block diagram of the lab-scale seed drill system in the Air Handling Lab at the University of Saskatchewan (Adapted from [71]).

In order to analyze the flowing seeds in a pipeline, a lab-scale air seeder in the Air Handling Lab at the University of Saskatchewan has been built to convey seeds through a small-scale pneumatic conveying system [12, 13]. A diagram of this system is displayed in Figure 3.1, which is adapted from [71]. The major modules of the seed drill system are shown in Figure 3.2.

(a) Air Fan

(b) Seed Hopper

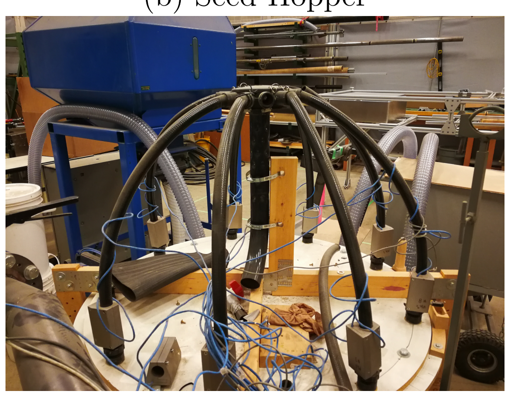

(c) Distributor

Figure 3.2: Photos of the lab-version seed drill system.

In this air seeder system, a PC running LabView (National Instrument, Austin, TX) is set to control the fan speed and the rotary valve airlock. An air speed element and an air speed transducer are connected to an NI USB-6009 multi-function data acquisition device (DAQ) from National Instruments, which can support the air speed feedback to the PC controller to keep the air from the air fan (Figure 3.2 a) in the pipeline with the designed value. The testing seeds are blown from seed hopper (Figure 3.2 b) into the pipeline. For the pipeline, there are two parts. The first part is the primary pipeline,which has an interior diameter of 57.3mm. The second part is eight secondary pipelines with an interior diameter of 25.4mm. There is a eight-outlet vertical distributor (Figure 3.2 c) to connect the two parts, which has a similar structure of the industrial seed drill. At the end of the secondary pipeline, a large sample hopper can collect the seeds from the pipeline. A computer and control software control the air fan speed and the rotary valve metering device to produce air flow and release seeds into the pipeline. A venturi meter was used to provide feedback on air flow to the controller. The properties of the tested materials from the studies of Binsirawanich et al. [72] are summarized and shown in Table 3.1.

Table 3.1: The Properties of the Tested Materials [72]

Material	Wheat	Canola
Density [kg/m^3]	1300	1150
Mean Diameter [mm]	4.08	1.83
Material Mass Flow Rate [kg/min]	0.66	1.56
Shape	Elongated	Spherical

3.2 Electrostatic Sensor

Considering the uniform detection characteristics throughout the sensing volume, the circular electrode is applied into the electrostatic sensor. Also the circular electrode does not affect the seed flow in the pipeline. As Figure 3.3 shows, the sensor including a circular electrode, and is connected to a DAQ device through transducer and amplifiers. When the charged seed flow inside the non-conductive tube and through the electrostatic sensor, the electrode in the sensor can detect the change of the charge distribution, and record the seed data to a data acquisition device.

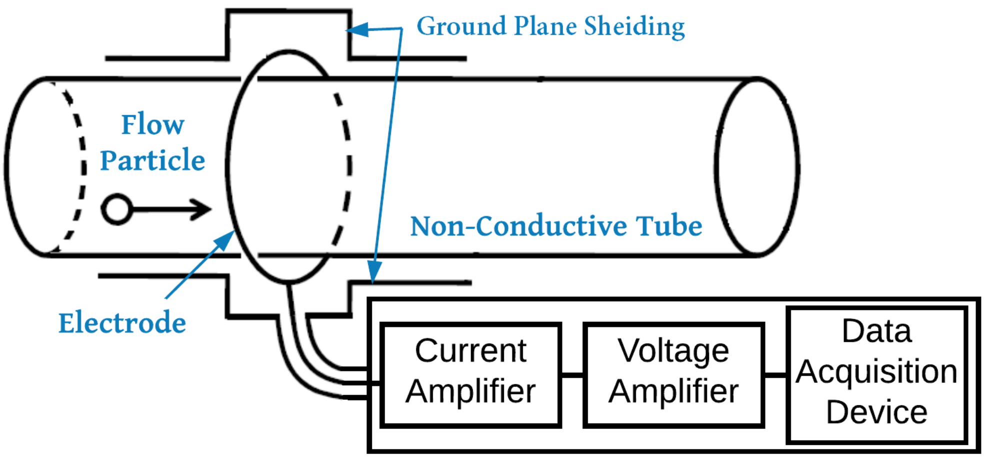

Figure 3.3: Electrostatic sensor schematic (Adapted from [12]).

The electrostatic flow rate instrument can be decomposed into the diagram demonstrated in Figure 3.4. The seneosr body for the system was designed for holding the electrode, the transducer, and the electrical connection between the two securely in place.

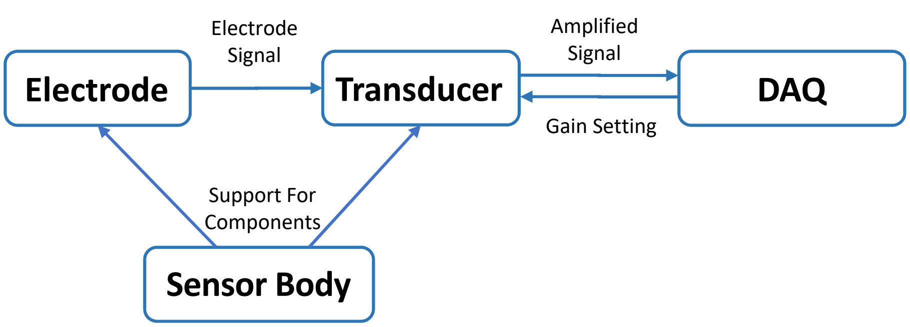

Figure 3.4: Block diagram of the electrostatic flow rate instrument (Adapted from [12])

A novel two-electrode electrostatic sensor based on seed electrostatic induction signal was developed in the Air Handling Lab at the University of Saskatchewan [12, 13]. Figure 3.5 shows the two-electrode electrostatic sensor.

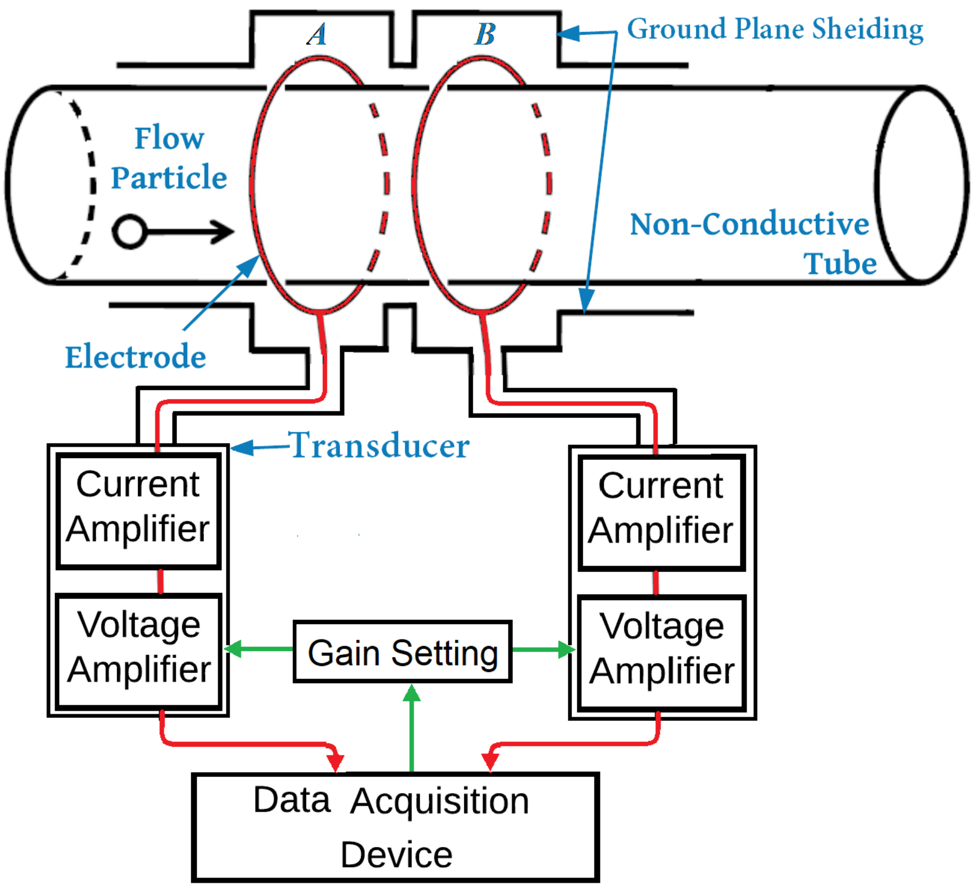

Figure 3.5: Two-electrode electrostatic sensor schematic.

Two independent seed signals are obtained from the ring electrode A and B. The current amplifier in each transducer converts the small seed signal into a voltage that can be measured by less sensitive amplifiers that can produce the higher power signal required by a DAQ device. The sensor is essentially a low-current to a voltage amplifier with a variable gain voltage amplifier connected to its output. In this design, the maximum gain for the voltage amplifier can be applied into the system is 1004, and can be set through the same DAQ device. The electrode is a ring type electrode that wraps around the pipeline with a same radius of the actual seed drill pipeline. This ring was constructed from 24 AWG enameled copper wire that is soldered directly to the transducer circuit board. The distance between the ring electrode A and B is Δd.

For the seed velocity measurement, the circular electrode was adjusted to adapt the primary pipeline with an interior diameter of 57.3 mm, which is shown as Figure 3.6 (a).

For the seed counting research, the electrostatic sensor was adjusted to adapt the secondary pipeline with an interior diameter of 25.4 mm, and bundled by ground plane shielding to avoid the electrostatic noise from environment, which is shown as Figure 3.6 (b). The two-electrode electrostatic sensor was connected to the DAQ device, shown in Figure 3.6 (c). The signal induced by seed can be transmitted to the supporting software in the PC for the further analysis.

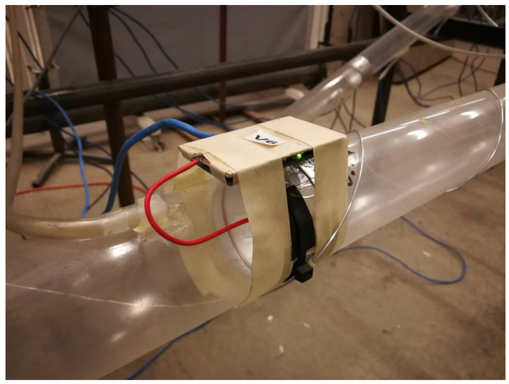

(a) Electrostatic sensor on the primary pipeline

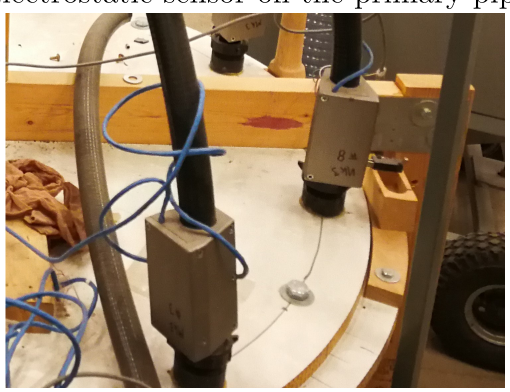

(b) Electrostatic sensor on the secondary pipeline

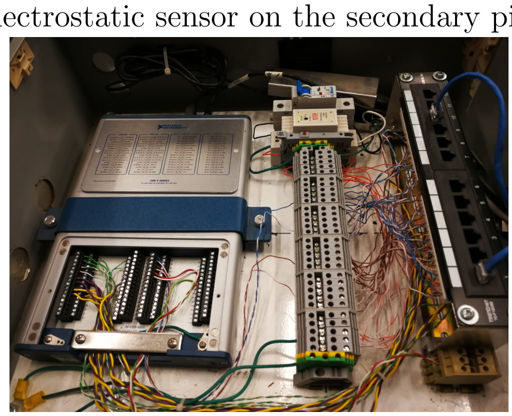

(c) DAQ

Figure 3.6: Photos of the electrostatic sensor system.

3.3 Signal Collection Software

Data collection software was developed using LabView, which was natively compatible with the DAQ NI USB-6353. The interface of the software is shown in Figure 3.7. In the interface, there were two windows that present the signals from the two independent electrode channels. The span of time displayed on the screen is 3 seconds, and the data were automatically stored in a data file. Two input boxes were designed for user to set the total gain in the voltage amplifier.

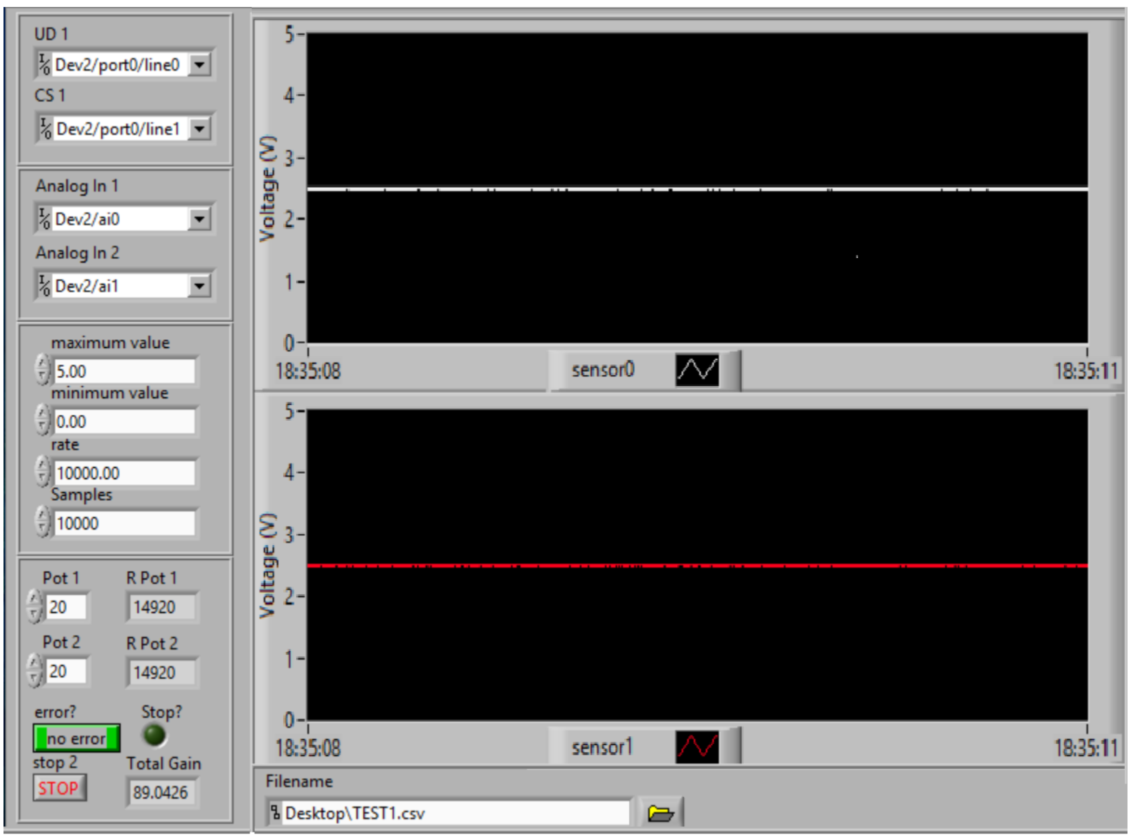

Figure 3.7: The supporting software for data collection.

4. Measuring Seed Velocity in a Pneumatic Conveying System

The velocity characteristics of the conveyed seed as they enter and travel through the flowing air in the pipeline of the pneumatic conveying system are widely unknown and difficult to measure on field equipment. By understanding the real-time velocity of seed, farmers can control the seed mass flow rate to reach relatively uniform sowing. This information can also be used to avoid seed setting in the pipeline. By analyzing the velocity distribution in the pipeline, the pneumatic conveying system can be controlled to improve efficiency and reduce power consumption.

In air seeders, air is the medium that the pneumatic conveying system uses to move the seed from a seed hopper to a destination. It is considered as a gas-solid flow [73, 74], which is known as a two phase flow with the particle-form solid carried by the gas flow. Recently, it is the gas-solid flow measurement in pneumatically conveyed agricultural products [75] on seed drills that have attracted interest in our air seeder research group. The movement of solid agriculture particles and the attendant gas flow patterns in the pipeline of seed drill are of particular interest, and there are a large number of experimental studies on the gas-solid flow. The method presented in this chapter is aimed at improving the signal processing for a two-electrode electrostatic sensor to determine the agricultural particle velocities in pneumatic conveying system in a seed drill.

The work was designed to be the first to adapt the existing electrostatic sensor with two circular electrodes to the primary pipeline of the lab version seed drill. This chapter introduced using the two-electrode electrostatic sensor to measure the seed velocity in an agricultural seeder apparatus that uses pneumatic conveying. A series of experiments was set to test the electrostatic sensor. Different algorithms based on cross-correlation were also compared. The other objective of this experiment was using the electrostatic sensor to measure the seed velocity at multiple air velocities and seed mass flow rates to better understand the behavior and look for opportunities to create a more efficient seeder through the use of particle tracking velocimetry. Velocity measurements were compared to results from other technology, it was proven that the electrostatic sensor is reliable velocimetry to apply to the pneumatic conveying system in the industrial environment.

4.1 Signal Processing Based on Cross-Correlation Principle

This section introduces the seed ESG signal for measuring seed velocity and two velocity measurement methods based on the cross-correlation principle.

4.1.1 Signal Analysis for Measuring Seed Velocity

The seed ESG signal is the recording of the electrical activity associated with seed passing the sensor through the pipeline. For the velocity measurement, the distance $\triangle d$ between these two electrodes can be easily measured. If the difference of time can be obtained from the collected data, the average speed of seed at the sensor's position was calculated by the Equation 4.1,

$$v = \frac{\triangle d}{\triangle t}. \tag{4.1}$$

Therefore, the key to the problem was to find the difference of time $\triangle t$ from the collected data. Figure 4.1 shows typical signals from the electrodeA and B (denoted as signal A and signal B hereafter) where the electrostatic sensor was aligned with the pipeline axis direction. Because of the proximity of the measuring electrodes, signals A and B have similar characteristics.

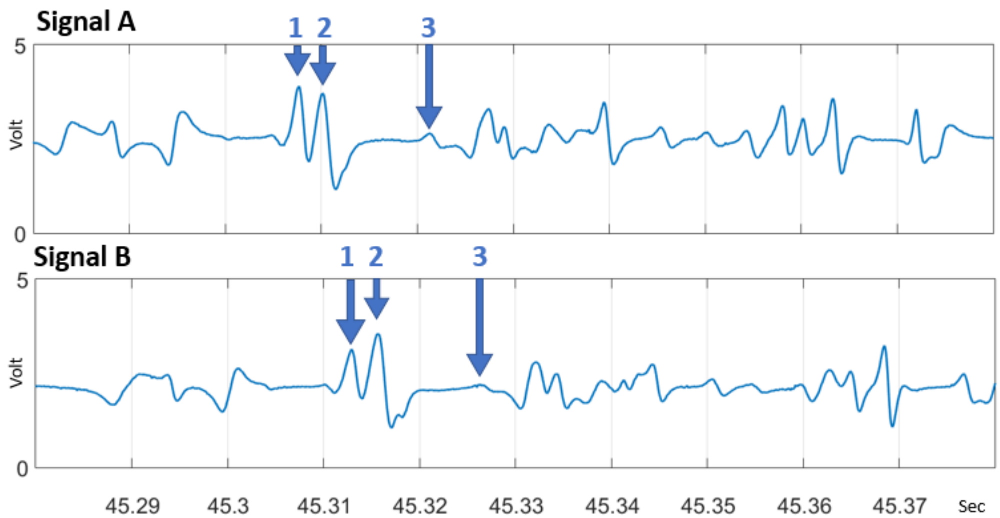

Figure 4.1: Example of ESG signals from the two electrodes.

In the real world, there are large number of seeds moving in the pipeline of seed drills in a short time. It is impossible to identify each seed in the actual sowing process. For example, in the Figure 4.1, three peak points are marked in the signal A. The three points should be match with the three marked points in the signal B in order. The maximum value in the signal A is the Mark 1. However, in the signal B, the maximum is the Mark 2. Obviously, the two maximum points are not produced by the same seed. The Mark 3 peak in the signal A is much more obvious it in the signal B. These all may cause errors in the final velocity calculation result.

A viable approach was to sample data and then take the average of the sampled seed velocity. By observing the two seed signal data sets in the tiny time, the shape of the signal waveforms are very similar. Two methods based on cross-correlation principle were used to obtain the time difference $\triangle t$ and the seed velocity v along the direction of the pipe at the electrostatic sensor position. One is the fixed time window cross-correlation method, the other is the threshold detection cross-correlation method.

4.1.2 Fixed Time Window Cross-Correlation Method

Figure 4.2 shows the steps of the algorithm of the fixed time window cross-correlation method. In this method, depending on the user's requirements, the window length is decided by the required velocity update time. A window in the signal A is determined and the same size window from signal B compared to it. In the signal B, a most similar signal with a same windows length could be found, and the time delay between the two signals is determined by the argument of the maximum of the cross-correlation.

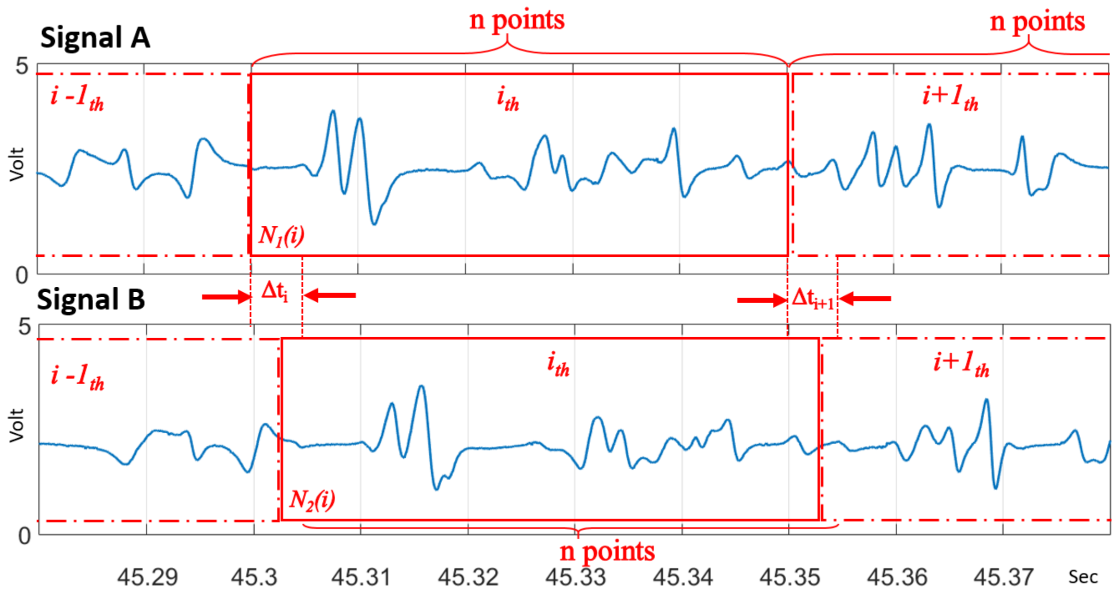

Figure 4.2: ESG signals from the two electrodes with the fixed time window on each signal channel.

Fixed Time Window Cross-Correlation Algorithm

1. Choose a suitable window with n points in the first signal data set with the start point N_1. The start point N_1 and the time window length n can be designed by users depending on the required velocity update time t_r and F_s is the sampling frequency, which is

$$n = t_r \times F_s. \tag{4.2}$$

2. Apply a same length window in the second signal. In order to more accurately find the matching signal and reduce some unnecessary calculations, and because of the fact that the particle velocity is always slower than the air velocity, in the second signal the start point N_2 is set to

$$N_2 = N_1 + \frac{\triangle d}{v_{air}} * F_s, \tag{4.3}$$

where υ_{air} is the set air velocity, F_s is the sampling frequency in the system, $\triangle d$ is the distance of the two electrodes.

3. Calculate the cross-correlation C between the first window and those possible second windows

$$C[n] = \sum_{m=1}^{n} f_1^*[m]\, f_2[m+n]. \tag{4.4}$$

4. Obtain the delay points n_{delay}, when the cross-correlation $C[n]$ reaches the maximum.

5. The time difference can be computed by Equation 4.5. The seed average velocity can then be computed by Equation 4.1:

$$\triangle t = \frac{n_{delay}}{F_s} + \frac{\triangle d}{\upsilon_{air}}. \tag{4.5}$$

4.1.3 Threshold Detection Cross-Correlation Method

Figure 4.3 shows the schematic diagram of the threshold detection cross-correlation method. In this method, a threshold value λ is set for signal A to activate the start point N_1 of a signal window. The window length ω should be at least larger than a single seed waveform to make sure that it contains enough of the characteristics to match the waveform in signal B. After acquiring the sampling window in signal A, the rest of the task is using the cross-correlation principle to measure the time difference $\triangle t$, which is similar to the Fixed Time Window Cross-Correlation Method.

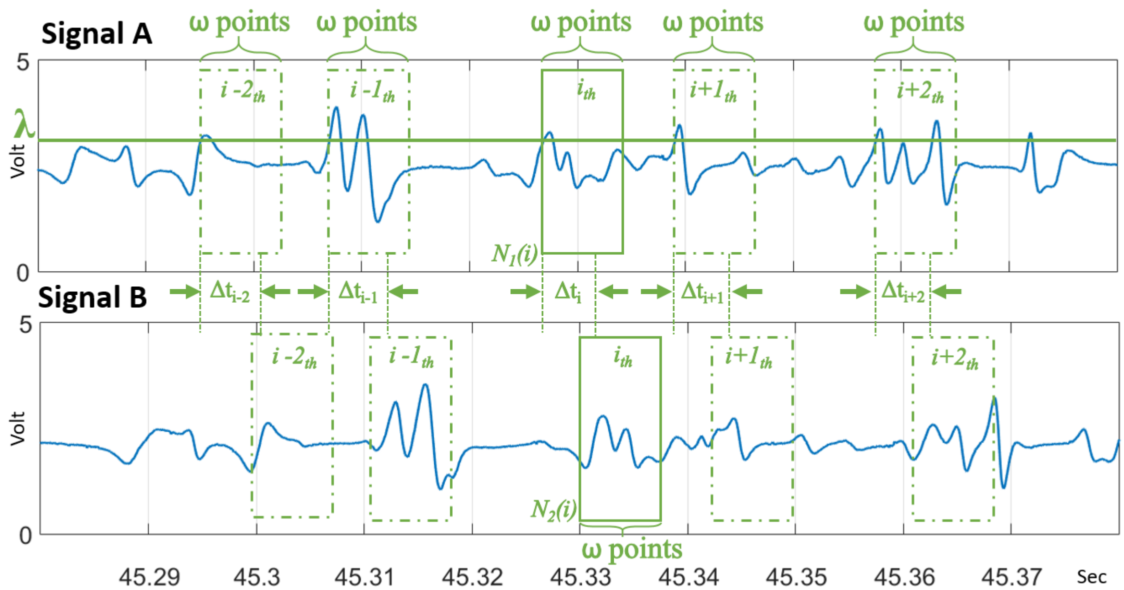

Figure 4.3: ESG signals from the two electrodes with threshold detection algorithm.

Threshold Detection Cross-Correlation Algorithm

1. Set a threshold value λ, and in the first signal data set, once the signal larger than the threshold value λ, the time is marked as the start point, N_1.

2. Choose a suitable window with length ω, which can at least cover one seed signal waveform, from the start point N_1.

3. The rest is as same as the step 2-6 of the Fixed Time Window Cross-Correlation Algorithm.

4.2 Performance Evaluation and Discussion

In this section, the experimental setup for the seed velocity measurement is described, and the results from the experiments are discussed.

4.2.1 Experimental Setup

In order to verify the validity and the flexibility of the two-electrode seed velocity measurement system, experiments were performed in the lab-version seed drill machine. The seed drill acrylic pipeline has a radius of $57.3\,mm$, which is same as the actual seed drill machine. Wheat seed was used as the conveyed particle for each of the tests performed.

To prove the two-electrode electrostatic sensor, a reference velocity measurement system PTV was also installed on the pipeline by Kyle Tschritter [76]. PTV is used to track the motion of particles in a flow through a series of images. From the images, the instantaneous velocity of the particles can be estimated which provides insight into the behavior of the fluid in which the particles are embedded. The distance from the Fan to the outlet of the seed hopper is $6\,m$, and the laser system was installed on the other side of the seed hopper $10\,m$ away. The electrostatic sensor was installed just at the outlet of the laser, which can be considered to be at the same position. The two electrodes in the electrostatic sensor has a distance of $31\,mm$.

According to previous trial experience, the gain applied in the sensor's amplifier was set to 89, which can offer a sensitive seed signal in the system sampling range. To measure the velocity under different situations, 23 testing groups with different fan speed and seed mass flow rate were tested. Each testing group lasted for at least 25 seconds and the sampling frequency was $10000\,Hz$, resulting in 2.5×10^5 points or more in each testing group. MatLab (The MathWorks Inc., Natick, MA) was used to process the collected data. Table 4.1 shows the testing groups conditions. The lab temperature was 20 °C and atmospheric pressure was $94.79\,kPa$.

Table 4.1: Setting for the Testing Groups

Setting		
Test	**Air Velocity (m/s)**	**Mass Flow Rate (kg/min)**
1	12	1
2		2
3		3
4	15	1
5		2
6		3
7		4
8		5
9		6
10	20	1
11		2
12		3
13		4
14		5
15		6
16	25	3
17		4
18		5
19		6
20	30	3
21		4
22		5
23		6

4.2.2 Numerical Results and Analysis

In this section, results from tests at 12, 15, 20, 25 and 30 m/s air velocity with a mass feed rate of 3 kg/min, are examined in different methods of signal processing. Figure 4.7 to 4.6 shows the measured velocity results for the 25 seconds testing seed signal. From the experiment, it was noted that some seeds often clump together on the bottom of the pipeline in the group with 12 m/s air velocity and 3 kg/min mass feed rate.

Figure 4.4 indicates the fixed time window cross-correlation method with the time window length of 0.25 sec and Figure 4.5 shows that of 0.5 sec. From the two different length of time window graph, the results are nearly the same, which indicates the length of the time window does not markedly affect the velocity measurement results.

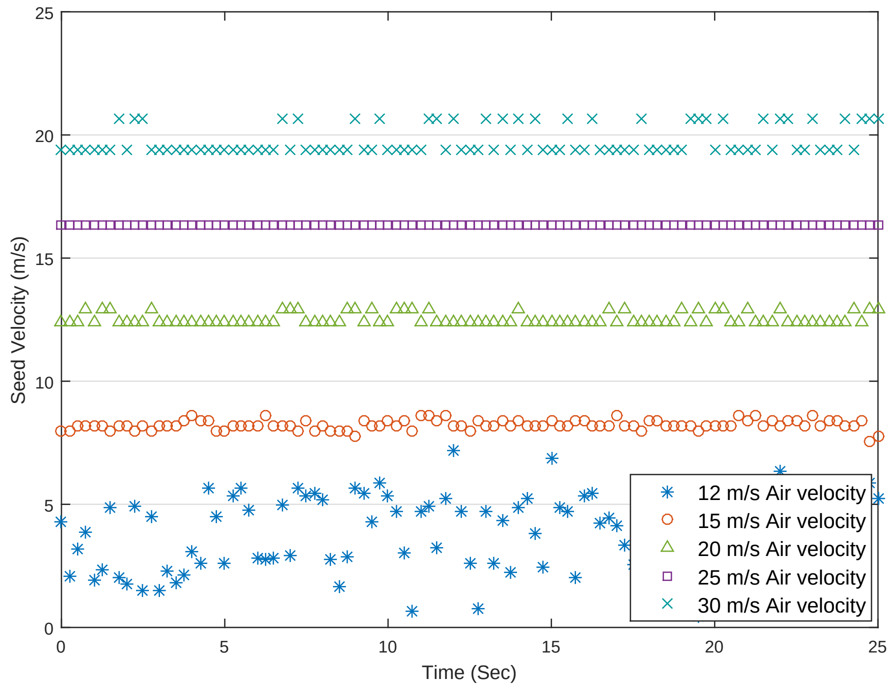

Figure 4.4: Velocity measurement graph for the 0.25 sec fixed time window method from the tests at 12, 15, 20, 25 and 30 m/s air velocity with a mass feed rate of 3 kg/min.

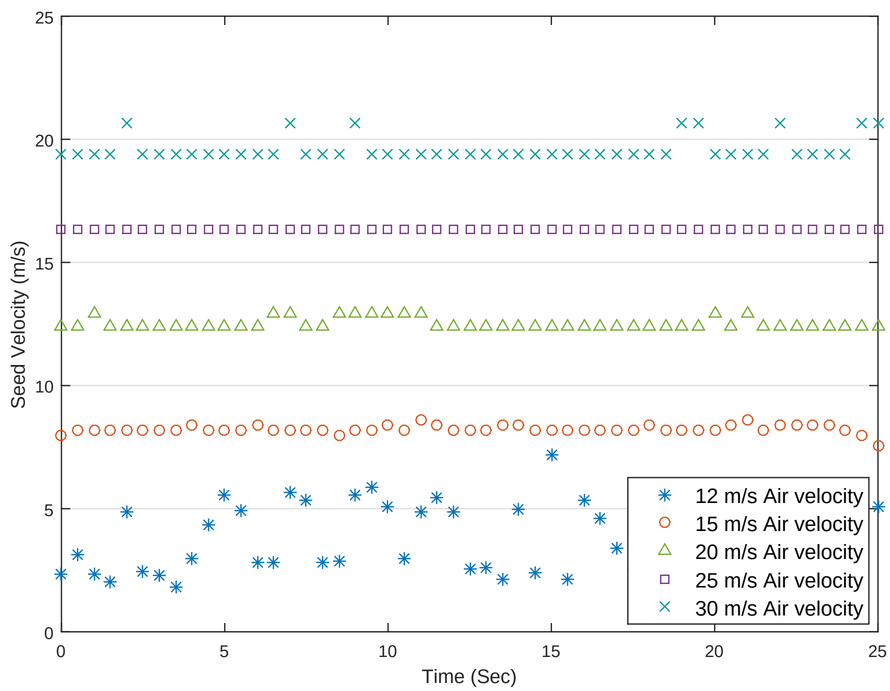

Figure 4.5: Velocity measurement graph for the 0.5 sec fixed time window method from the tests at 12, 15, 20, 25 and 30 m/s air velocity with a mass feed rate of 3 kg/min.

Figure 4.6 shows the velocity results from the threshold detection cross-correlation method, and the threshold value was set to 2.8 $volts$. In this method, the seed velocity is measured from the seed whose signal magnitude is greater than the threshold value. From the result graph, it is not smooth as the fixed time window velocity measurement result, but the averages of the seed velocity almost are the same.

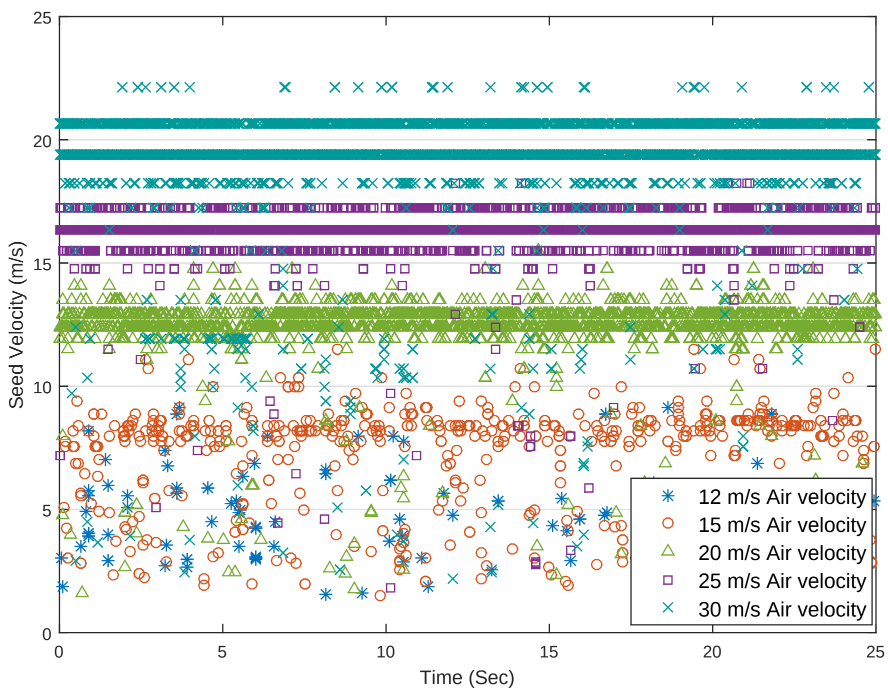

Figure 4.6: Velocity measurement graph for the threshold detection method with a threshold value of 2.8 $volts$ from the tests at 12, 15, 20, 25 and 30 m/s air velocity with a mass feed rate of 3 kg/min.

From Figure 4.4 to 4.6, the fixed time window method produced a smoother velocity graph than the threshold detection method. Under a mass flow rate of 3 kg/min, the seed velocity curve with a high air velocity is more stable than that of 12 m/s air velocity. By observing the different length of the fixed time window, the velocity result changes slightly.

The PTV method provides the horizontal and vertical components of each tracked seed velocity. To compare with the results measured by the two-electrode electrostatic sensor, only the horizontal part was taken into consideration. Figure 4.7 shows the results from PTV tests at 12, 15, 20, 25 and 30 m/s air velocity with a mass feed rate of 3 kg/min combined. In this figure, the x-axis shows the seed horizontal velocity U results, and the y-axis indicates the seed velocity in the vertical direction V in the pipeline. From the five testing groups, the average seed velocities in the horizontal direction results are $4.13\,m/s$, $8.33\,m/s$, $12.31\,m/s$, $15.61\,m/s$, and $18.98\,m/s$, respectively; while, the standard deviation (SD) of these velocity results are 2.31, 1.64, 1.58, 2.06 and 2.29 m/s [76].

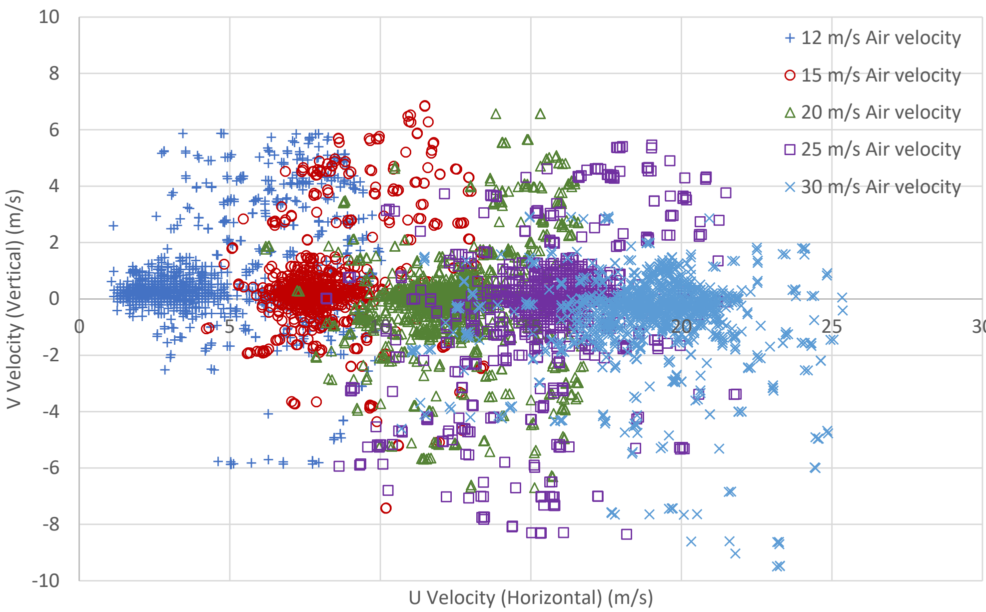

Figure 4.7: Velocity Measurement Results from PTV from the tests at 12, 15, 20, 25 and 30 m/s air velocity with a mass feed rate of 3 kg/min [76].

Along with the known air velocity for each test, the slip ratio between the air and seed velocities in each group was also calculated. The average velocity of the horizontal axis and the SD for each test was calculated as noted in Table 4.2 below. For the PTV method, the velocity results were calculated from the valid particles in the images. For the fixed time window cross-correlation method, the velocities were measured every 0.25 sec or 0.5 sec from the 25 sec period of the testing seed signals. For the threshold detection method, the velocity measurement was activated by the designed threshold value.

The slip ratio is a good representation of the relation between the seed and the airflow, which is a two-phase gas-solid flow in this experiment, as Equation 4.6 shows,

$$Slip\,ratio\,\% = 100 \times \frac{Seed\;Velocity}{Air\;Velocity}. \tag{4.6}$$

Table 4.2: Complete Results for All Measurement Tests

Setting			PTV				0.25 sec Time Window				0.5 sec Time Window				Threshold Detection			
Test	Air Velocity (m/s)	Mass Flow Rate (kg/min)	Average Velocity (m/s)	Std. Dev	Slip Ratio	Number of Valid Points	Average Velocity (m/s)	Std. Dev	Slip Ratio	Number of trials represented	Average Velocity (m/s)	Std. Dev	Slip Ratio	Number of trials represented	Average Velocity (m/s)	Std. Dev	Slip Ratio	Number of trials represented
1	12	1	6.84	1.18	0.57	623	6.45	0.31	0.54	104	6.40	0.12	0.53	52	5.58	1.78	0.47	261
2		2	5.80	1.43	0.48	1716	5.05	1.34	0.42	104	5.18	1.09	0.43	52	4.78	1.76	0.40	240
3		3	4.13	2.31	0.34	1552	3.78	1.54	0.32	104	3.45	1.43	0.29	52	4.38	1.87	0.36	103
4	15	1	8.75	1.36	0.58	1859	9.08	0.19	0.61	104	9.08	0.16	0.61	52	8.59	1.74	0.57	280
5		2	8.75	1.59	0.58	1246	8.65	0.18	0.58	104	8.65	0.14	0.58	52	8.10	1.93	0.54	545
6		3	8.33	1.64	0.56	914	8.18	0.22	0.55	104	8.19	0.17	0.55	52	7.24	2.02	0.48	580
7		4	8.09	1.65	0.54	1160	7.86	0.51	0.52	104	7.83	0.19	0.52	52	6.65	2.24	0.44	723
8		5	7.95	1.57	0.53	1212	6.35	2.33	0.42	104	7.04	1.46	0.47	52	6.36	2.41	0.42	916
9		6	7.84	1.66	0.52	2883	5.45	2.04	0.36	104	5.73	1.64	0.38	52	6.00	2.31	0.40	1196
10	20	1	12.58	1.62	0.63	1452	12.98	0.29	0.65	104	12.95	0.25	0.65	52	12.50	2.08	0.63	774
11		2	12.33	1.86	0.62	2405	12.85	0.17	0.64	104	12.84	0.19	0.64	52	12.66	1.09	0.63	1949
12		3	12.31	1.58	0.62	1872	12.53	0.22	0.63	104	12.51	0.21	0.63	52	12.45	1.26	0.62	3425
13		4	12.12	1.79	0.61	3007	12.38	0.13	0.62	104	12.38	0.09	0.62	52	12.20	1.31	0.61	4943
14		5	11.75	1.63	0.59	2260	12.13	0.25	0.61	104	12.13	0.25	0.61	52	11.97	1.31	0.60	7089
15		6	11.54	1.57	0.58	2928	12.00	0.18	0.60	104	11.98	0.15	0.60	52	11.85	1.43	0.59	9663
16	25	3	15.61	2.06	0.62	1115	16.32	0.00	0.65	104	16.32	0.00	0.65	52	16.26	1.01	0.65	6040
17		4	15.30	2.21	0.61	1418	16.25	0.22	0.65	104	16.24	0.24	0.65	52	16.06	1.08	0.64	8244
18		5	15.35	1.50	0.61	923	16.15	0.33	0.65	104	16.14	0.33	0.65	52	15.96	1.02	0.64	10092
19		6	15.25	2.56	0.61	1797	16.01	0.39	0.64	104	16.03	0.39	0.64	52	15.93	0.89	0.64	12059
20	30	3	18.98	2.29	0.63	1265	19.77	0.60	0.66	104	19.60	0.49	0.65	52	19.49	2.03	0.65	8214
21		4	19.18	2.13	0.64	1249	19.60	0.49	0.65	104	19.60	0.49	0.65	52	19.75	1.19	0.66	10214
22		5	18.84	1.89	0.63	1073	19.42	0.25	0.65	104	19.42	0.25	0.65	52	19.67	1.02	0.66	12677
23		6	18.68	2.20	0.62	1758	19.40	0.18	0.65	104	19.40	0.18	0.65	52	19.51	1.01	0.65	14581

From the experiment data, the following results were noted:

1. For test 1 to 9, the air velocity was set to the lowest setting $12\,m/s$ and $15\,m/s$. For the test 2, 3, 8, 9, when the mass flow rate was high, it was noted that some seeds would often clump together along the bottom of the pipe and plug the pipe. It could produce a large measured velocity difference between the PTV and the electrostatic sensor. But no matter which method was applied, the deviation of velocity under the air velocity of $12\,m/s$ or $15\,m/s$ is obviously higher than the other three groups. Moreover, from Table 4.2, the slip ratios for the tests under the air velocity of $12\,m/s$ and $15\,m/s$ are significantly lower than other three air velocity testing groups.

2. For test 10 to 23, there was no seed-clumping phenomenon in the pipe noted during these tests, which means the air velocity was high enough to entrain the seed in the air flow. With the increasing seed mass flow rate, the change of the measured seed velocity is slight for all four measurement methods. The slip ratio for the test 10 to 23 stays relatively constant at about 0.65 from the cross-correlation methods.

3. From all of the experimental data, the two-electrode electrostatic sensor was able to measure the velocity of the flowing seed in the pipeline. Beside the tests with clumping seeds, the standard deviations of the rest all tests are under 0.6 for the fixed time window method; while, for the PTV and threshold detection method, the standard deviations are between about 1 to 2.5.

4. The results from PTV provided a good reference to ensure the two-electrode electrostatic sensor was working correctly. The seed velocity for each test was graphed in comparison to the seed mass flow rate as shown in Figure 4.8. Table 4.3 summarizes the seed velocity measurement results from the electrostatic sensor compared with the PTV results. From the test groups with the air velocity of 12 and 15 m/s, some of the velocity results have a large difference, about 10 to 30. The reason might be that the PTV technique only took the valid seeds in images and ignored the clumping seeds. However, in a lower air velocity groups, there often were some clumping seeds, and the electrostatic sensor measured the clumping seed ESG signals, which might produce the

obvious difference from the PTV velocity measurement results. Moreover, from the test groups with the air velocity of 20, 25, and 30 m/s, there were few clumping seeds, and the differences between the two methods are relatively tiny, between 1.6% and 6.1%. From these tests, it was confirmed that the two-electrode electrostatic sensor has the ability to measure the seed velocity in a pneumatic conveying system.

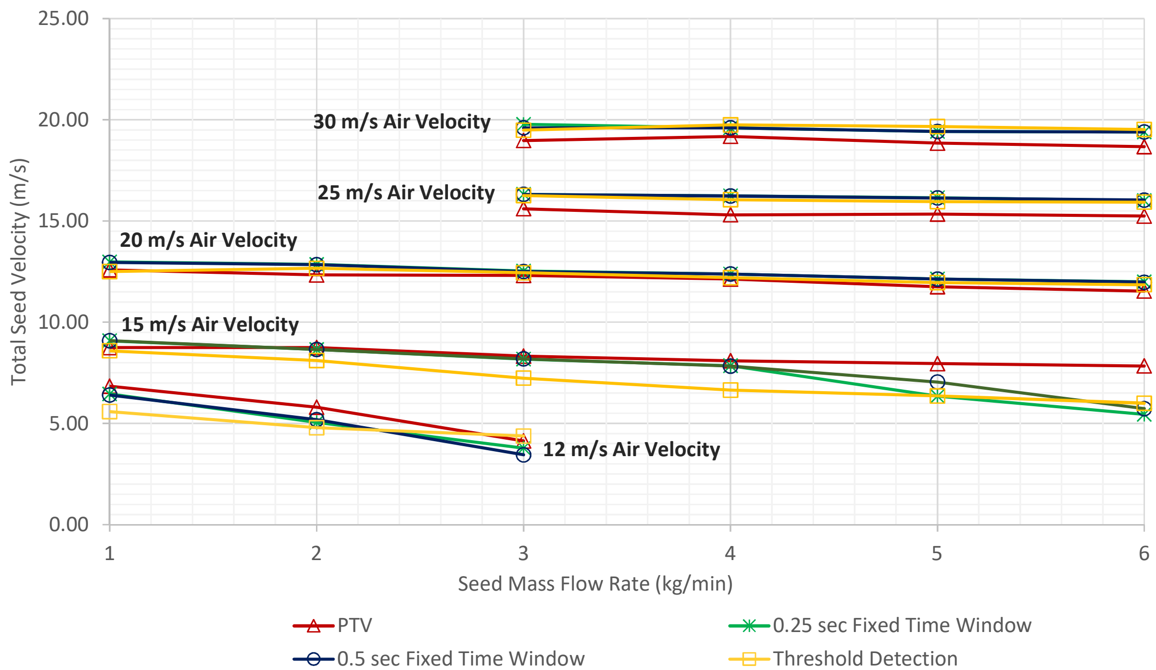

Figure 4.8: Velocity measurement graph for PTV and electrostatic sensor with different algorithms.

Table 4.3: Comparison with PTV and Electrostatic Sensor Measurement Results

Setting			PTV	0.25 sec Time Window		0.5 sec Time Window		Threshold Detection	
Test	Air Velocity (m/s)	Mass Flow Rate (kg/min)	Average Velocity (m/s)	Average Velocity (m/s)	$\frac{\lvert U_{Seed} - U_{PTV} \rvert}{U_{PTV}}$	Average Velocity (m/s)	$\frac{\lvert U_{Seed} - U_{PTV} \rvert}{U_{PTV}}$	Average Velocity (m/s)	$\frac{\lvert U_{Seed} - U_{PTV} \rvert}{U_{PTV}}$
1	12	1	6.84	6.45	6.16%	6.40	6.41%	5.58	18.42%
2		2	5.80	5.05	13.05%	5.18	10.67%	4.78	17.62%
3		3	4.13	3.78	8.47%	3.45	16.50%	4.38	5.96%
4	15	1	8.75	9.08	3.78%	9.08	3.82%	8.59	1.88%
5		2	8.75	8.65	1.12%	8.65	1.16%	8.10	7.42%
6		3	8.33	8.18	1.75%	8.19	1.63%	7.24	13.09%
7		4	8.09	7.86	2.90%	7.83	3.27%	6.65	17.80%
8		5	7.95	6.35	20.08%	7.04	11.36%	6.36	19.95%
9		6	7.84	5.45	30.45%	5.73	26.86%	6.00	23.48%
10	20	1	12.58	12.98	3.15%	12.95	2.93%	12.50	0.66%
11		2	12.33	12.85	4.20%	12.84	4.08%	12.66	2.67%
12		3	12.31	12.53	1.74%	12.51	1.58%	12.45	1.08%
13		4	12.12	12.38	2.13%	12.38	2.13%	12.20	0.63%
14		5	11.75	12.13	3.26%	12.13	3.26%	11.97	1.83%
15		6	11.54	12.00	3.97%	11.98	3.81%	11.85	2.70%
16	25	3	15.61	16.32	4.55%	16.32	4.55%	16.26	4.18%
17		4	15.30	16.25	6.20%	16.24	6.09%	16.06	4.91%
18		5	15.35	16.15	5.25%	16.14	5.20%	15.96	4.02%
19		6	15.25	16.01	4.99%	16.03	5.14%	15.93	4.46%
20	30	3	18.98	19.77	4.17%	19.60	3.26%	19.49	2.67%
21		4	19.18	19.60	2.17%	19.60	2.17%	19.75	2.96%
22		5	18.84	19.42	3.09%	19.42	3.09%	19.67	4.39%
23		6	18.68	19.40	3.86%	19.40	3.86%	19.51	4.48%

4.3 Conclusion

In the proposed seed velocity measurement system, a two-electrode electrostatic sensor was applied for the seed velocity measurement. The objectives set for this experiment were to use the electrostatic sensor and two cross-correlation methods to measure wheat seed in a pneumatic conveying system. A PTV system was used to provide a reference data set. Using the existing equipment in the Air Handling Lab at the University of Saskatchewan, tests were performed where the air velocity was set to 12, 15, 20, 25 and 30 m/s and the seed mass flow rate was varied between 1 kg/min to 6 kg/min in 1 kg/min increments. The seed electrostatic signals were collected by the two electrodes, and transmitted to the DAQ connected to a PC.

In total, 23 tests were run and the velocity of the particles were measured and recorded. The results of the tests provided a good view of the velocity of the seed in the pneumatic conveying system. It showed that when the air velocity is relatively low and the mass flow rate is relatively high, the wheat seed can not be successfully transported, resulting in velocity measurement results having a large deviation. This situation causes the calculated slip ratio to be lower than the normal value in the lab version air seeder system. The lower air speed requires a greater distance to accelerate particle to their ultimate slip velocity. It suggests that the the maximum slip ratio in this air seeder system between the flowing air and the wheat seed is approximately 0.65, and if it is lower than 0.5, some seeds would clump together along the bottom of the pipeline and even clog the pipeline.

5. Seed Counting in a Pneumatic Conveying System

Accurate seed counting during the process of sowing has the potential to help precision in agriculture. Due to environmental factor, the number of seeds sown is hard to measure using an air seeder. An electrostatic sensor was applied to detect the seed ESG signal. However, for various reasons, such as overlapping waveform from multiple particles, the experimental results of the counting accuracy are lower than acceptable. To reduce the counting error rate, pattern recognition technology and related experimental improvements were applied to the seed counting project.

It was noted that, there was not necessarily a gap between each seed signal or waveform peak. Moreover, the charge carried by each seed was different so that the signal waveform amplitude was random in a certain range. Based on the seed signal waveforms and the known seed number, waveform features were developed using a pattern recognition method and training groups. The parameters obtained from the training groups were then applied to the testing groups. Comparing the testing group seed number with the manual counting results, the performance of the pattern recognition method was evaluated and demonstrated the potential for high accuracy counting results.

In this chapter, the whole process of this method is demonstrated, including the acquiring the ESG signal, signal denoising by compressive sensing, signal segmentation, feature extraction and selection, and a multiple classification approach. Two kinds of seed, wheat and canola, were treated as the experimental objects to verify the applicability of the seed counting method. The flowing seed counting system was evaluated through four different scenarios.

5.1 Signal Processing Based on Pattern Recognition Technique

In this section, the seed ESG signal for seed counting is analyzed, and the simulation and analysis for the signal model is discussed. Also, the signal processing method based on pattern recognition technique is described.

5.1.1 Signal Analysis for Seed Counting

A model that uses a Gaussian distribution [77] as the induced charge waveform was developed. The decision to use a Gaussian shape came from examining the data and deciding that this was an accurate representation of the induced particle waveform:

$$G(t, \mu, \epsilon, A) = A \cdot \frac{1}{\epsilon\sqrt{2\pi}} \exp(-\frac{1}{2}(\frac{t-\mu}{\epsilon})^2). \tag{5.1}$$

where, t is the time of the seed arriving the electrode, μ is mean of the distribution, ϵ is stand deviation, and A is the gain for the signal waveform amplitude.

Because what is actually measured is the change in charge, the waveform used in modeling is the derivative of a Gaussian:

$$G'(t, \mu, \epsilon, A) = A \cdot \frac{\mu - t}{\epsilon^3\sqrt{2\pi}} \exp(-\frac{1}{2}(\frac{t-\mu}{\epsilon})^2). \tag{5.2}$$

For a single particle, there are three parameters that should be considered: the magnitude of the signal, the width of the signal, the particle polarity. The number of points in the waveform is controlled by the sampling frequency chosen. The width of the waveform is affected by the speed of the particles and the amount of charge. The particle polarity carried by each seed is random, and particles with the opposite charge will cause the inverse charge and current waveforms.

ESG signal is the recording of the electrical activity associated with seed passing through the electrode. Each seed has a certain amount of charge, and produces an electrostatic waveform as it moves past the electrode. After the superposition of the individual seed signals motor units (MUs), the ESG signal is produced.

ESG signal decomposition is the process of resolving a composite ESG signal into its constituent motor unit potential trains (MUPTs), which can be considered as a classification problem. For one seed, it can produce one kind signal waveform, which is shown as the Figure 5.1. A particle with the opposite charge will cause the inverse current waveform. The equation of the signal waveform can be represented as

$$f_1 = G_1'(t_1, \mu_1, \epsilon_1, A_1). \tag{5.3}$$

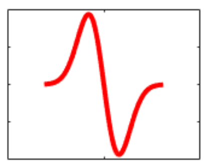

Figure 5.1: One seed electrostatic waveform template.

In most situations, seeds carry different amount of charge and travel at different speeds, so each seed ESG MU and signal waveform is different. Also, the opposite charge seeds will produce the inverse ESG signal. The equation of the two seed signal template can be represented as

$$f_2 = G_1'(t_1, \mu_1, \epsilon_1, A_1) + G_2'(t_2, \mu_2, \epsilon_2, A_2). \tag{5.4}$$

By analyzing these two seed signal templates, all of the templates can be divided into six cases by different feature orders based on turn (without peak and valley), peak and valley, and zero-cross point. Figure 5.2 shows two random seed overlap waveform template cases. The blue lines indicate the two seed individual waveforms, and the red one shows the superposition of the two waveforms. Figure 5.3 shows the orders of the features for the six cases.

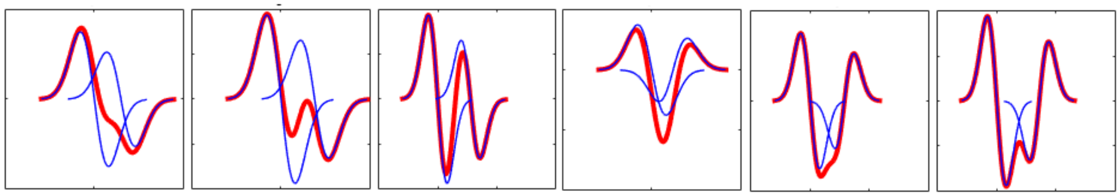

case 1 case 2 case 3 case 4 case 5 case 6

Figure 5.2: Two random seeds potential electrostatic waveform template cases.

Case 1	Turn	Peak/Valley	Zero-Cross	Turn	Turn	Peak/Valley	Turn		
Case 2	Turn	Peak/Valley	Zero-Cross	Peak/Valley	Peak/Valley	Peak/Valley	Turn		
Case 3	Turn	Peak/Valley	Zero-Cross	Peak/Valley	Zero-Cross	Peak/Valley	Zero-Cross	Peak/Valley	Turn
Case 4	Turn	Peak/Valley	Zero-Cross	Peak/Valley	Zero-Cross	Peak/Valley	Turn		
Case 5	Turn	Peak/ Valley	Zero-Cross	Peak/Valley	Turn	Turn	Zero-Cross	Peak/Valley	Turn
Case 6	Turn	Peak/Valley	Zero-Cross	Peak/Valley	Peak/Valley	Peak/Valley	Zero-Cross	Peak/Valley	Turn

Figure 5.3: The features for the two random seeds waveform template cases.

The three seed electrostatic waveform template equation is

$$f_3 = G_1'(t_1, \mu_1, \epsilon_1, A_1) + G_2'(t_2, \mu_2, \epsilon_2, A_2) + G_3'(t_3, \mu_3, \epsilon_3, A_3). \tag{5.5}$$

Similarly, the three random seed electrostatic waveform templates can be divided into 108 cases based on the different feature orders.

Figure 5.4 shows three random seeds with the same polarity overlap waveforms.

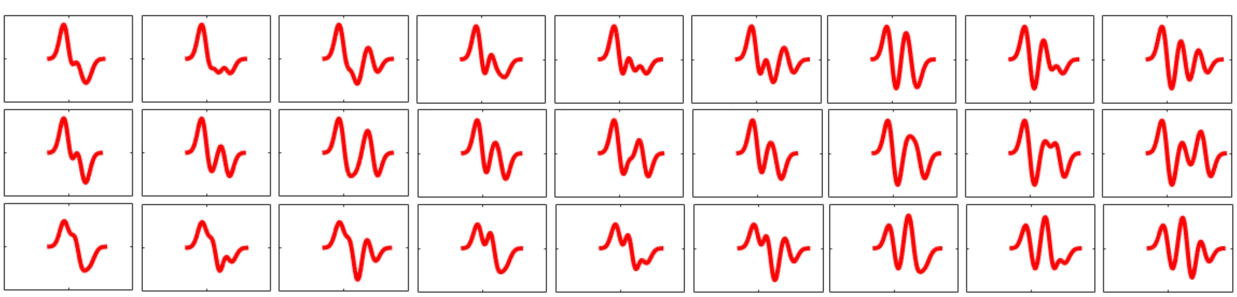

Figure 5.4: Three random seeds with the same polarity potential electrostatic waveform templates.

Figure 5.5 shows three random seeds with the different polarity overlap waveforms.

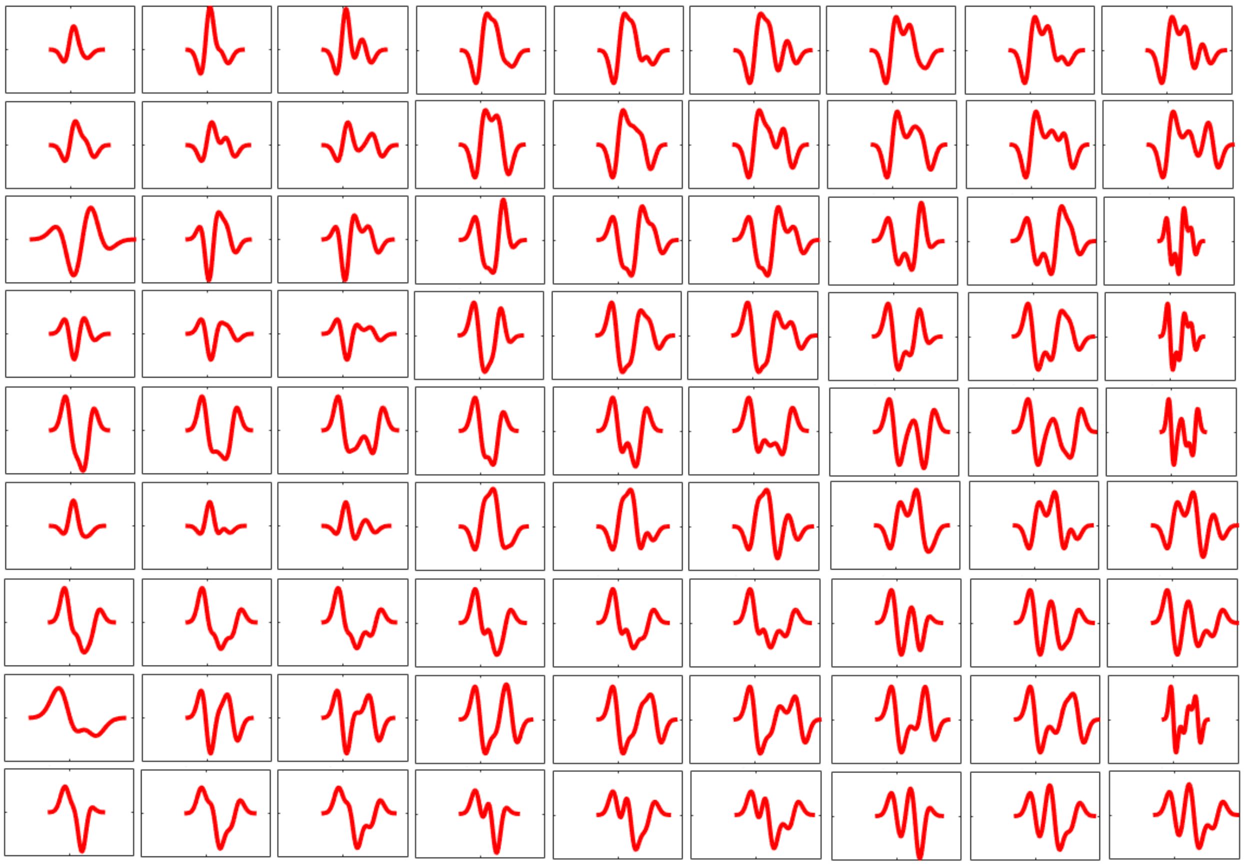

Figure 5.5: Three random seeds with the different polarity potential electrostatic waveform templates.

In general, the equation of the n seed cluster waveform templates can be represented as

$$f_n = \sum_{i=1}^{n} G'_i(t_i, \mu_i, \epsilon_i, A_i). \tag{5.6}$$

Based on analysis the real seed ESG signals, the phenomenon of seed signals overlapping is common, and the number of seeds in a cluster signal can reach to more than hundred. It is difficult and infeasible to exhaustively analyze all possible signal templates. Therefore, we cannot just simply find out all the templates and match them to the real seed ESG signal. This is possible only if a robust pattern recognition algorithm is developed.

Because of the complicated waveform templates, the simple match method could not be applied directly. After acquiring the ESG signal, the first task was signal denoising and signal segmentation, which was then followed by feature extraction and the main task of classification. In the main classification task, each MUP reference set was obtained using training groups, and then applied to the testing groups. Figure 5.6 shows the main steps of the counting approach for signal processing.

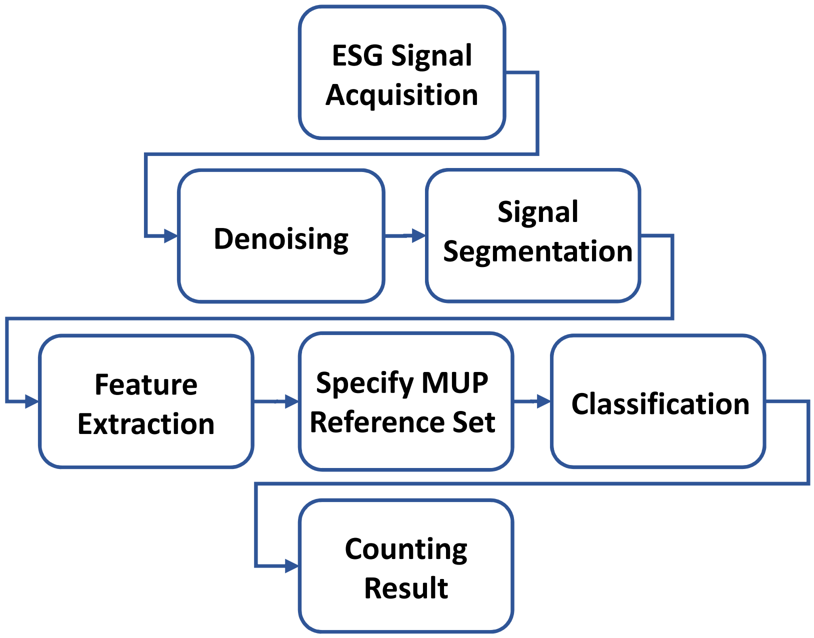

Figure 5.6: Flowchart of ESG signal processing.

5.1.2 ESG Signal Denoising by Compressive Sensing

Denoising is the step that must be carried out. Because the number of seeds passing through the sensor varies over time, a simple band pass filter can not be used for denoising. The compressive sensing approach [78, 79] is a feasible method for the signal denoising.

Sparse and structured signal decomposition is based on time-frequency adjacency in Gabor representations [80]. The Gabor transform of a signal $x(t)$ is defined by this formula

$$\Phi_x(t, f) = \int_{-\infty}^{\infty} e^{-\pi(\tau-t)^2} e^{-j2\pi f\tau} x(\tau) d\tau. \tag{5.7}$$

The basic conception of persistent time-frequency compressive sensing is to consider thresholding operators [81] as

$$S_{\lambda,\xi}(c) = c_{k,j}(1 - \xi(c))^{+}, \tag{5.8}$$

where $c_{k,j}$ is a sequence of time-frequency coefficients, and + means a non-negative function. In this research, the persistent empirical Wiener (PEW) operator [82] is applied as the thresholding operator.

In the PEW thresholding operator, the applied basic threshold function is ξ^{L}, which is the least absolute shrinkage and selection operator (LASSO),

$$\xi^{L}(c_{k,j}) = \frac{\lambda}{|c_{k,j}|}, \tag{5.9}$$

where λ is the threshold level for the shrinkage.

The neighborhood smoothed shrinkage operator applied was the persistent LASSO ξ^{WGL},

$$\xi^{WGL} = \xi^{L} \circ \eta_{N}, \tag{5.10}$$

where, $\eta_N(c_{k,j}) = \sqrt{\left(\sum_{(k,j)' \in N(k,j)} \omega_{(k,j)}\left(k,j\right)' — c_{k,j}|^2\right)}$, the time-frequency neighborhood smoothing function, and $N(k,j) = \left\{(k,j)' : \omega_{(k,j)}\left(k,j\right)'\right\}$is the neighborhood with the weight $\omega_{(k,j)}$.

Furthermore, changing the thresholding slope, $\xi^{*} = \xi^{2}$, the further threshold operator, ξ^{PEL}, is obtained, which is

$$\xi^{PEL} = (\xi^{WGL})^{2}. \tag{5.11}$$

Algorithm for Signal Denoising

1. Apply the Gabor transform on the ESG signal X with the Noise Z, and obtain its time-frequency distribution $\Phi(X + Z)$.

2. Choose a threshold level λ for the shrinkage. The larger λ, the sparser the solution.

3. Shrink the time-frequency coefficients $\Phi(X + Z)$ to Y with the threshold operator as the LASSO estimator.

4. Apply the Inverse Gabor transform on Y to reconstruct the signal X' after denoising.

Figure 5.7 shows the steps of the algorithm of signal denoising.

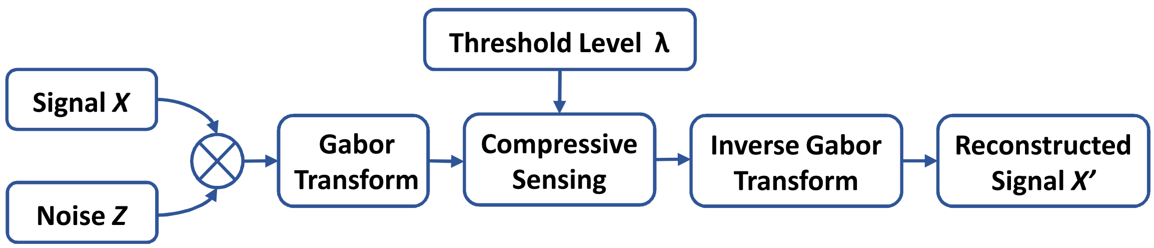

Figure 5.7: Compressive sensing denoising schematic diagram with Gabor transform.

For simulation analysis, a simulated ESG signal with $25\,dB$ Guassion noise, which is obtained from the real ESG signal noise level, has been applied by the compressive sensing denoising methods. The signal simulates that 300 seeds pass the electrostatic sensor in one second. The threshold level λ is set as 0.03. Figure 5.8 shows the simulated clean signal, the clean signal with noise, and the denoised signal. Figure 5.9 shows the three signals in the time-frequency distribution.

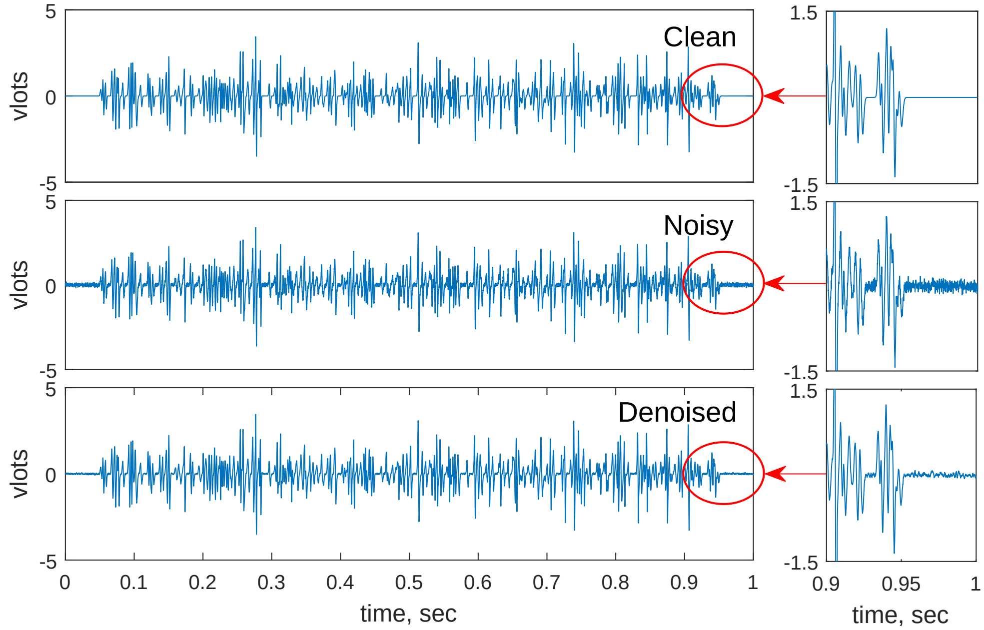

Figure 5.8: ESG signal denoising simulation by compressive sensing. The image on the right side is an enlarged view of the red arrow part of the signal.

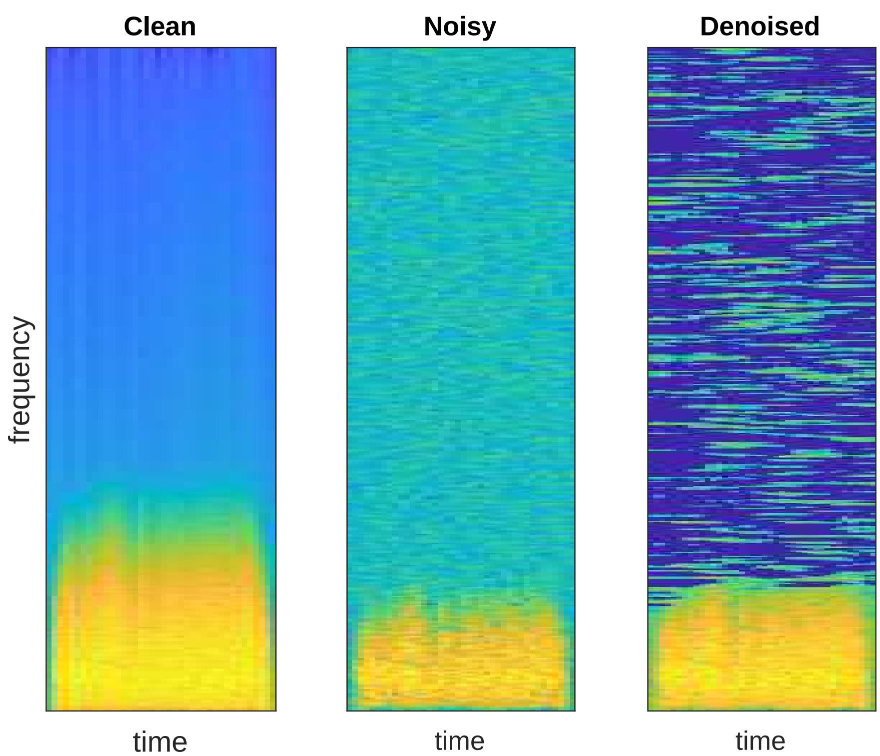

Figure 5.9: ESG signal denoising simulation in time-frequency distribution.

5.1.3 Signal Segmentation for MUP

The objective of ESG signal decomposition is the extraction of relevant seed information from analysis of individual MUP waveforms and MU patterns. After the ESG signal denoising, the next step is the segmentation of the signal and detection of possible MUP waveforms. The ESG signal waveform is generated by each seed moving through the electrostatic sensor, and the seed cluster waveform can be separated by their inter-discharge intervals (IDIs) as shown in Figure 5.10.

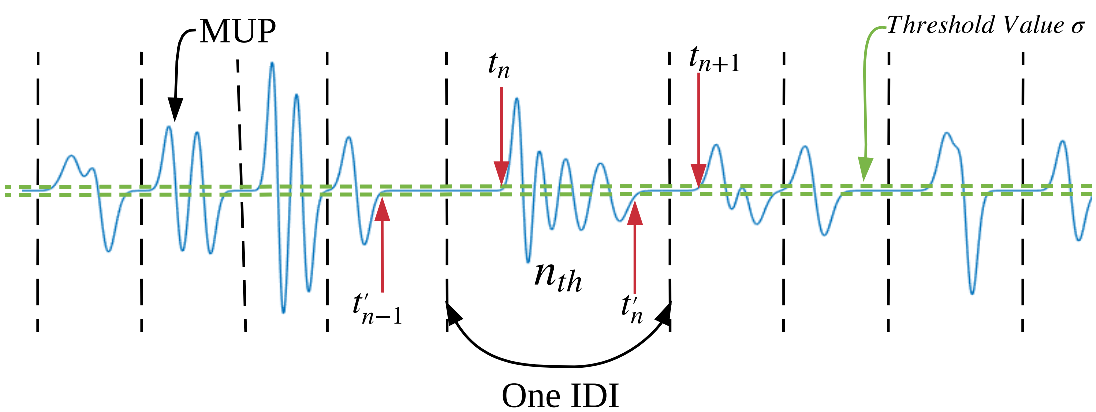

Figure 5.10: ESG signal segmentation by IDIs.

The shapes of MUPs can offer the cluster of seed information, which can help getting the number of seeds for each IDI. Within this model, all the IDIs within the MU firing pattern are independent. ESG signals do not have a certain gap between each discharging MU. IDI can help to analyze each cluster waveform.

Algorithm for Signal Segmentation

1. To detect a MUP, a signal magnitude threshold value σ and a zero-cross section time t_c are assumed.

2. Once the magnitude of signal is greater than the threshold value σ, the n_{th} MUP is detected at the time t_n.

3. When the detected signal value is less than the threshold value σ and the duration

time is more than the zero-cross section time t_c, the last point of the signal magnitude larger than σ can be marked as the end of the MUP at the time t'_n.

4. The system is ready to detect the $n+1_{th}$ MUP.

5. For the n_{th} IDI, it occurs at $t_{nstart} = \frac{(t_n + t'_{n-1})}{2}$, and ends at $t_{nend} = \frac{(t_{n+1} + t'_n)}{2}$.

5.1.4 Feature Extraction and Selection for MUPTs

To compare with the analysis of the MUPT waveforms, six feature extraction methods were developed.

1. *Threshold Detection*

   In the Threshold Detection, the value is compared with a threshold value. The counter is incremented by one when the current value exceeds the threshold value. The problem is if there are two or more seeds though the electrostatic sensor in a very close distance, then the value of the data in this process will always be greater than that of the threshold value.

2. *Full Width Half Maximum*

   The Full Width Half Maximum (FWHM) was computed for an individual particle depend on the speed of particle and then compared to the result for the entire cluster. The results of this comparison was then used to determine the class of the cluster.

3. *Cluster Width*

   The width of a single particle was compared with the width of the total cluster. Both widths were computed using a similar threshold to determine the start and end of the waveform. The results of this comparison was then used to determine the class of the cluster.

4. *Peak and Valley Detection*

   Similar to the threshold detection algorithm, the peak detection method examine the negative and positive waveform separately. Then the number of seeds can be obtained though the peak and valley count results.

5. *Number of Turns*

   Each waveform has a certain number of turns. Like the peak and valley, the number of turns is one of the MUP shape parameters. The number of turns for one seed waveform is four. For multiple seeds, the number of turns could be different, and the distance of two turns is still related to the shape of the number of seed waveform.

6. *Energy Comparison*

   The feature, energy comparison computes the energy for one seed, which has considered the width and amplitude for one seed signal waveform. The number seeds in a group is related to the total energy of the group seeds waveform. In mathematics, we can use the first or second norm to compute the seed energy.

After these six features were tested by simulated and actual ESG signals, four of the features were applied to the seed counting signal processing*: Cluster Width, Peak and Valley Detection, Number of Turns,* and *Energy Comparison.*

5.1.5 Multiple Classifier Approach

According to the complexity of the ESG signal, the traditional classification task has a low accuracy for the counting result. When a large number of seed through the electrostatic sensor continues, the superposition of the waveform is very serious, and seeds cannot be separated one by one. In order to improve the performance of the classification, the multiple classifier approach has been applied to the ESG signal. The classifier system basic architecture is shown in Figure 5.11.

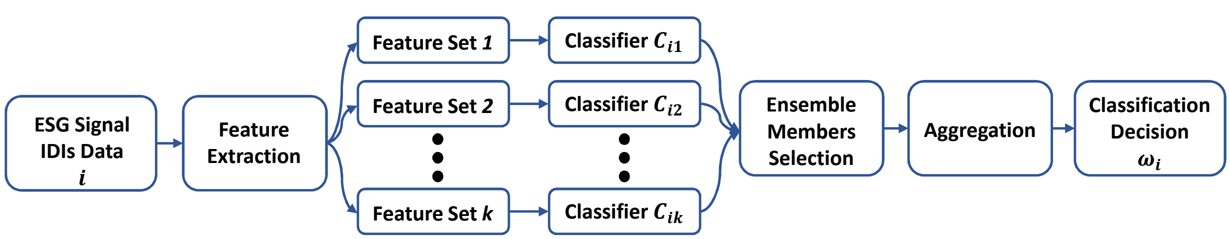

Figure 5.11: Multiple classifier system basic architecture.

Different classifiers can make their own decisions for the individual MUP waveforms which are parallel and independent. Then the ensemble members selection stage can choose each base classification result for further analysis. The aggregation module was based on the average rule. For M IDIs $\{\omega_i,\ i = 1, 2, ..., M\}$, the aggregation module is used for combine K different base classifier results $\{n_{ik},\ i = 1, 2, ..., M;\ k = 1, 2, ..., K\}$ with the decision confidences $\{C_{ik},\ i = 1, 2, ..., M;\ k = 1, 2, ..., K\}$. Therefore, the combined classifier decision for ω_i with the average rule confidence is

$$\omega_i = \frac{\sum_{k=1}^{k} C_{ik} \cdot n_{ik}}{K}. \tag{5.12}$$

5.2 Performance Evaluation and Discussion

In this section, the experimental setup is described, and the results from the experiments is discussed.

5.2.1 Experimental Setup

The experiment subjects were wheat seed. The air speed was 26 m/s, which is controlled by a fan. The the motor controller can release seed into the pipeline with a rate of 78 rpm. For the electrostatic sensor, a suitable gain was set to obtain a detected signal with a high resolution but not saturating. In the experiment, the gain applied was 186. Two electrostatic sensors were adapted to the secondary pipeline with a interior diameter of 25.4 mm. For the conveying air conditions, the air humidity was 54.3 $\%RH$ and the temperature was 23.1 $°C$. The sampling frequency was 10000 Hz.

There were three wheat seed groups, having $n_1 = 6161$, $n_2 = 7267$, and $n_3 = 6402$ seeds by hand counting, respectively. For pattern recognition, leave-one-out cross-validation was used in the signal analysis. Two of the three groups were treated as the training groups and the third was the testing group. In each group, the seed passed through two electrostatic sensors with a distance of 33 mm, with DAQ collect two data sets from the two sensors at the same time. Therefore, in total, there were 6 sets of ESG signal data for the three wheat groups. The counting results by the pattern recognition method were evaluated by the correct classification rate (CCr). The accuracy CCr is the ratio of the number of result from pattern recognition and the manual counting result, which is

$$CCr\% = (1- \mid \frac{\text{number of seeds classified}}{\text{manully counting result}} - 1 \mid) \times 100. \tag{5.13}$$

Then, the error rate is

$$Error\ Rate = 100\% - CCr\%. \tag{5.14}$$

5.2.2 Numerical Results and Analysis

After acquiring the wheat ESG signals from the experiment, the first task was signal denoising. Figure 5.12 shows the three wheat seed groups in the time-frequency distribution. For each group, there were two sensors to collect the ESG signal data.

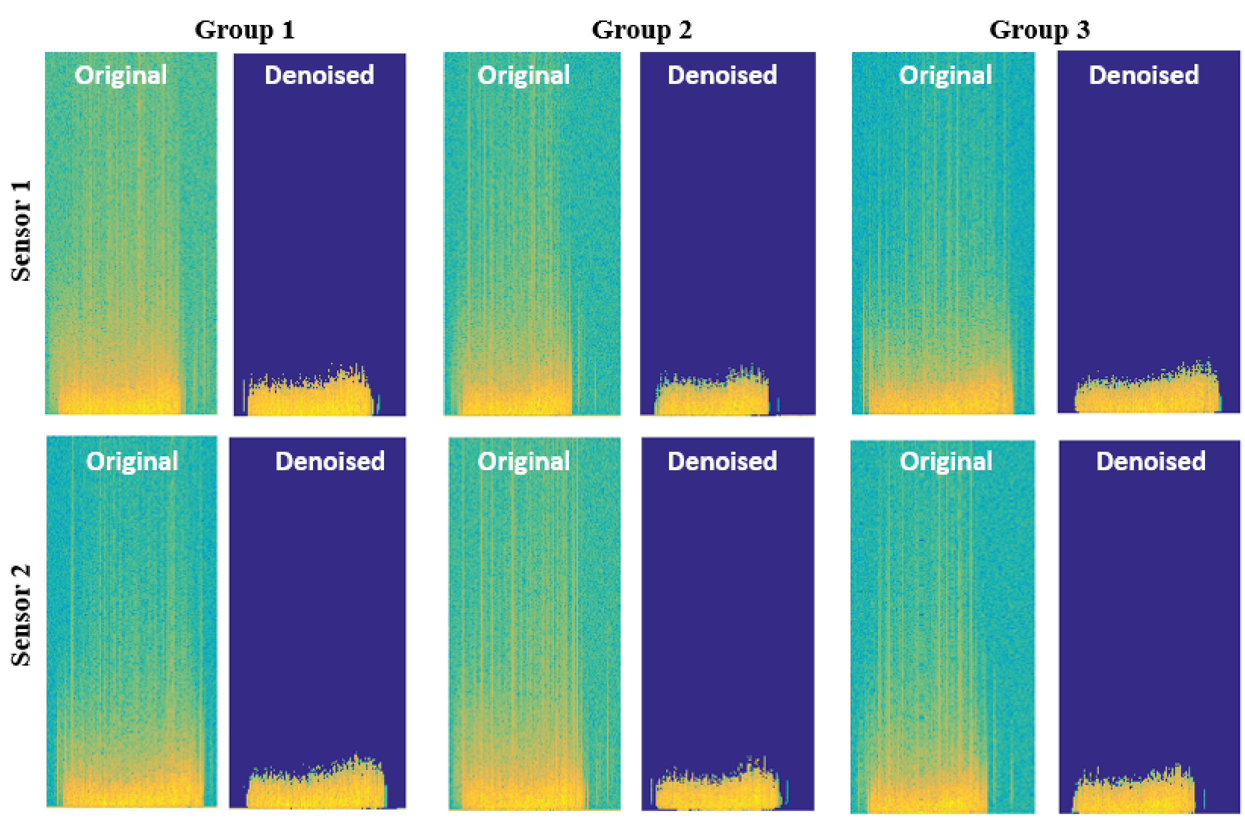

Figure 5.12: Original ESG signals and denoised signals in the time-frequency domain.

Applying the signal segmentation for the six group signals, the cluster MUs from the denoised signal were obtained. For the six groups, the number of IDIs for each denoised signal by signal segmentation is shown in the Table 5.1.

Table 5.1: Number of IDIs Calculated from Each Denoised ESG Signal

	Sensor 1	Sensor 2
Group 1	328	351
Group 2	302	338
Group 3	254	293

For the feature extraction, four features were developed, which are *Cluster Width, Peak and Valley Detection, Number of Turns,* and *Energy Comparison.* The feature of *Peak and Valley Detection* and *Number of Turns* can be extracted directly from the ESG signal. For the features of *Cluster Width* and *Energy Comparison*, training groups were needed to obtain the reference set for the average waveform width and norm energy of each seed in the real ESG signals. From the training groups, the total waveform width and seed energy were acquired from each sensor signal, and then divided by the known seed number of the training groups. The width reference and energy reference for the testing groups were calculated. Table 5.2 shows the reference set value for each testing group.

Table 5.2: MUP Feature Reference Set for Testing Group

Training Group		Width Reference	Energy Reference	Testing Group
Group 2	Group 3	23.4228	6.6211	Group 1
Group 3	Group 1	24.6999	6.3318	Group 2
Group 1	Group 2	23.8756	6.1255	Group 3

Figure 5.13 shows the performance of four features for the counting wheat seed processing results. In this figure, the first blue bar in each group shows the seed number by manually counting, and the rest of the four bars shows the counting results by the four features individually. Table 5.3 shows the CCr and the error rate for the individual four features counting results.

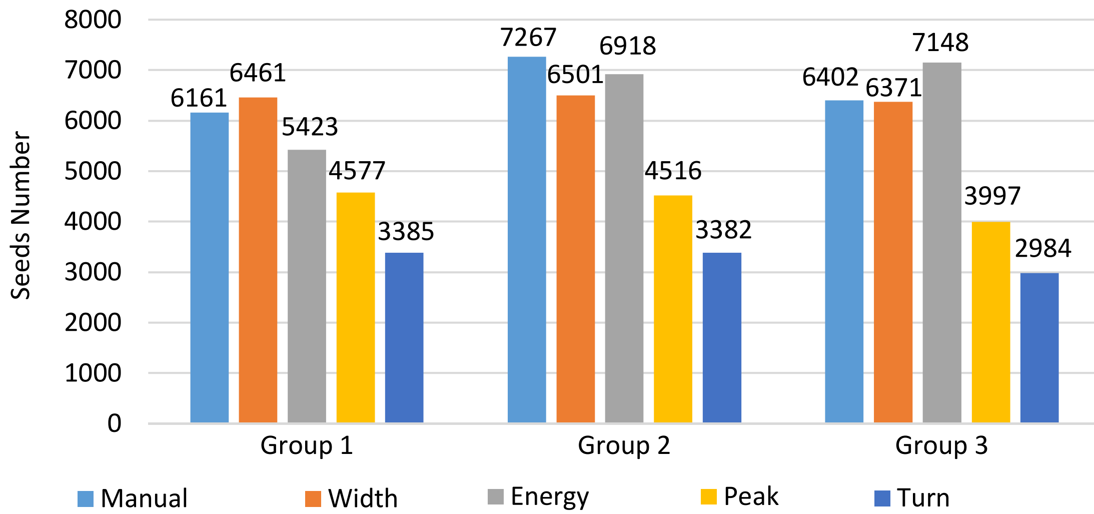

Figure 5.13: Counting results by four features for the three wheat groups.

Table 5.3: The CCr and Error Rate for the Four Features Counting Results

	Group 1			Group 2			Group 3		
	Number	*CCr*	Error Rate	NUM	*CCr*	Error Rate	NUM	*CCr*	Error Rate
Width	6461	95.13%	4.87%	6501	89.46%	10.54%	6371	99.52%	0.48%
Energy	5423	88.02%	11.98%	6918	95.20%	4.80%	7148	88.35%	11.65%
Peak	4577	74.29%	25.71%	4516	62.14%	37.86%	3997	62.43%	37.57%
Turn	3385	54.94%	45.06%	3382	46.54%	53.46%	2984	46.61%	53.39%
Multiple	5942	96.45%	3.55%	6710	92.34%	7.66%	6760	94.41%	5.59%

Obviously, for the three wheat groups, the error rates for the feature of *Peak and Valley Detection* and *Number of Turns* are unacceptable and much higher than the feature of *Cluster Width* and *Energy Comparison*. The CCr for the Width and Energy feature in the three wheat groups is at least 88%, but for the Peak and Turn feature it only about 60% to 75%. Therefore, in the task of multiple classification, the ensemble members selection stage only chose the *Cluster Width* and *Energy Comparison* classifier results for further analysis in the aggregation module. The Figure 5.14 shows the wheat seed multiple classifier approach counting results by the combined classifier decision with average rule confidence.

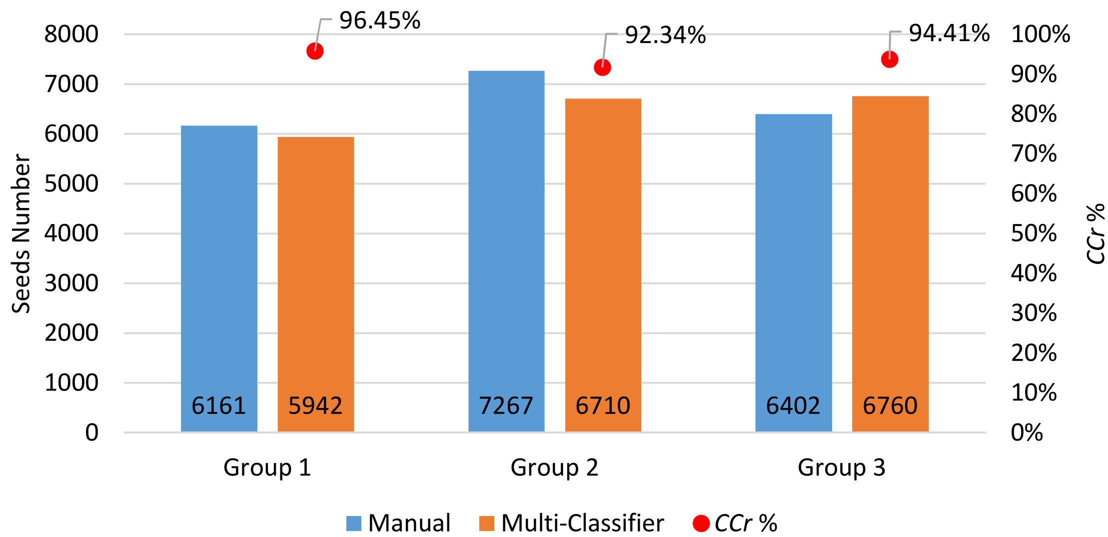

Figure 5.14: Counting results and CCr by the multiple classifier approach for the three wheat groups. Blue bar shows the manual counting results, and orange bar shows the multi-classifier couting results.

From the wheat seed counting results, all of the three testing groups accuracy rates is above 90%, which is in an acceptable range. The average of the CCr from the three testing wheat groups is 94.40% with the Standard Deviation (SD) of 2.05%. Moreover, in the following, the counting results are presented to investigate how the expected performance behaviors differ for collecting data by one electrostatic sensor, for denoising with an standard filter, for different kinds of seeds, and for an overflowed signal.

1. Number of Collecting Data Sensors: Two VS One

In order to investigate the influence of different number of the sensors, each data set can be treated as an individual testing set. From three two-sensor data sets, there are eight different combinations for three one-sensor data sets. Each combination of the three one-sensor data sets can get the three groups counting results. So, totally, there are 24 counting results by one sensor. From Figure 5.15, the two sensor result has a better mean accuracy rate at 94.40% with a low sample SD of 2.06%. If only one of ESG signal in each group was applied in the seed counting system, the average accuracy rate of the counting result is 92.26% with a sample SD of 5.44%. Using two electrostatic sensors to collect the ESG signal has a potential to improve the stability of counting system performance.

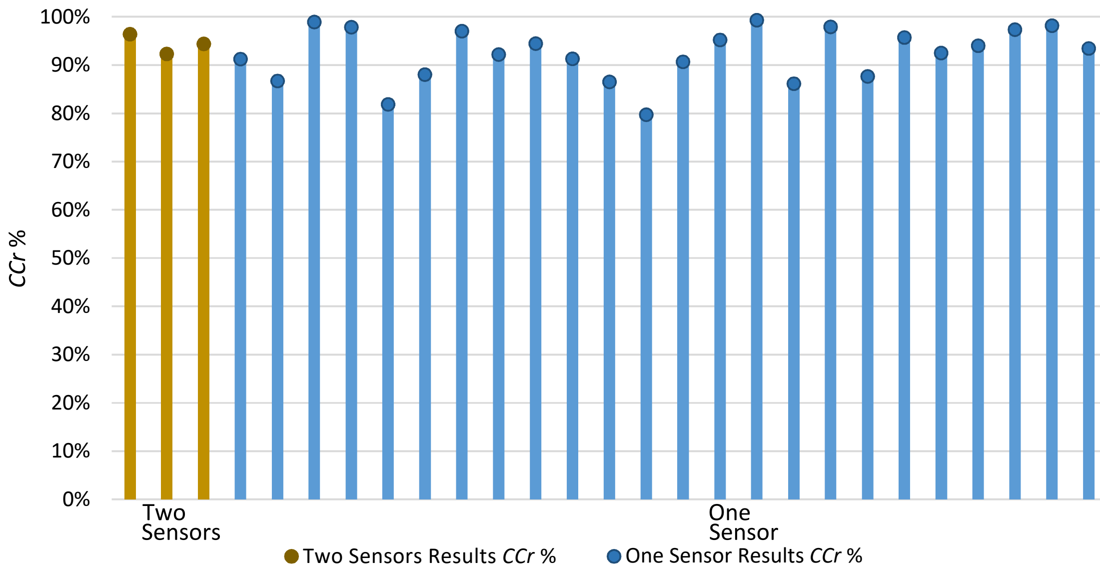

Figure 5.15: The CCr of counting results by two sensors and one sensor.

2. Denoising Methods: Sparse Sensing VS Normal Filter

In order to show the sparse sensing denoising performance, a normal standard low-pass filter has been designed and applied to the seed counting system to compare with the sparse sensing method. Through simulation and study the real ESG signal, the seed information signal is distributed within $600Hz$. So, a simple standard 6_{th} order Butterworth low-pass filter with a cut-off frequency $600Hz$ was used for the comparison. Figure 5.16 shows the accuracy rate results for the multiple classifier approach with applying the sparse sensing denoising method and the normal filter.

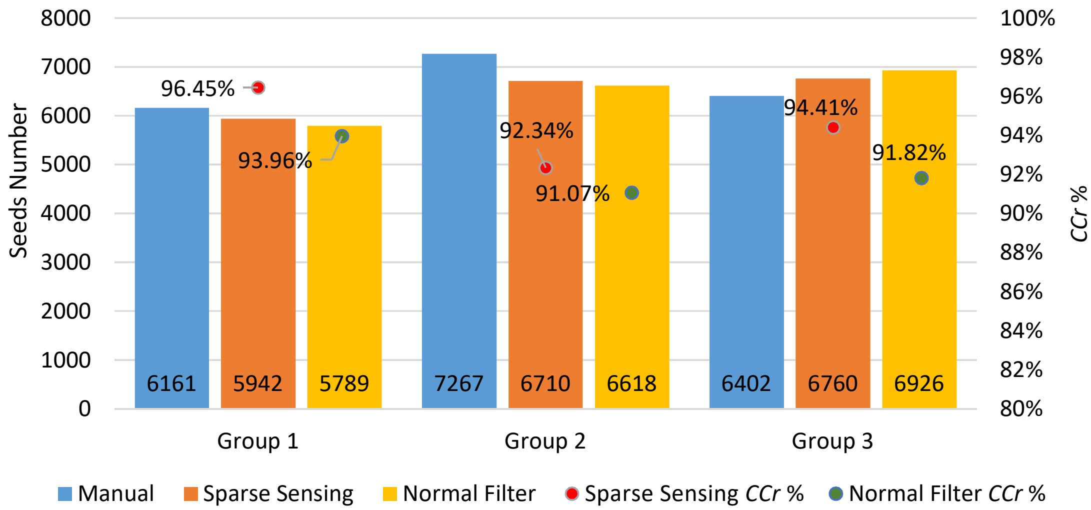

Figure 5.16: Wheat seed counting results by different denoising method. Blue bar shows the manual counting results, orange bar shows the counting results from the sparse sensing denoising, and yellow bar shows the the counting results from the normal filter denoising.

Compared with the counting results from the normal filter denoising methods, although the difference was tiny, the sparse sensing results had a 1% to 3% increase in the three experimental wheat groups.

3. Different Seed Type: Canola

In order to prove that the seed counting system has applicability for other kinds seeds. Three canola seed groups have been also applied to the system to confirm its applicability. Because of the different property of experimental seed, the experiment condition of three canola seed groups was set differently. The three groups respectively contain 7921, 8373, and 9053 canola seed. The gain was set to 550 to obtain a good resolution ESG signal. The air speed was controlled 14 m/s with the seed roller of 24 rpm. Table 5.4 shows the reference set value for each canola testing group. Figure 5.17 shows the canola seed multiple classifier approach counting results.

Table 5.4: MUP Feature Reference Set for Canola Testing Group

Training Group		Width Reference	Energy Reference	Testing Group
Group2	Group3	16.7672	8.5257	Group1
Group3	Group1	16.7311	8.3182	Group2
Group1	Group2	16.7965	8.1650	Group3

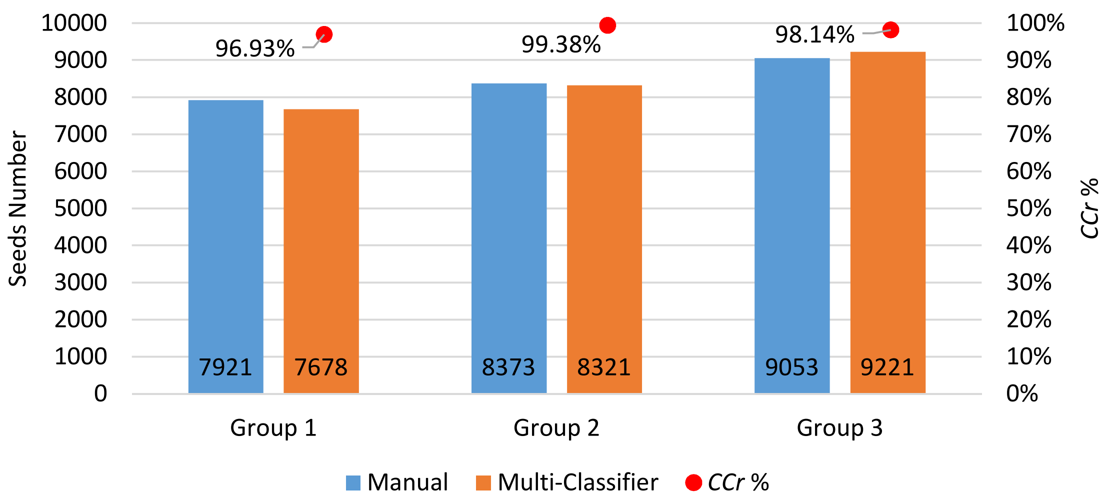

Figure 5.17: Counting results by the multiple classifier approach for the three canola groups. Blue bar shows the manual counting results, and orange bar shows the multi-classifier couting results.

From the canola seed counting results, all of the three testing groups, the accuracy rate is above 96%, which is higher than the wheat seed CCr. The means of the canola CCr from the three testing groups is 98.15% with the SD of 1.22%. Obviously, this canola seed experiment using this pattern recognition counting seed method can prove this counting system has universal applicability for any other kinds seed.

4. Inappropriate Gain: Overflowed ESG Signal

During data collection for the ESG signal experiment, the initial preparation work was to set a suitable gain for the detected signal. The gain could not be too small in case the ESG signal could not offer enough seed information or a good resolution signal, while the gain could not be too large in case the signal overflowed the DAQ sampling range resulting in a wrong feature classification decision. In order to analyze the effect of an inappropriate gain, a comparison group with a much higher gain of 200 was designed for the three wheat seed groups. Figure 5.18 (a) shows the ESG signal with a standard gain, and the overflow signal is shown as Figure 5.18 (b),

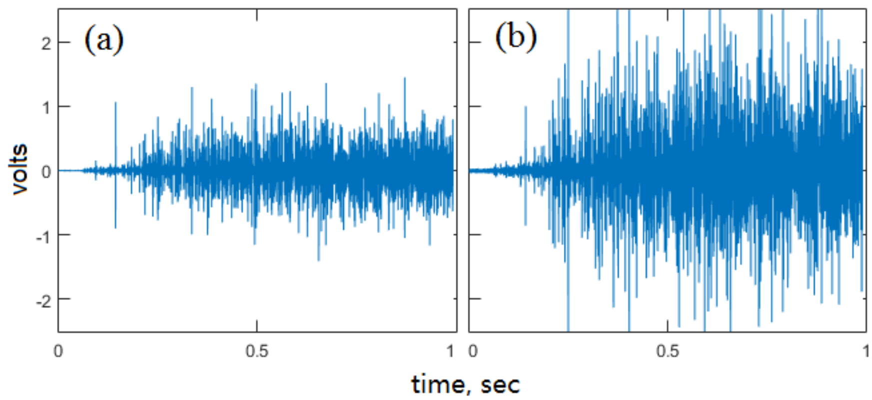

Figure 5.18: The standard ESG signal (a) and the overflowed signal (b).

Figure 5.19 shows the counting results of the overflow wheat seed ESG signals and the counting method is totally the same as the standard signal. The blue bar in the figure shows the manual counting results, and the orange bar shows the counting system results. From the results, the accuracy CCr of the counting result is too low to accept, which is indicated by the red mark in the figure.

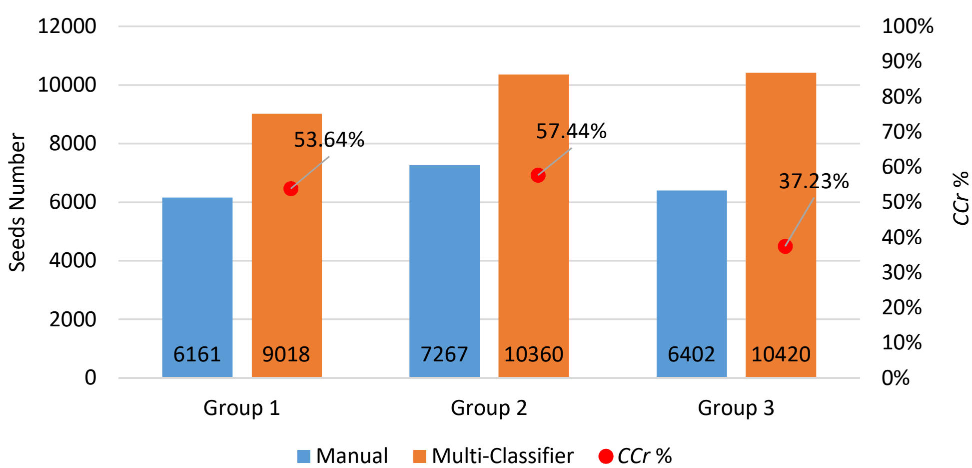

Figure 5.19: Counting results by the multiple classifier approach for the three canola groups. Blue bar shows the manual counting results, and orange bar shows the counting system results.

The overflow signal caused relatively low accuracy results based on the *Cluster Width* and *Energy Comparison* classifier approach. Seed energy was sensitive to the applied gain, resulting in the results of *Energy Comparison* classifier were abnormal, so the overflowed ESG signal needs to be analyzed from the four basic features. In Figure 5.20, the four individual feature classifier decision results have been shown and compared with manual results. Obviously, the number counting results from the energy comparison classifier were much higher than other three classifier results. Table 5.5 shows the accuracy CCr and the error rate of the three overflow signals counting results.

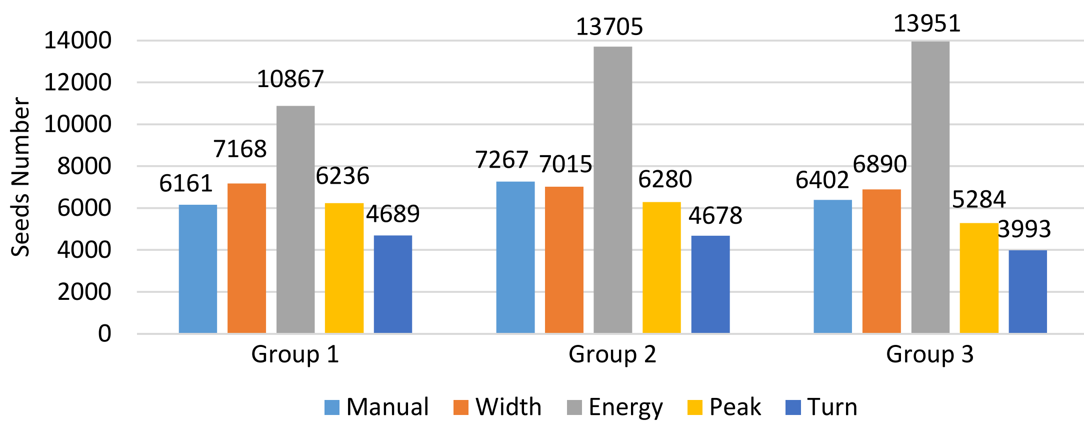

Figure 5.20: Wheat seed counting results for the overflow ESG signal.

Table 5.5: The CCr and Error Rate for the Overflow ESG Signal Counting Results

	Group 1 (6161 Seeds)			Group 2 (7267 Seeds)			Group 3 (6402 Seeds)		
	Number	*CCr*	Error Rate	NUM	*CCr*	Error Rate	NUM	*CCr*	Error Rate
Width	7168	83.66%	16.34%	7015	96.53%	3.47%	6890	92.38%	7.62%
Energy	10867	23.62%	76.38%	13705	11.41%	88.59%	13951	-17.91%	117.91%
Peak	6236	98.79%	1.21%	6280	86.41%	13.59%	5284	82.53%	17.47%
Turn	4689	76.11%	23.89%	4678	64.37%	35.63%	3993	62.36%	37.64%

From the four features individual counting results, the feature of *Energy Comparison*, which was applied in the standard ESG signal, has a worse performance than the overflowed ESG signal due to the incomplete MUP waveform. By comparison, the features of *Cluster*

Width and *Peak and Valley Detection* have an acceptable counting results, which has an average CCr of 90.85% for the *Cluster Width* and 89.24% for the *Peak and Valley Detection*. Thus, in the process of the multiple classification task, the feature selection should be *Cluster Width* and *Peak and Valley Detection* for the overflowed signals.

In Figure 5.21, it shows the updated multiple classifier approach counting results for the wheat overflow signals. According to the counting results, the average of the accuracy CCr is 92.59% with the SD of 2.16%. Compared with the standard ESG signal counting results, the accuracy rate is about 1.5% lower. Therefore, if the gain is inappropriately set in the initial preparation work, it does not means that the overflow ESG signal is not useful. If a suitable feature classification decision were chosen in the multiple classifier stage, the counting results still could have an accuracy above 90%, even though the counting result is not as good as the standard ESG signal.

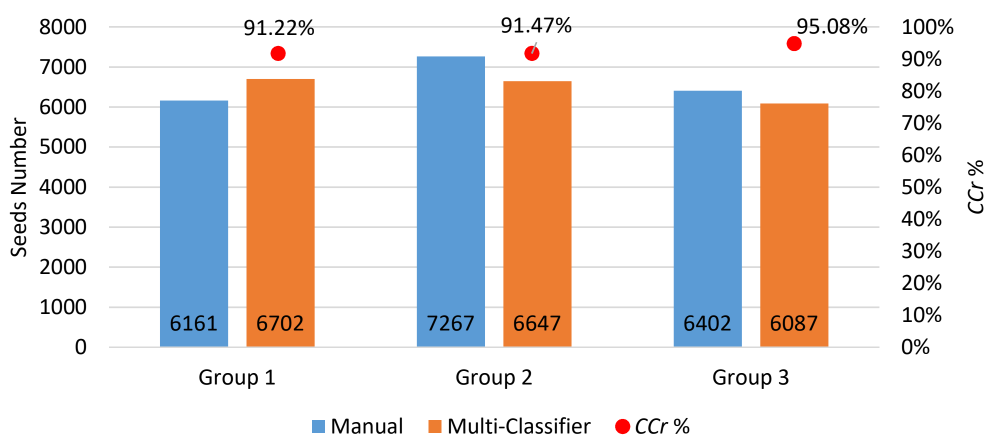

Figure 5.21: Counting results by the updated multiple classifier approach for the three overflow wheat groups. Blue bar shows the manual counting results, and orange bar shows the counting system results for the overflowed signals.

5.3 Conclusion

In the proposed method of counting flowing seed in the pipeline based on pattern recognition, signal denoising with the compressive sensing method was applied to the collected ESG signal. Sparse and structured signal decomposition was based on time-frequency adjacency in Gabor representations, and the persistent empirical Wiener operator was used in the compressive sensing to be the thresholding operator. After the signal denoising, signal segmentation can divide a denoised ESG signal into several seed cluster IDIs for MUPs. Through research the seed cluster MUPs, four features of the ESG signal, *Cluster Width, Peak and Valley Detection, Number of Turns,* and *Energy Comparison*, were developed and applied into the feature selection stage. Then, in the multiple classification, each feature classifier made its own decision for the individual cluster MUP waveform. From the testing groups, the *Cluster Width* and *Energy Comparison* feature reference sets of the cluster MUP waveforms can be obtained, and then were used into the classification task for the testing groups. Also the features that have acceptable counting results were chosen to be the selected features in the ensemble members selection module. The aggregation module based on the average rule calculated the classification decision from the selected features for each cluster MUP waveform.

From the three wheat seed test groups, the seed counting results have an average accuracy rate of 94.40% with the SD of 2.05%. Also, the three canola test groups were applied the same seed counting method, and the average accuracy rate of the canola seed groups is 98.15% with a 1.22% SD. It is shown that the counting system has the applicability for some other kinds of seeds. Also, if the ESG signal is overflowed, some other features need to be applied in the classification task to make an appropriate decision result, but it is better that the counting system have a suitable gain set to collect the ESG signal. To this end, the performance behaviors of the counting system were examined for various scenarios with respect to different seed types and inappropriate gain in the collecting process.

6. Conclusion

In this chapter, the summary of the research steps are discussed first. Then, the potential future developments of the project are addressed.

6.1 Summary of the Research

Pneumatic transport is widely used in the modern agriculture process. Velocity measurement and counting for the flowing seed in the seed drill pipeline have been attracting the interest of many researchers for a long time, which can help researchers to analyze the seed data and improve the value of each seed. The objectives set for this research were to use the electrostatic sensor to analyze the moving seed velocity and the number of the seeds in a pneumatic conveying system.

By using the existing lab-scale air seeder system and electrostatic sensors in the Air Handing Lab at the University of Saskatchewan, the seed velocity measurement experiments and seed counting experiments were taken.

For measuring seed velocity, a two-electrode electrostatic sensor was used to detect the flowing seed signal in a seed drill system. The electrostatic sensor was adjusted to adapt the primary pipeline of the pneumatic conveying system with an interior diameter of 57.3 mm. There were 23 testing experiments under the different settings of the air velocity and seed mass flow rate. The air velocity was set to 12 m/s, 15 m/s, 20 m/s, 25 m/s, and 30 m/s, and the range of the seed mass flow rate was set from 1 kg/min to 6 kg/min. Each electrode in the electrostatic sensor detected a ESG signal. After acquiring the seed ESG signals, the two cross-correlation methods in MatLab were applied for velocity analysis. One was the fixed time window cross-correlation method, and the other was the threshold detection cross correlation method. In the fixed time window method, the window length is decided by the required velocity update time depending on the user's requirements. While, in the threshold detection method, a threshold value was set to activate the velocity measurement with a window length of full seed waveform at least. Reference data based on the PTV technique was required to test the accuracy of velocity measurement results based on the electrostatic sensor technique.

In the 23 testing groups, it was noted that some seeds were settling and clumping together and then block the transmission of seeds in four groups which have a relatively low air velocity and a relatively high mass flow rate. Besides the four clumping seed groups, the velocity measurement results have an agreement rate of above 93.80% with the PTV results. Also, the testing results show that a good view of the behavior of the seed in the pneumatic conveying system is almost the same as the reference group, which means that the two-electrode electrostatic sensor has reliability in the industrial environment.

In this research study, a proposed method was also proposed for seed counting included compressive sensing denoising and multi-classification pattern recognition. The electrostatic sensor was adjusted to adapt the secondary pipeline with an interior diameter of 25.4 mm. After acquiring the ESG signal, the first task was removing the noise in the original ESG signal. Because ESG signal is sparse ,which is the prerequisite of compressive sensing, the denoising method is based on the compressive sensing. The stage of the compressive sensing is in the time-frequency distribution by the Gabor Transform, and the basic conception of persistent time-frequency compressive sensing is to consider thresholding operators. Then, the signal segmentation stage helped to extract relevant seed information from analysis of individual MUP waveform and MU patterns. Next, the feature extraction and selection picked up the useful information about the seed number in the ESG signal. From training groups, the feature reference set were obtained and applied into each feature classifier for testing groups. Based on the average rule, the final classifier decision was made for the testing groups.

There were three wheat seed groups and three canola seed groups for the seed counting experiments. Leave-one-out cross-validation was used in the signal analysis. Two of the three groups were treated as the training groups and the third was the testing group. From two testing groups, the reference set of each feature was obtained and applied into testing groups. The pattern recognition counting results were compared with the manual counting results. By this seed counting approach, the average accuracy of the counting results reached to 94.40% with the SD of 2.05% in wheat testing seed and 98.15% with a 1.22% SD in canola testing seed.

6.2 Future Directions

Throughout, this thesis proposed two important characters for the flowing seed in the pneumatic conveying system, respectively in Chapter 2 and 3. There still are some potential future contributions for a natural next extension to this thesis.

In this thesis, only a two-electrode electrostatic sensor was used on the conveying pipeline. In the future, multiple sensors could be added along the pipeline to analyze the velocity distribution for the flowing seed along the pipeline, which can help operators to understand the relation between the pipeline length and seed movement velocity in the pneumatic conveying system and find the minimum velocity required for successful transportation of the seed.

Also for the seed count estimate, more sensor nodes can help analyze the seed information to improve the accuracy rates of the measurement results. And as mentioned in Chapter 4, there were seed-clumping phenomena happening in some testing groups. In the future, the minimum requirement for the seed conveying under the different settings also could be one possible direction.

Moreover, a wireless transmission system can be designed for the ESG signal acquisition. ESG signal transmitted by wired network limits the applications for the device. If the signal data is transmitted by wireless, the electrostatic sensor will be more flexibly installed on the pipeline, which can improve the applicability of the seed detection system.

Last but not least, it is important to study the influence of environment factors, such as humility and temperature. In the real seed sowing process, a different working environment might change some characters of the seed, which may cause a different result. In the lab, the environment is relatively stable. Therefore, it is worthwhile to investigate the effect of the environment before any practical application.

Appendix A: Velocity Graphs Results for the $0.25 sec$ Fixed Time Window Method

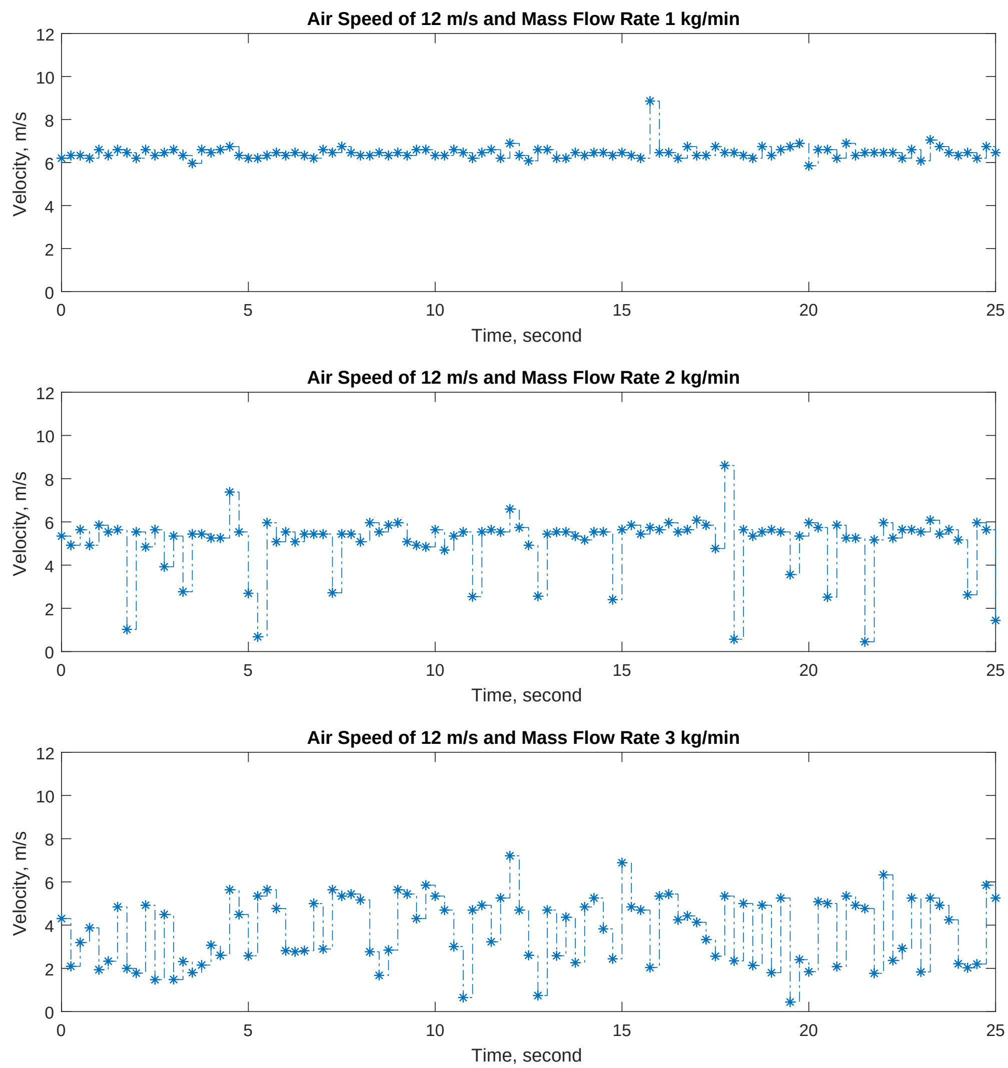

Figure A.1: Velocity measurement graph for the $0.25\, sec$ fixed time window method from the tests at $12\ m/s$ air velocity with a mass feed rate of 1, 2 and 3 kg/min.

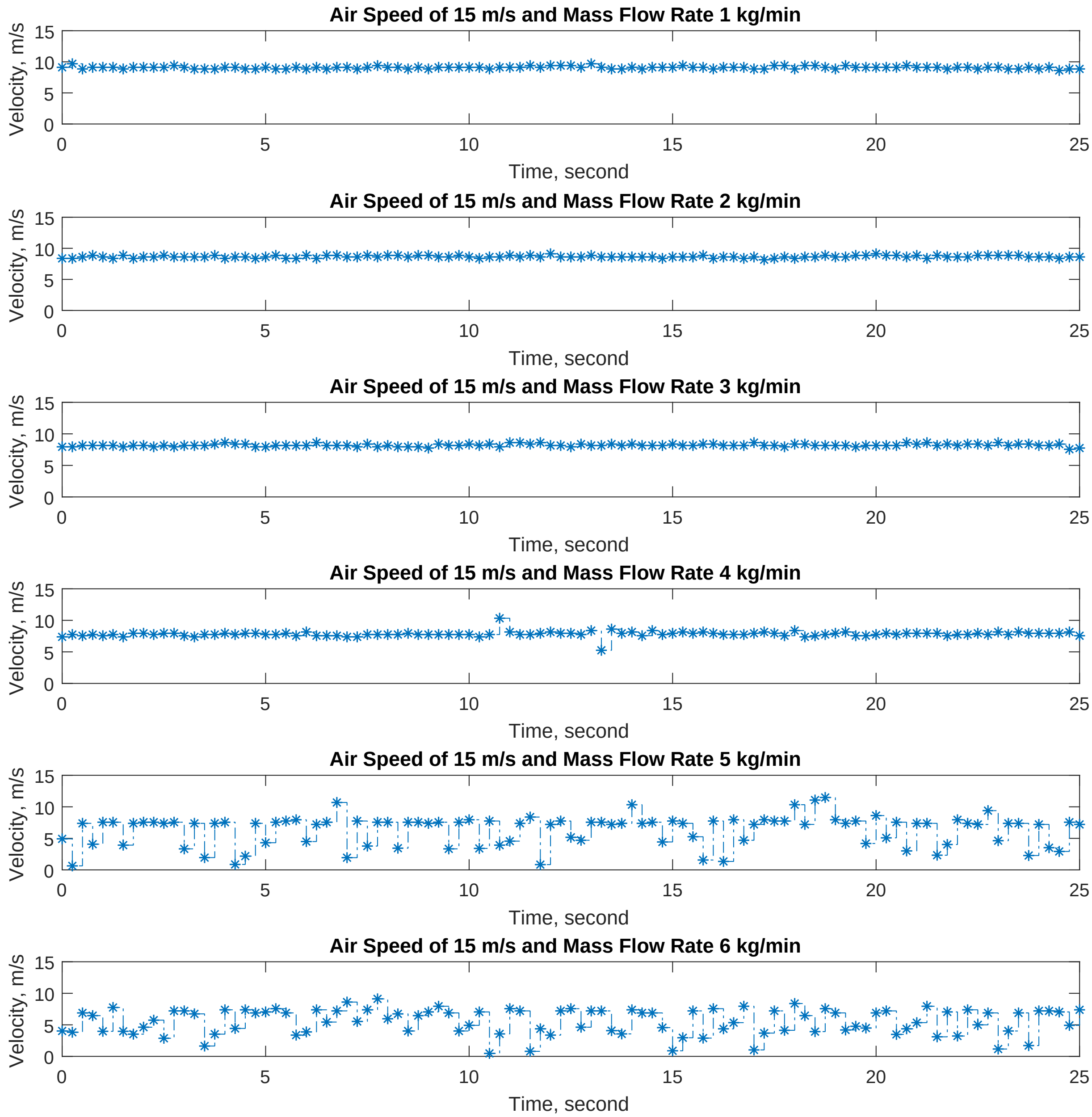

Figure A.2: Velocity measurement graph for the 0.25 sec fixed time window method from the tests at 15 m/s air velocity with a mass feed rate of 1, 2, 3, 4, 5 and 6 kg/min.

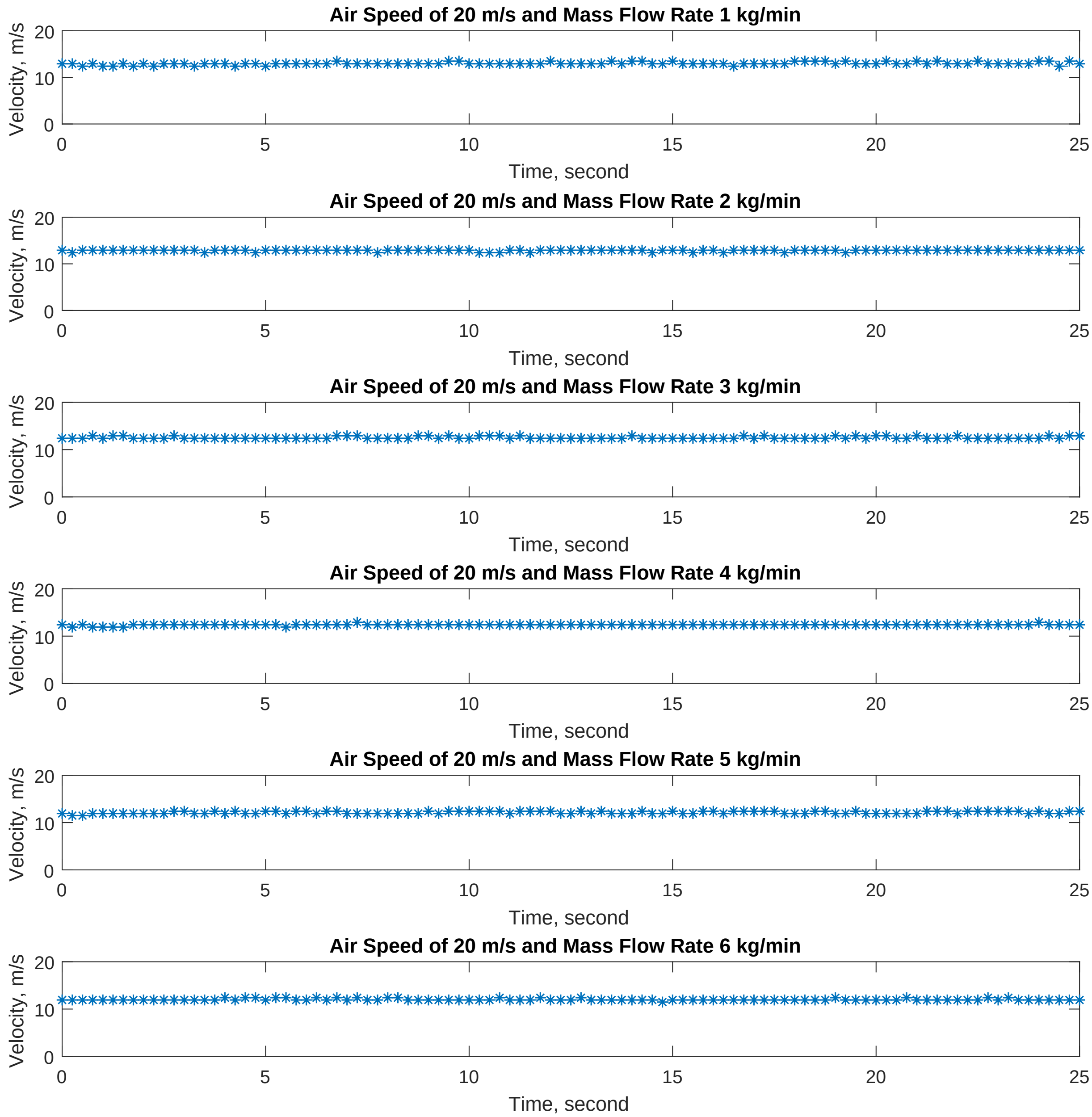

Figure A.3: Velocity measurement graph for the 0.25 sec fixed time window method from the tests at 20 m/s air velocity with a mass feed rate of 1, 2, 3, 4, 5 and 6 kg/min.

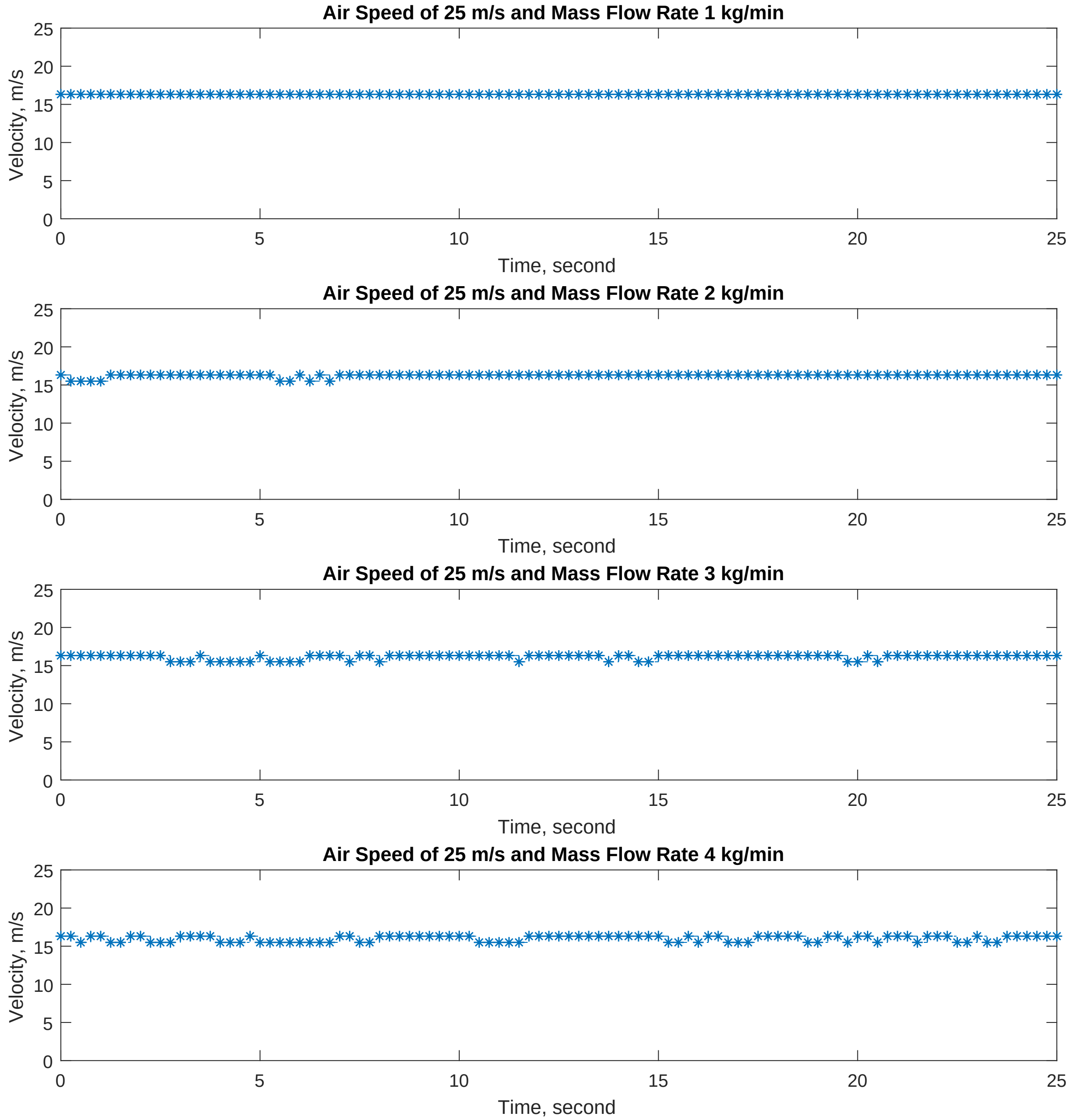

Figure A.4: Velocity measurement graph for the 0.25 sec fixed time window method from the tests at 25 m/s air velocity with a mass feed rate of 3, 4, 5 and 6 kg/min.

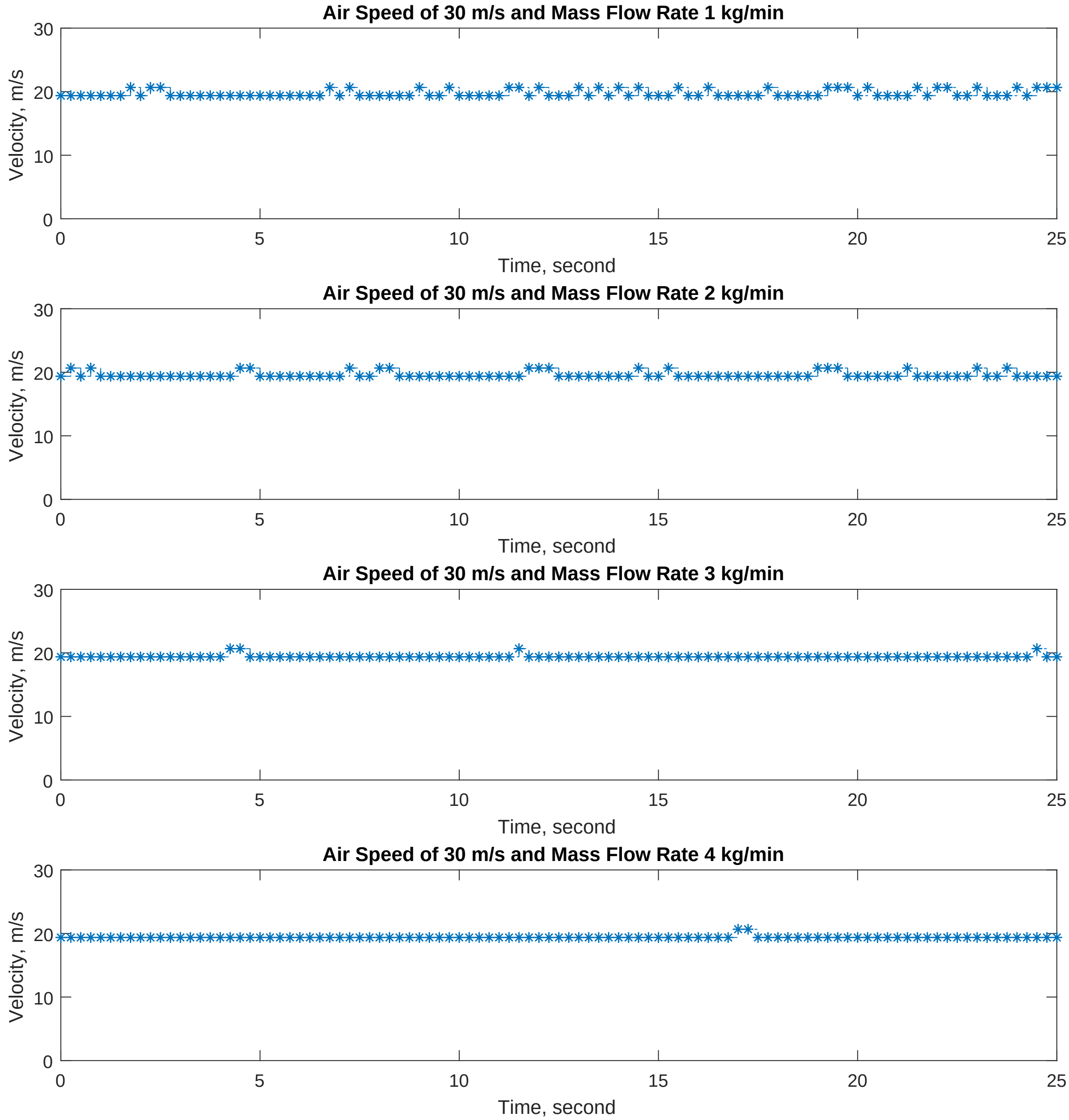

Figure A.5: Velocity measurement graph for the 0.25 sec fixed time window method from the tests at 30 m/s air velocity with a mass feed rate of 3, 4, 5 and 6 kg/min.

Appendix B: Velocity Graphs Results for the $0.5 sec$ Fixed Time Window Method

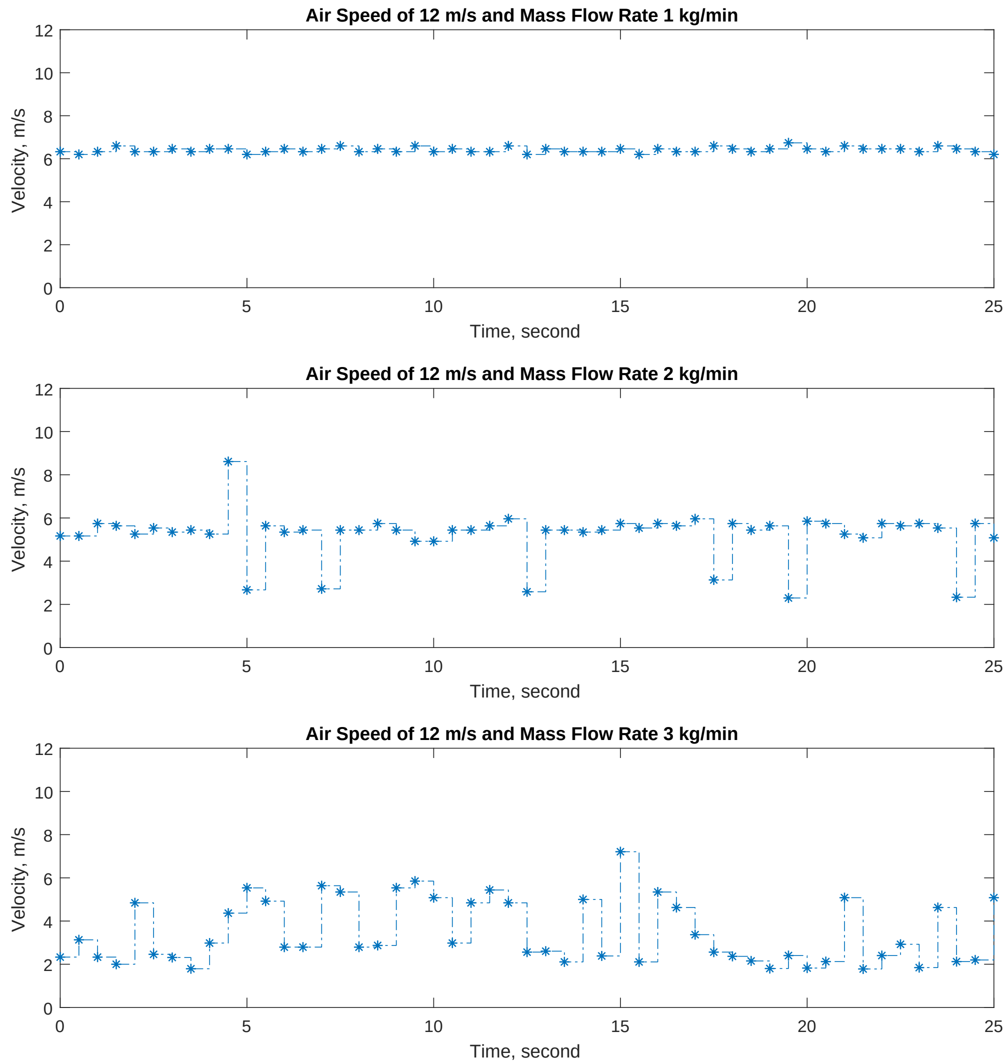

Figure B.1: Velocity measurement graph for the $0.5\,sec$ fixed time window method from the tests at 12 m/s air velocity with a mass feed rate of 1, 2 and 3 kg/min.

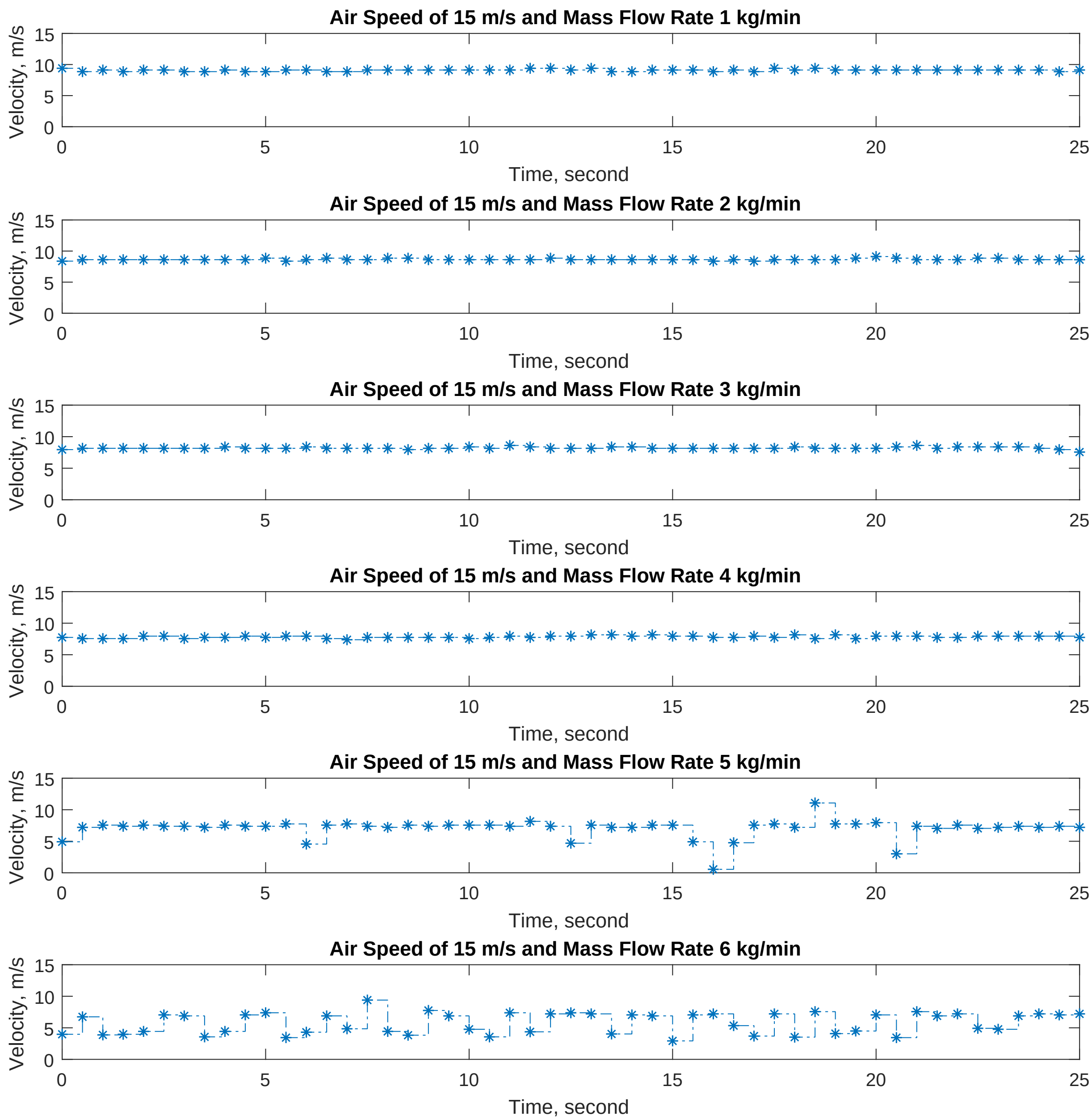

Figure B.2: Velocity measurement graph for the 0.5 sec fixed time window method from the tests at 15 m/s air velocity with a mass feed rate of 1, 2, 3, 4, 5 and 6 kg/min.

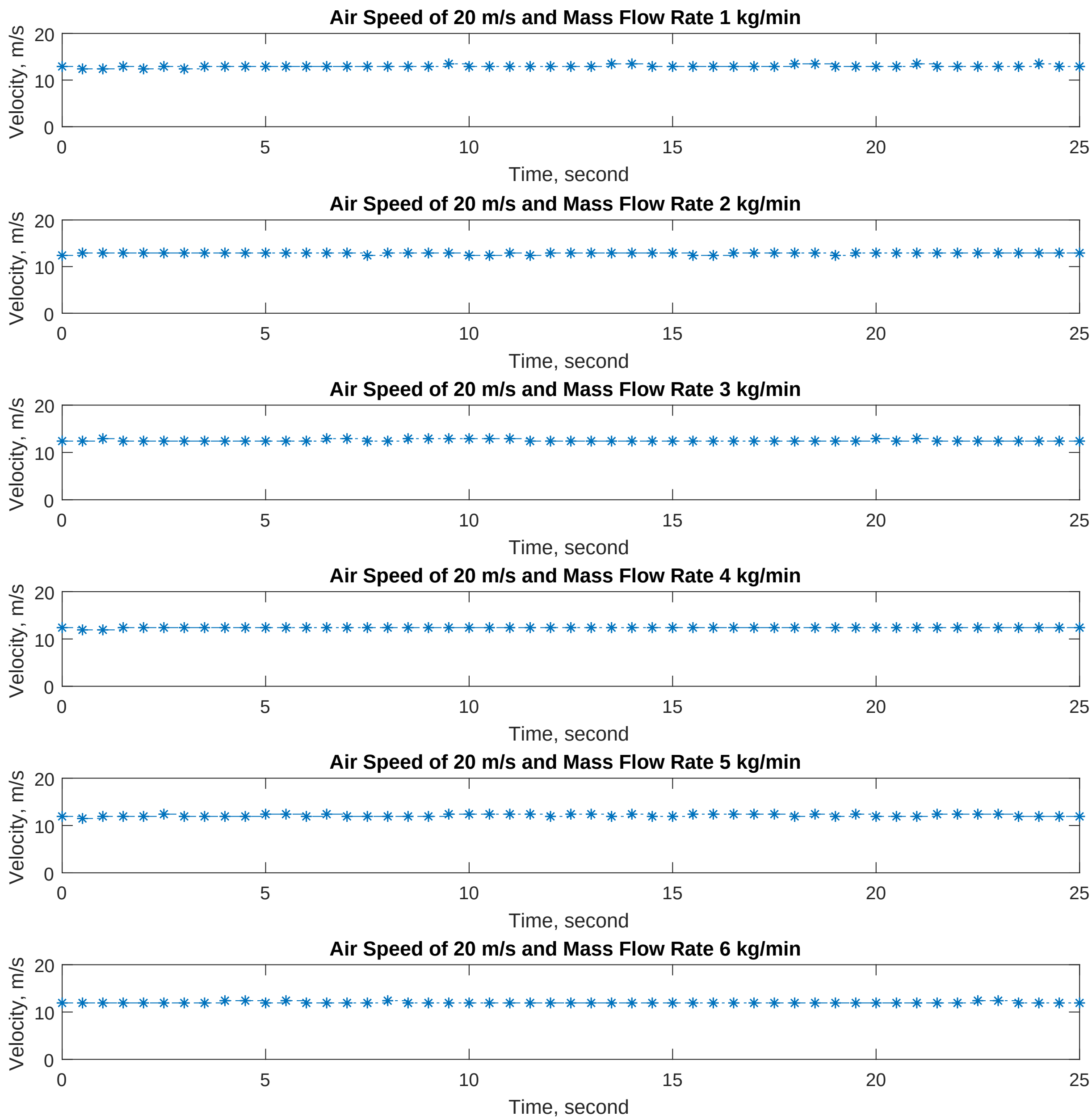

Figure B.3: Velocity measurement graph for the 0.5 sec fixed time window method from the tests at 20 m/s air velocity with a mass feed rate of 1, 2, 3, 4, 5 and 6 kg/min.

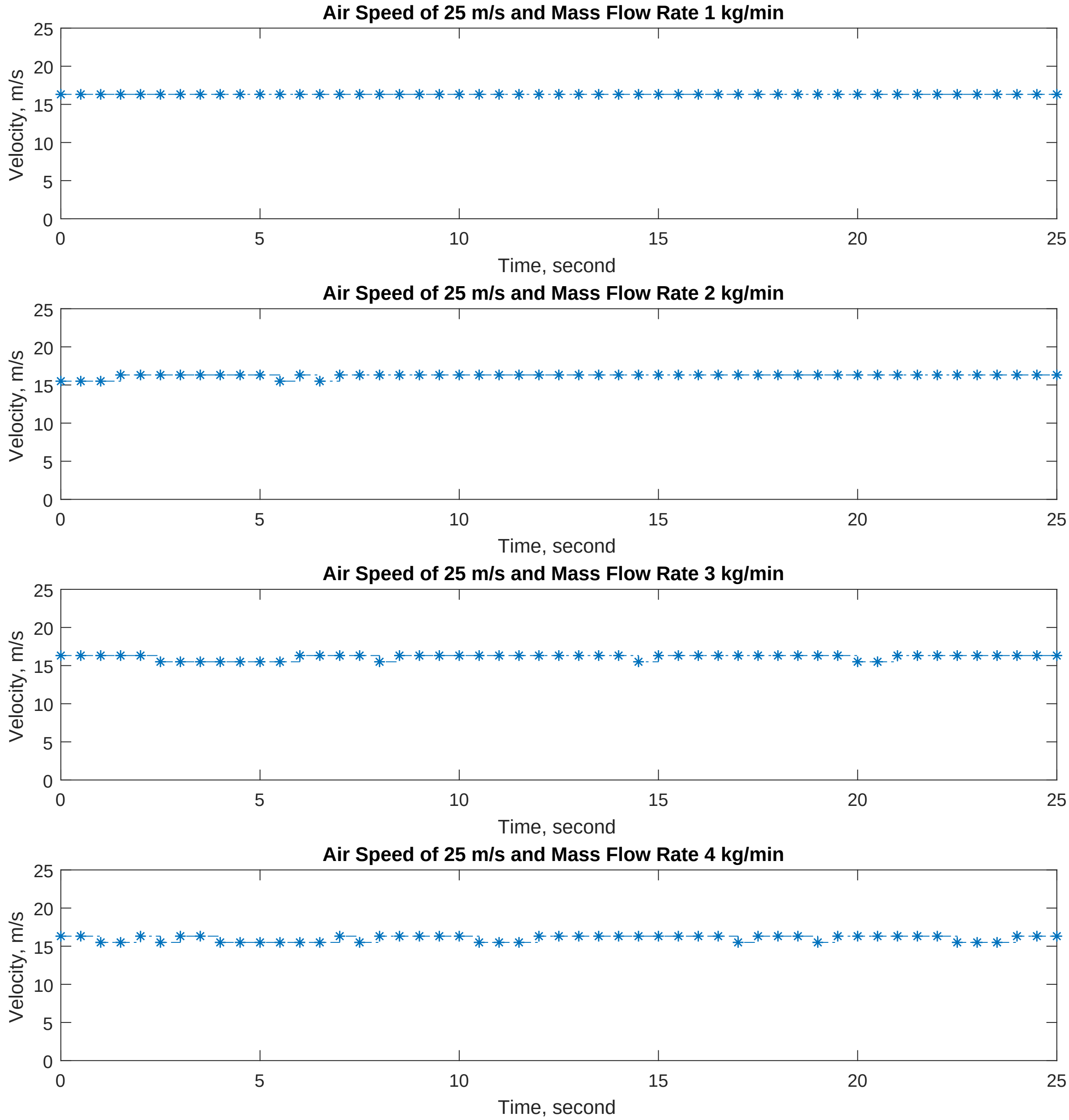

Figure B.4: Velocity measurement graph for the 0.5 sec fixed time window method from the tests at 25 m/s air velocity with a mass feed rate of 3, 4, 5 and 6 kg/min.

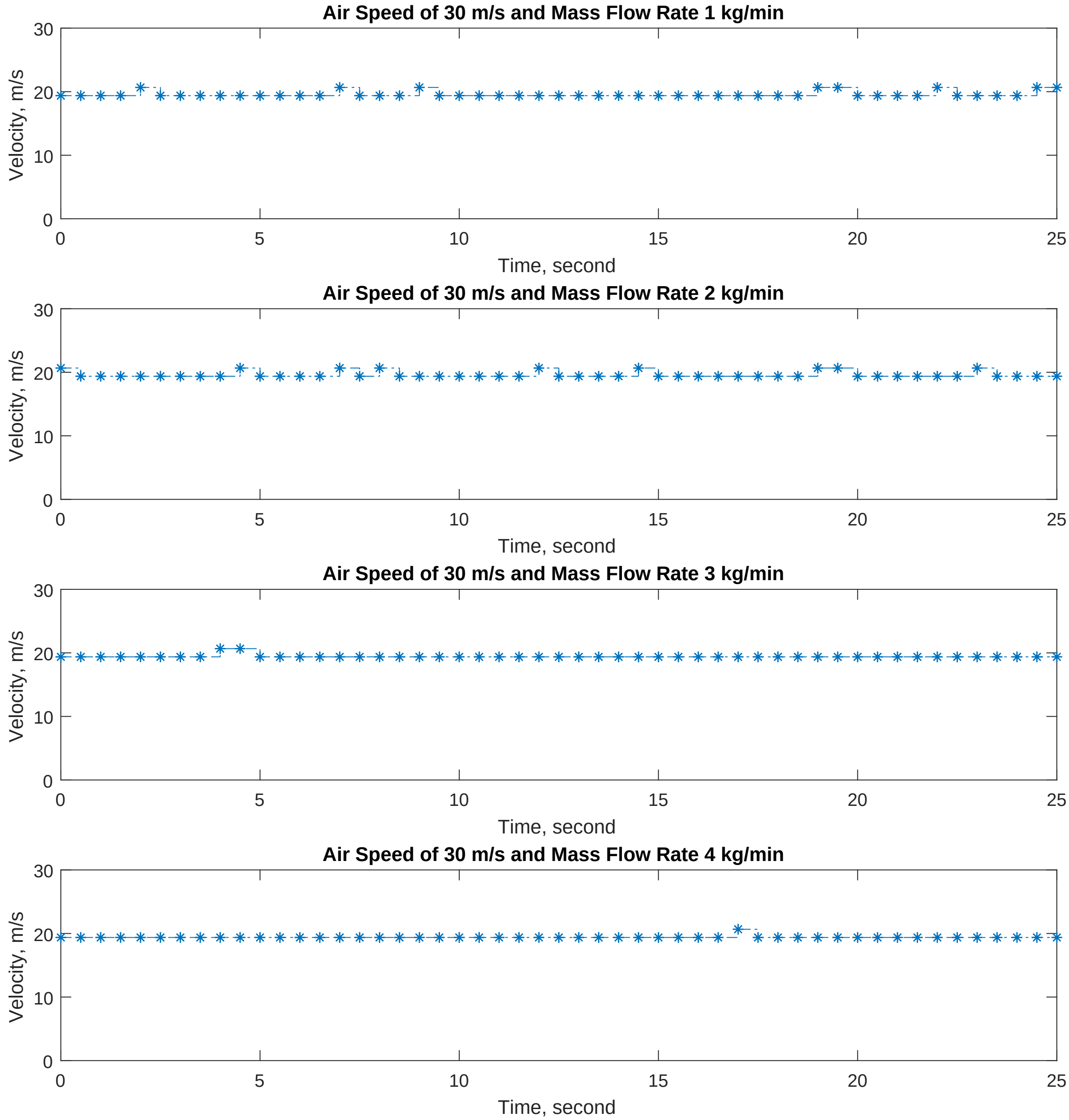

Figure B.5: Velocity measurement graph for the 0.5 sec fixed time window method from the tests at 30 m/s air velocity with a mass feed rate of 3, 4, 5 and 6 kg/min.

Appendix C: Velocity Graphs Results for the Threshold Detection Method

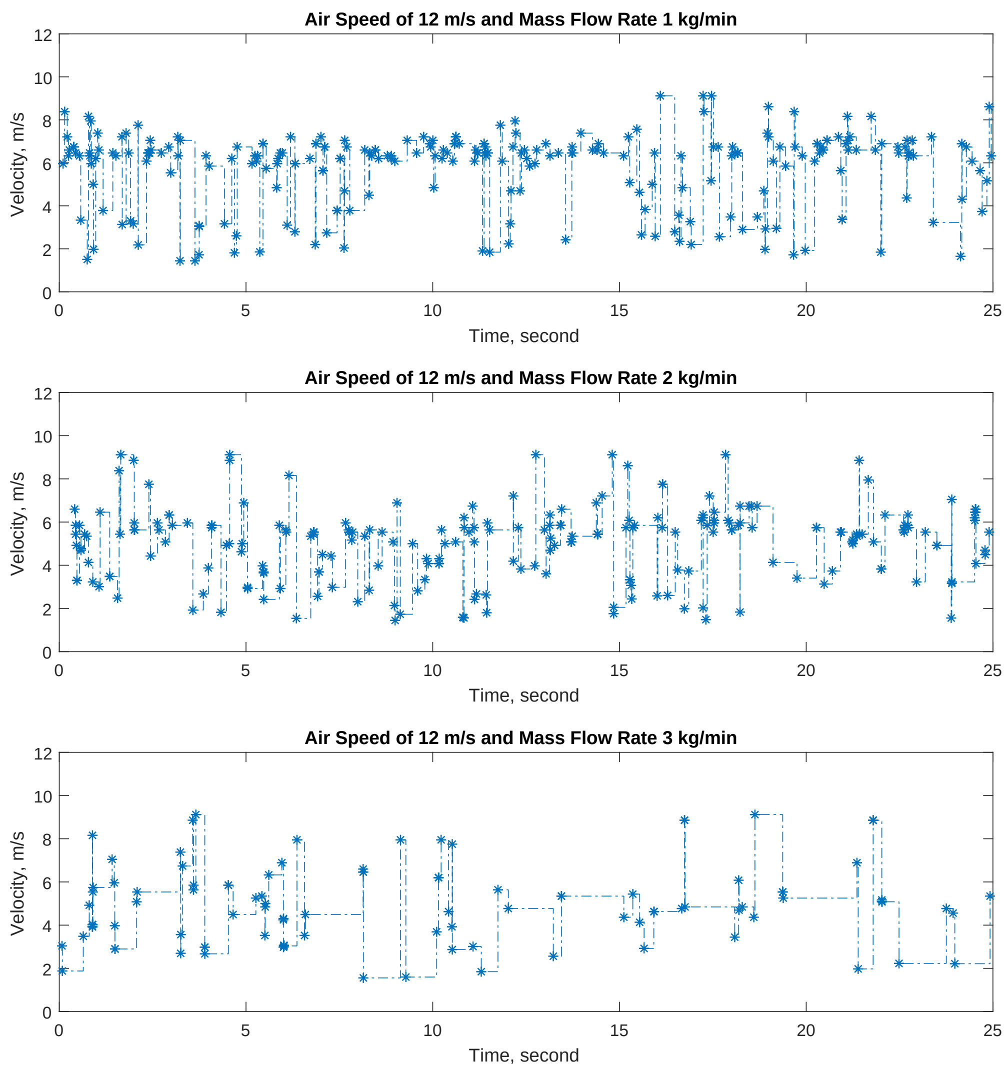

Figure C.1: Velocity measurement graph for the threshold detection method from the tests at 12 m/s air velocity with a mass feed rate of 1, 2 and 3 kg/min.

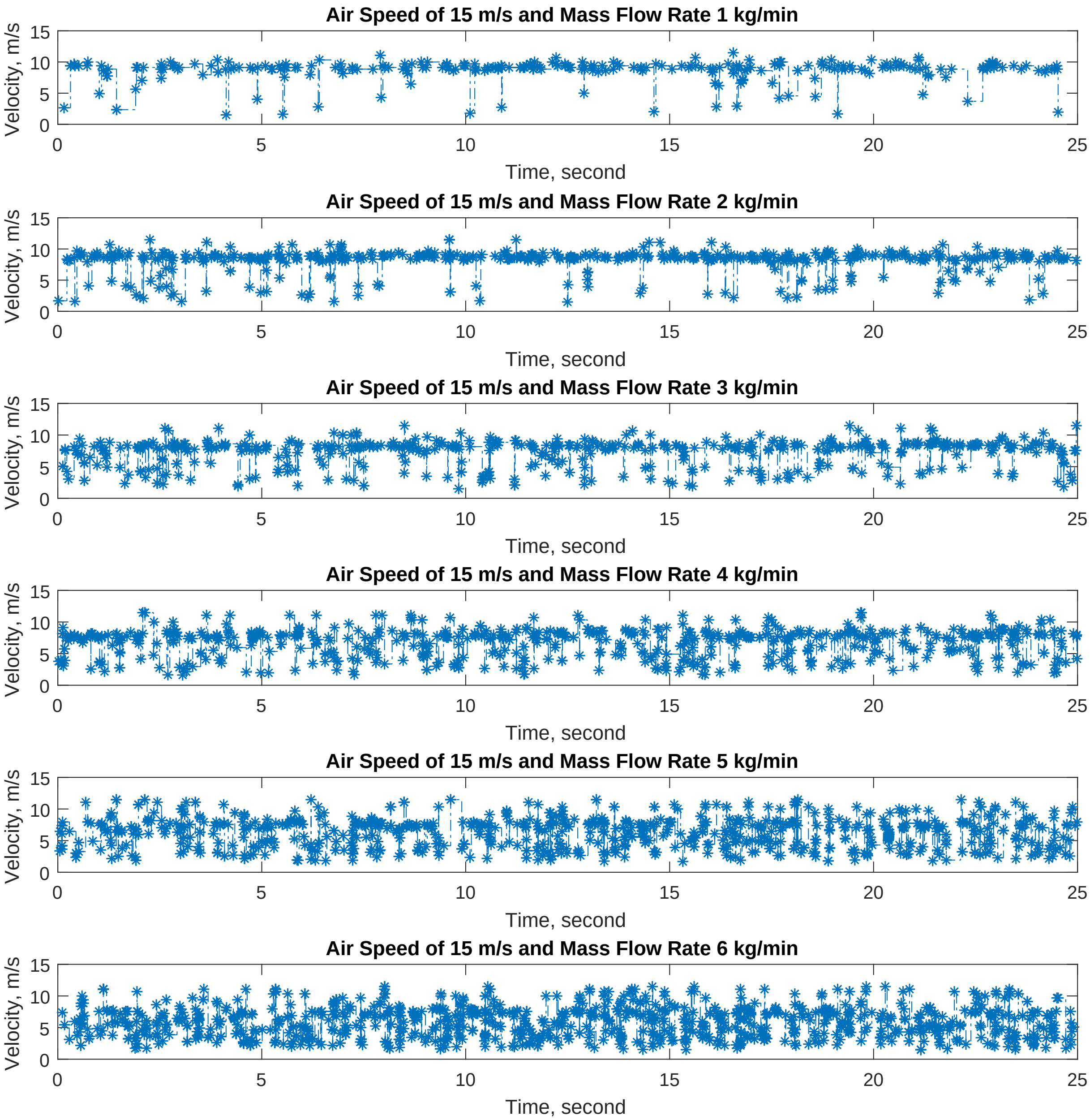

Figure C.2: Velocity measurement graph for the threshold detection method from the tests at 15 m/s air velocity with a mass feed rate of 1, 2, 3, 4, 5 and 6 kg/min.

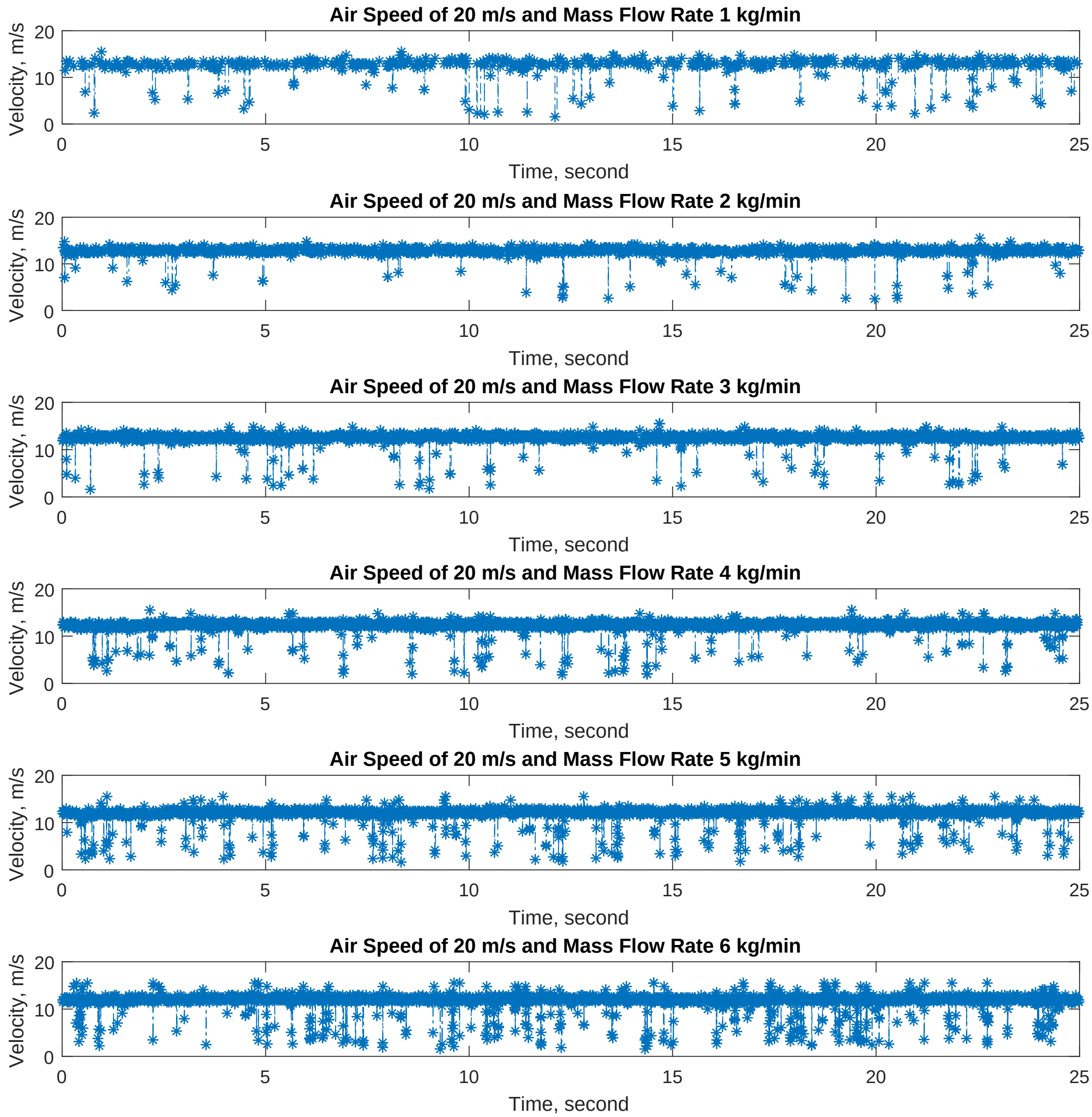

Figure C.3: Velocity measurement graph for the threshold detection method from the tests at 20 m/s air velocity with a mass feed rate of 1, 2, 3, 4, 5 and 6 kg/min.

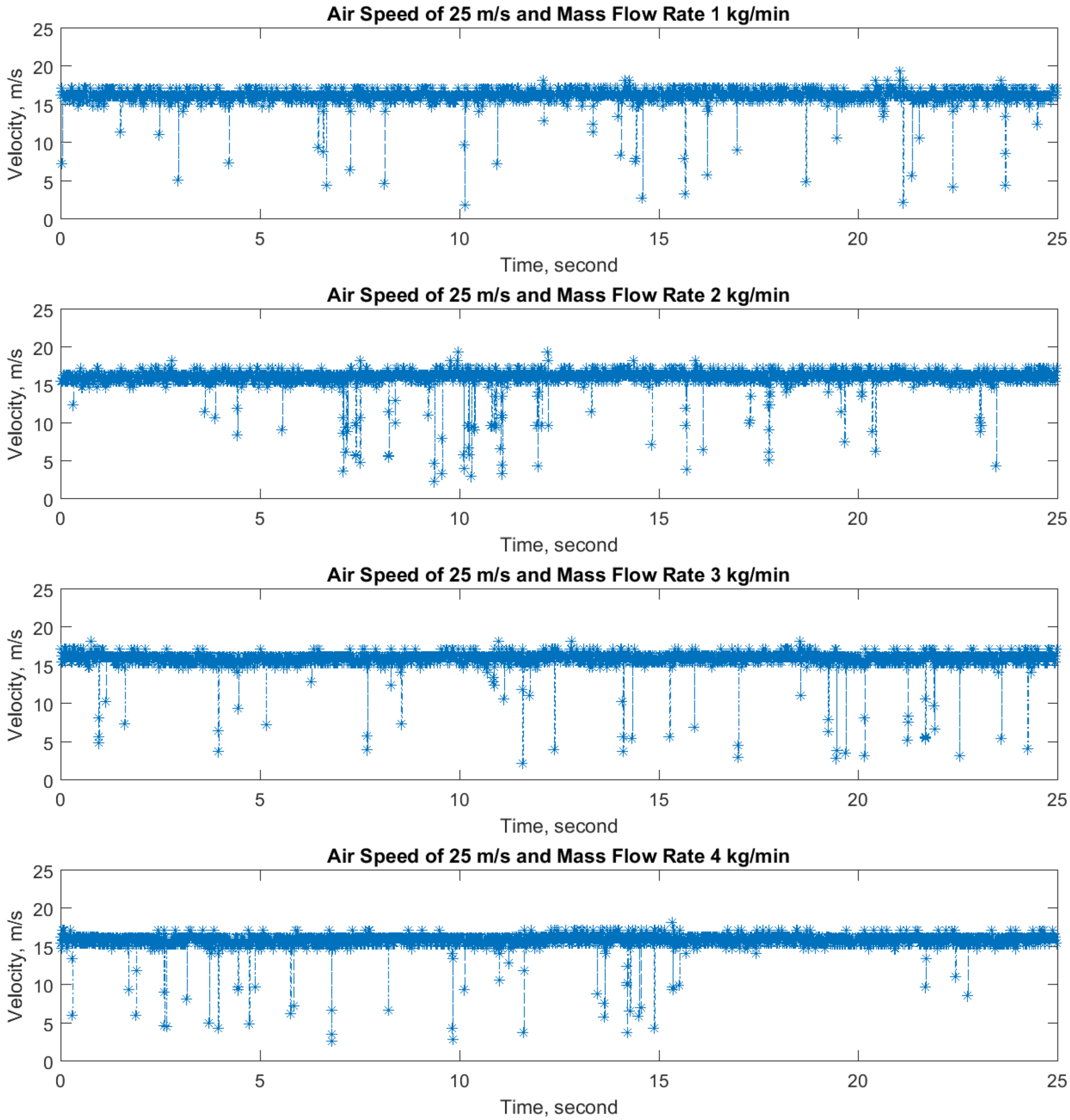

Figure C.4: Velocity measurement graph for the threshold detection method from the tests at 25 m/s air velocity with a mass feed rate of 3, 4, 5 and 6 kg/min.

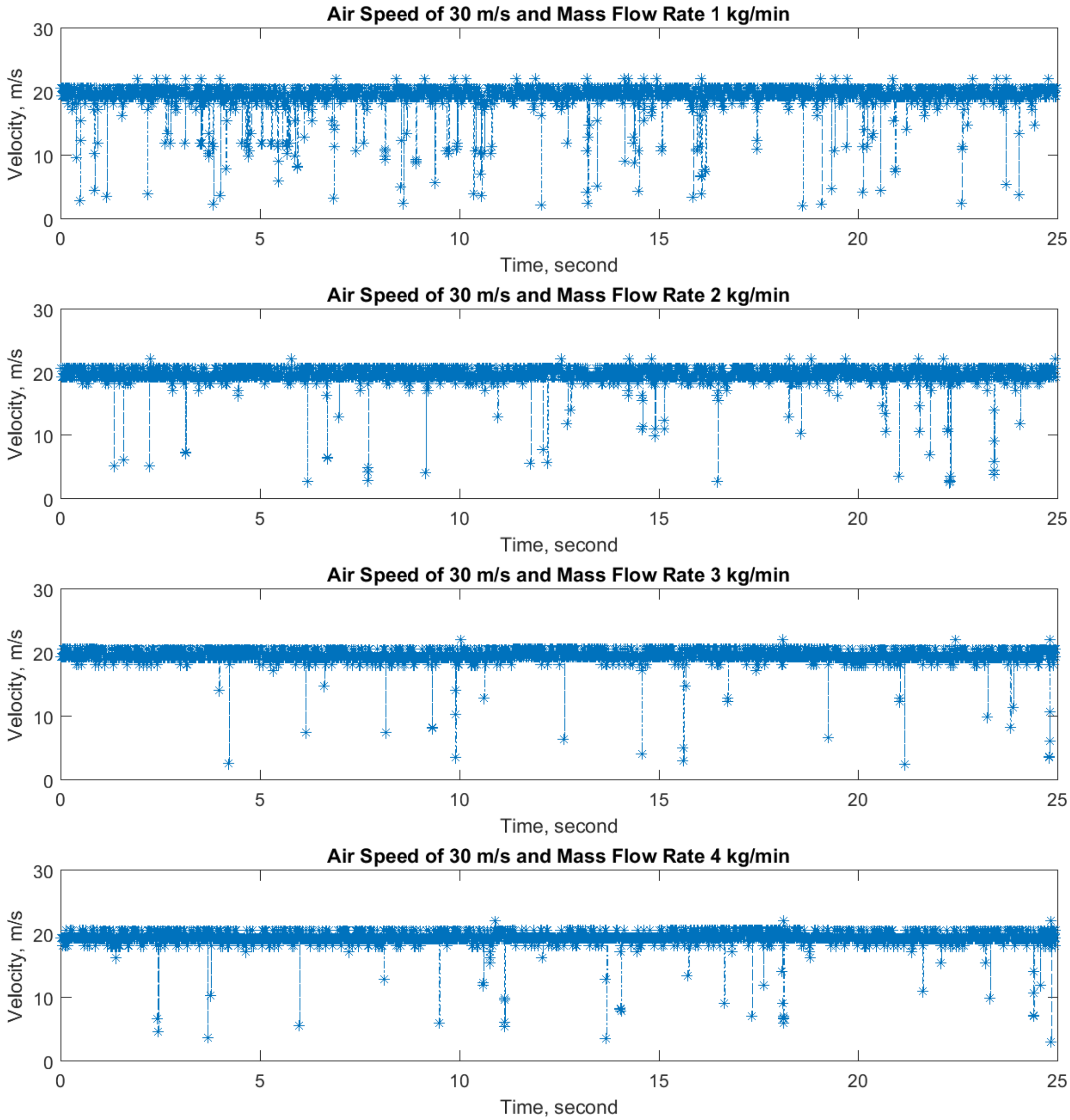

Figure C.5: Velocity measurement graph for the threshold detection method from the tests at 30 m/s air velocity with a mass feed rate of 3, 4, 5 and 6 kg/min.

Appendix D: Seeds ESG Signal Acquisition Program

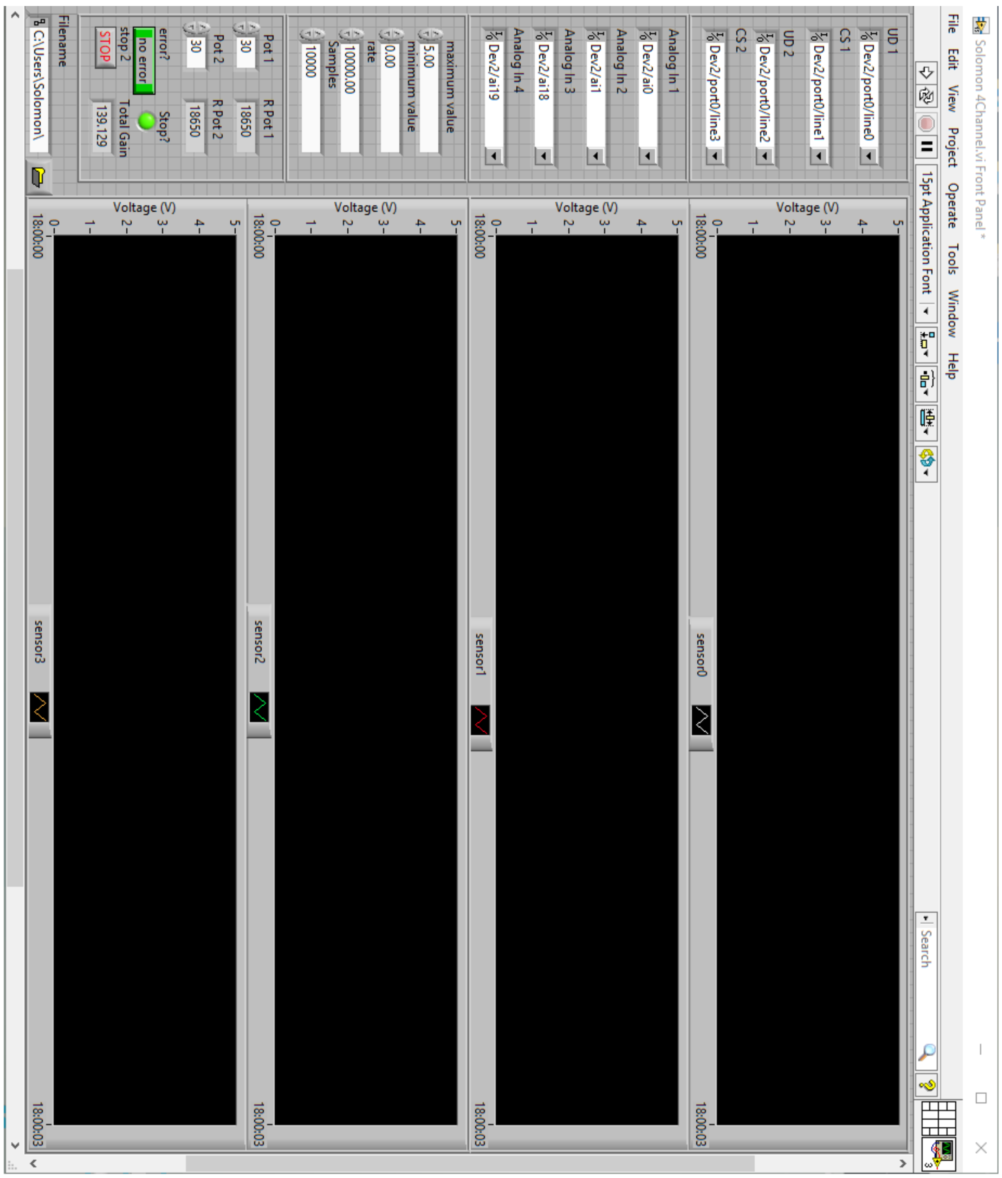

Figure D.1: The LabView Signal Acquisition Program Front Panel for Two Electrostatic Sensors.

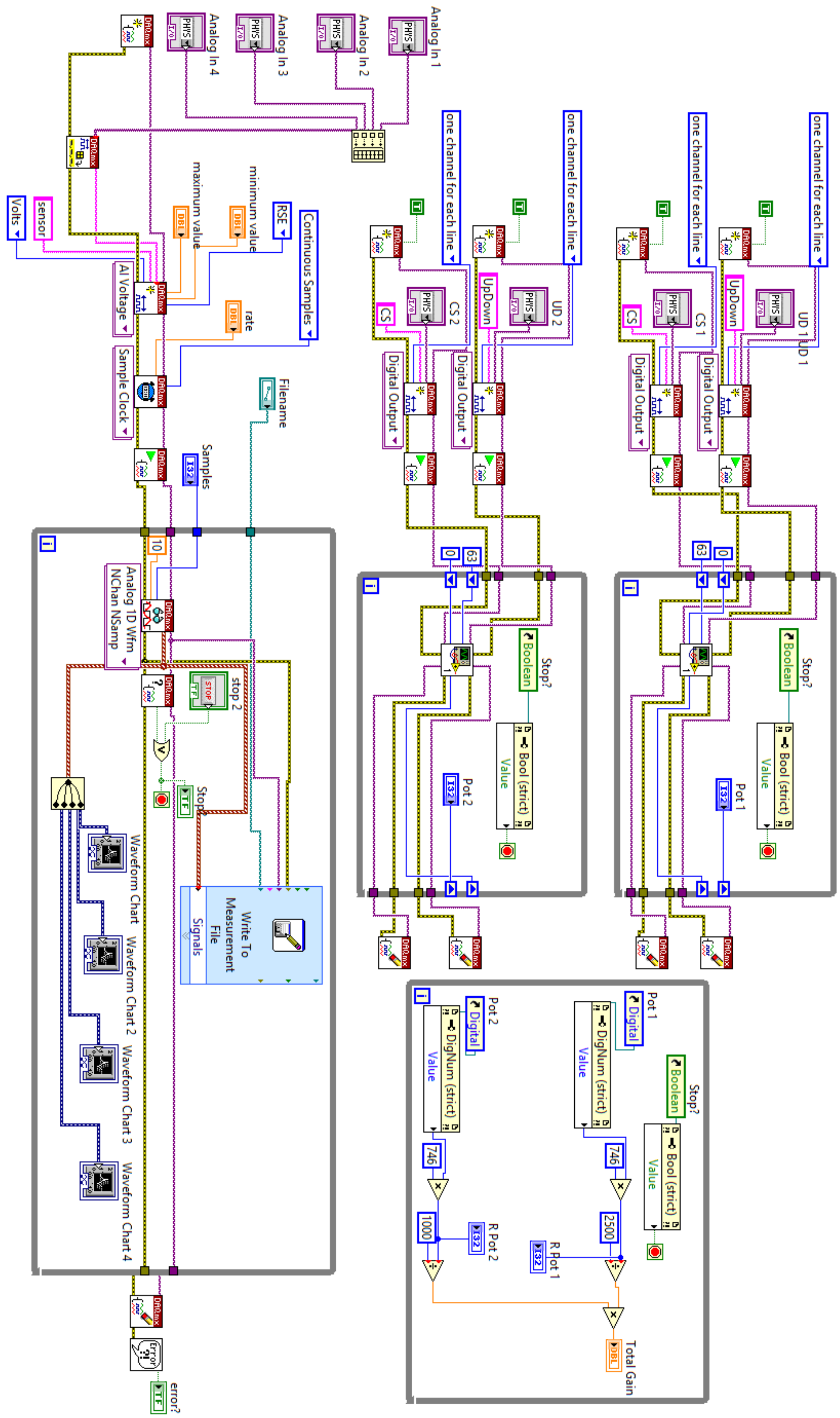

Figure D.2: The LabView Signal Acquisition Program Block Diagram for Two Electrostatic Sensors.

References

[1] R. Gebbers and V. I. Adamchuk, "Precision agriculture and food security," *Science*, vol. 327, no. 5967, pp. 828–831, 2010.

[2] Y. S. Tey and M. Brindal, "Factors influencing the adoption of precision agricultural technologies: a review for policy implications," *Precision Agriculture*, vol. 13, no. 6, pp. 713–730, 2012.

[3] P. Bilsborrow, J. Cooper, C. Tétard-Jones, D. Średnicka-Tober, M. Barański, M. Eyre, C. Schmidt, P. Shotton, N. Volakakis, I. Cakmak, *et al.*, "The effect of organic and conventional management on the yield and quality of wheat grown in a long-term field trial," *European Journal of Agronomy*, vol. 51, pp. 71–80, 2013.

[4] D. Rindos, *The Origins of Agriculture: An Evolutionary Perspective.* Academic Press, 2013.

[5] G. E. Klinzing, F. Rizk, R. Marcus, and L. Leung, *Pneumatic Conveying of Solids: A Theoretical and Practical Approach*, vol. 8. Springer Science & Business Media, 2011.

[6] P. Nikolić, V. Bugarski, D. Matić, and F. Kulić, "Modern supervisory control system in a pneumatic transport system: Practical realization," *Journal on Processing and Energy in Agriculture*, vol. 18, no. 2, pp. 91–93, 2014.

[7] W. Wei, G. Qingliang, W. Yuxin, Y. Hairui, Z. Jiansheng, and L. Junfu, "Experimental study on the solid velocity in horizontal dilute phase pneumatic conveying of fine powders," *Powder Technology*, vol. 212, no. 3, pp. 403–409, 2011.

[8] R. Marcus, *Pneumatic Conveying of Solids.* Springer Science & Business Media, 2012.

[9] D. Mills, *Pneumatic Conveying Design Guide.* Butterworth-Heinemann, 2003.

[10] R. Anderson, L. Zhang, Y. Ding, M. Blanco, X. Bi, and D. P. Wilkinson, "A critical review of two-phase flow in gas flow channels of proton exchange membrane fuel cells," *Journal of Power Sources*, vol. 195, no. 15, pp. 4531–4553, 2010.

[11] G. Rudinger, *Fundamentals of Gas Particle Flow*, vol. 2. Elsevier, 2012.

[12] D. M. Pastl and S. D. Noble, "Design and testing of an electrostatic particle sensor for lean-phase pneumatic conveying," p. 1, American Society of Agricultural and Biological Engineers, 2014.

[13] S. D. Noble and D. M. Pastl, "System and method for monitoring agricultural product delivery," Oct. 28 2014. US Patent 8,869,629.

[14] W. C. Hinds, *Aerosol Technology: Properties, Behavior, and Measurement of Airborne Particles*. John Wiley & Sons, 2012.

[15] K.-H. O. Mertins, B. D. Batcheller, and D. L. Hauck, "Seed monitoring system for counting seeds as they are dispensed through a seed planting tube," July 22 1997. US Patent 5,650,609.

[16] K.-H. O. Mertins, B. D. Batcheller, D. L. Hauck, C. J. Skarie, and J. T. Jacobson, "Seed monitoring system for counting seeds as they are dispensed through seed tubes in an air seeding system," Dec. 8 1998. US Patent 5,847,389.

[17] S. Donadono and L. Massimilla, "Mechanisms of momentum and heat transfer between gas jets and fluidized beds," in *Proceedings of the Second Engineering Foundation Conference on Fluidization, Engineering Foundation, New York*, pp. 375–380, 1978.

[18] I. Finnie, J. Wolak, and Y. Kabil, "Erosion of metals by solid particles," *Journal of Materials*, vol. 2, no. 3, p. 682, 1967.

[19] Y. Wu, X. Wu, L. Yao, G. Gréhan, and K. Cen, "Direct measurement of particle size and 3D velocity of a gas-solid pipe flow with digital holographic particle tracking velocimetry," *Applied Optics*, vol. 54, no. 9, pp. 2514–2523, 2015.

[20] H. Maas, A. Gruen, and D. Papantoniou, "Particle tracking velocimetry in three-dimensional flows," *Experiments in Fluids*, vol. 15, no. 2, pp. 133–146, 1993.

[21] J. Lesinski, B. Mizera-Lesinska, J. Fanton, and M. Boulos, "Laser doppler anemometry measurements in gas-solid flows," *AIChE Journal*, vol. 27, no. 3, pp. 358–364, 1981.

[22] S. Woodhead, A. Pittman, and S. J. Ashenden, "Laser doppler velocimetry measurements of particle velocity profiles in gas-solid two-phase flows," in *Instrumentation and Measurement Technology Conference, 1995. IMTC/95. Proceedings. Integrating Intelligent Instrumentation and Control., IEEE*, p. 770, IEEE, 1995.

[23] H.-E. Albrecht, N. Damaschke, M. Borys, and C. Tropea, *Laser Doppler and phase Doppler measurement techniques.* Springer Science & Business Media, 2013.

[24] A. O. Ojo, B. Fond, B. G. Van Wachem, A. L. Heyes, and F. Beyrau, "Thermographic laser doppler velocimetry," *Optics letters*, vol. 40, no. 20, pp. 4759–4762, 2015.

[25] A. Saoud, V. Mosorov, and K. Grudzien, "Measurement of velocity of gas-solid swirl flow using electrical capacitance tomography and cross correlation technique," *Flow Measurement and Instrumentation*, vol. 53, pp. 133–140, 2017.

[26] P. Herbert, T. Gauthier, C. Briens, and M. Bergougnou, "Application of fiber optic reflection probes to the measurement of local particle velocity and concentration in gas-solid flow," *Powder Technology*, vol. 80, no. 3, pp. 243–252, 1994.

[27] J.-X. Zhu, G.-Z. Li, S.-Z. Qin, F.-Y. Li, H. Zhang, and Y.-L. Yang, "Direct measurements of particle velocities in gas-solids suspension flow using a novel five-fiber optical probe," *Powder Technology*, vol. 115, no. 2, pp. 184–192, 2001.

[28] X. Lai and H. Torp, "Interpolation methods for time-delay estimation using cross-correlation method for blood velocity measurement," *IEEE Transactions on Ultrasonics, Ferroelectrics, and Frequency Control*, vol. 46, no. 2, pp. 277–290, 1999.

[29] T. A. Scambos, M. J. Dutkiewicz, J. C. Wilson, and R. A. Bindschadler, "Application of image cross-correlation to the measurement of glacier velocity using satellite image data," *Remote Sensing of Environment*, vol. 42, no. 3, pp. 177–186, 1992.

[30] R. D. Keane and R. J. Adrian, "Theory of cross-correlation analysis of PIV images," *Applied Scientific Research*, vol. 49, no. 3, pp. 191–215, 1992.

[31] M. Volk, C. Bean, I. Lokmer, N. Perez, and J. Ibanez, "Tracking velocity changes from ambient noise and repeating airgun shots in tenerife," in *AGU Fall Meeting Abstracts*, 2015.

[32] M. Friderike Volk, C. Bean, I. Lokmer, and D. Craig, "Apparent changes in seismic wave velocity related to microseism noise source variations," in *EGU General Assembly Conference Abstracts*, vol. 16, p. 13045, 2014.

[33] J. Liu, J. R. Grace, and X. Bi, "Novel multifunctional optical-fiber probe: I. Development and validation," *AIChE journal*, vol. 49, no. 6, pp. 1405–1420, 2003.

[34] J. Liu, J. R. Grace, and X. Bi, "Novel multifunctional optical-fiber probe: II. High-density CFB measurements," *AIChE journal*, vol. 49, no. 6, pp. 1421–1432, 2003.

[35] G. H. Fathauer, "Ultrasonic sensor," May 6 1975. US Patent 3,881,353.

[36] W. Reid, D. Buckley, and W. Mason, "A photoelectric seed counting detector," *Journal of Agricultural Engineering Research*, vol. 21, no. 2, pp. 213–215, 1976.

[37] Z. Mussadiq, B. Laszlo, L. Helyes, and C. Gyuricza, "Evaluation and comparison of open source program solutions for automatic seed counting on digital images," *Computers and Electronics in Agriculture*, vol. 117, pp. 194–199, 2015.

[38] T. Liu, W. Wu, W. Chen, C. Sun, C. Chen, R. Wang, X. Zhu, and W. Guo, "A shadow-based method to calculate the percentage of filled rice grains," *Biosystems Engineering*, vol. 150, pp. 79–88, 2016.

[39] W. Liu, Y. Han, F. Bretz, F. Wan, and P. Yang, "Counting by weighing: know your numbers with confidence," *Journal of the Royal Statistical Society: Series C (Applied Statistics)*, 2016.

[40] J.-L. Starck, E. J. Candès, and D. L. Donoho, "The curvelet transform for image denoising," *IEEE Transactions on image processing*, vol. 11, no. 6, pp. 670–684, 2002.

[41] L. Pasti, B. Walczak, D. Massart, and P. Reschiglian, "Optimization of signal denoising in discrete wavelet transform," *Chemometrics and Intelligent Laboratory Systems*, vol. 48, no. 1, pp. 21–34, 1999.

[42] E. J. Candès and M. B. Wakin, "An introduction to compressive sampling," *IEEE Signal Processing Magazine*, vol. 25, no. 2, pp. 21–30, 2008.

[43] L. Zhu, Y. Zhu, H. Mao, and M. Gu, "A new method for sparse signal denoising based on compressed sensing," in *2009 Second International Symposium on Knowledge Acquisition and Modeling*, vol. 1, pp. 35–38, IEEE, 2009.

[44] R. G. Baraniuk, "Compressive sensing [lecture notes]," *IEEE Signal Processing Magazine*, vol. 24, no. 4, pp. 118–121, 2007.

[45] R. G. Baraniuk, V. Cevher, M. F. Duarte, and C. Hegde, "Model-based compressive sensing," *IEEE Transactions on Information Theory*, vol. 56, no. 4, pp. 1982–2001, 2010.

[46] M. F. Duarte and Y. C. Eldar, "Structured compressed sensing: From theory to applications," *IEEE Transactions on Signal Processing*, vol. 59, no. 9, pp. 4053–4085, 2011.

[47] C. A. Metzler, A. Maleki, and R. G. Baraniuk, "From denoising to compressed sensing," *IEEE Transactions on Information Theory*, vol. 62, no. 9, pp. 5117–5144, 2016.

[48] T. Pavlidis, *Structural pattern recognition*, vol. 1. Springer, 2013.

[49] H. Jeffries, M. Berman, A. Poularikas, C. Katsinis, I. Melas, K. Sherman, and L. Bivins, "Automated sizing, counting and identification of zooplankton by pattern recognition," *Marine Biology*, vol. 78, no. 3, pp. 329–334, 1984.

[50] L. Devroye, L. Györfi, and G. Lugosi, *A Probabilistic Theory of Pattern Recognition*, vol. 31. Springer Science & Business Media, 2013.

[51] J. Albus, R. Anderson, J. Brayer, R. DeMori, H.-Y. Feng, S. Horowitz, B. Moayer, T. Pavlidis, W. Stallings, P. Swain, *et al.*, *Syntactic Pattern Recognition, Applications*, vol. 14. Springer Science & Business Media, 2012.

[52] J. M. De Sa, *Pattern Recognition: Concepts, Methods and Applications*. Springer Science & Business Media, 2012.

[53] D. Tkach, H. Huang, and T. A. Kuiken, "Study of stability of time-domain features for electromyographic pattern recognition," *Journal of Neuroengineering and Rehabilitation*, vol. 7, no. 1, p. 21, 2010.

[54] D. J. Lacks and R. M. Sankaran, "Triboelectric charging in single-component particle systems," *Particulate Science and Technology*, vol. 34, no. 1, pp. 55–62, 2016.

[55] D. J. Lacks and A. Levandovsky, "Effect of particle size distribution on the polarity of triboelectric charging in granular insulator systems," *Journal of Electrostatics*, vol. 65, no. 2, pp. 107–112, 2007.

[56] X. Qian, Y. Yan, J. Shao, L. Wang, H. Zhou, and C. Wang, "Quantitative characterization of pulverized coal and biomass–coal blends in pneumatic conveying pipelines using electrostatic sensor arrays and data fusion techniques," *Measurement Science and Technology*, vol. 23, no. 8, p. 085307, 2012.

[57] C. Xu, B. Zhou, D. Yang, G. Tang, and S. Wang, "Velocity measurement of pneumatically conveyed solid particles using an electrostatic sensor," *Measurement Science and Technology*, vol. 19, no. 2, p. 024005, 2008.

[58] J. Ma and Y. Yan, "Design and evaluation of electrostatic sensors for the measurement of velocity of pneumatically conveyed solids," *Flow Measurement and Instrumentation*, vol. 11, no. 3, pp. 195–204, 2000.

[59] Z. Wen, X. Ma, and H. Zuo, "Characteristics analysis and experiment verification of electrostatic sensor for aero-engine exhaust gas monitoring," *Measurement*, vol. 47, pp. 633–644, 2014.

[60] C. Xu, S. Wang, G. Tang, D. Yang, and B. Zhou, "Sensing characteristics of electrostatic inductive sensor for flow parameters measurement of pneumatically conveyed particles," *Journal of Electrostatics*, vol. 65, no. 9, pp. 582–592, 2007.

[61] J. Krabicka and Y. Yan, "Finite-element modeling of electrostatic sensors for the flow measurement of particles in pneumatic pipelines," *IEEE Transactions on Instrumentation and Measurement*, vol. 58, no. 8, pp. 2730–2736, 2009.

[62] L. Peng, Y. Zhang, and Y. Yan, "Characterization of electrostatic sensors for flow measurement of particulate solids in square-shaped pneumatic conveying pipelines," *Sensors and Actuators A: Physical*, vol. 141, no. 1, pp. 59–67, 2008.

[63] Y. Hu, L. Yang, L. Wang, X. Qian, and Y. Yan, "On-line continuous measurement of the operating deflection shape of power transmission belts through electrostatic sensing," in *Instrumentation and Measurement Technology Conference Proceedings (I2MTC), 2016 IEEE International*, pp. 1–5, IEEE, 2016.

[64] S. Morris, R. Wood, T. Harvey, and H. Powrie, "Use of electrostatic charge monitoring for early detection of adhesive wear in oil lubricated contacts," *Transactions-American Society of Mechanical Engineers Journal of Tribology*, vol. 124, no. 2, pp. 288–296, 2002.

[65] T. Harvey, S. Morris, L. Wang, R. Wood, and H. Powrie, "Real-time monitoring of wear debris using electrostatic sensing techniques," *Proceedings of the Institution of Mechanical Engineers, Part J: Journal of Engineering Tribology*, vol. 221, no. 1, pp. 27–40, 2007.

[66] T. Harvey, R. Wood, and H. Powrie, "Electrostatic wear monitoring of rolling element bearings," *Wear*, vol. 263, no. 7, pp. 1492–1501, 2007.

[67] J. Q. Zhang and Y. Yan, "On-line continuous measurement of particle size using electrostatic sensors," *Powder technology*, vol. 135, pp. 164–168, 2003.

[68] M. F. Rahmat and T. Tajdari, "Particles mass flow rate and concentration measurement using electrostatic sensor," *International Journal on Smart Sensing and Intelligent Systems*, vol. 4, no. 2, pp. 313–324, 2011.

[69] X. Qian, X. Huang, H. Yonghui, and Y. Yan, "Pulverized coal flow metering on a full-scale power plant using electrostatic sensor arrays," *Flow Measurement and Instrumentation*, vol. 40, pp. 185–191, 2014.

[70] X. Qian, X. Huang, Y. Hu, and Y. Yan, "Measurement of the mass flow distribution of pulverized coal in primary air pipes using electrostatic sensing techniques," in *Instrumentation and Measurement Technology Conference Proceedings (I2MTC), 2016 IEEE International*, pp. 1–5, IEEE, 2016.

[71] P. Binsirawanich, "Mass flow sensor development for an air seeding cart," M.S. thesis, Univeristy of Saskatchewan, Saskatchewan, Canada, 2011.

[72] P. Binsirawanich, S. D. Noble, and J. Gervais, "Velocity of conveyed seeds in an inclined transition tube," in *XVIIth World Congress of the International Commission of Agricultural and Biosystems Engineering (CIGR)*, 2010.

[73] L.-S. Fan and C. Zhu, *Principles of gas-solid flows.* Cambridge University Press, 2005.

[74] H. Zhou, Y. Huang, Y. Yang, G. Mo, J. Li, and K. Cen, "Experimental measurements of gas-solid flow and splitting mechanisms of a coal pipe splitter with a perpendicularly arranged upstream elbow," *Particuology*, vol. 25, pp. 143–150, 2016.

[75] S. Yin, B. Jin, W. Zhong, Y. Lu, Y. Shao, and H. Liu, "Gas-solid flow behavior in a pressurized high-flux circulating fluidized bed riser," *Chemical Engineering Communications*, vol. 201, no. 3, pp. 352–366, 2014.

[76] T. Kyle, "Measuring seed particle velocity in a pneumatic conveying system using particle tracking velocimetry," M.Eng. project report, Univeristy of Saskatchewan, Saskatchewan, Canada, 2017.

[77] N. Goodman, "Statistical analysis based on a certain multivariate complex gaussian distribution (an introduction)," *The Annals of Mathematical Statistics*, vol. 34, no. 1, pp. 152–177, 1963.

[78] Y. Tsaig and D. L. Donoho, “Extensions of compressed sensing,” *Signal Processing*, vol. 86, no. 3, pp. 549–571, 2006.

[79] C. A. Metzler, A. Maleki, and R. G. Baraniuk, “From denoising to compressed sensing,” *IEEE Transactions on Information Theory*, vol. 62, no. 9, pp. 5117–5144, 2016.

[80] S.-H. Cho, G. Jang, and S.-H. Kwon, “Time-frequency analysis of power-quality disturbances via the gabor–wigner transform,” *IEEE Transactions on Power Delivery*, vol. 25, no. 1, pp. 494–499, 2010.

[81] K. Siedenburg and M. Dörfler, “Audio denoising by generalized time-frequency thresholding,” in *Audio Engineering Society Conference: 45th International Conference: Applications of Time-Frequency Processing in Audio*, Audio Engineering Society, 2012.

[82] K. Siedenburg, “Persistent empirical Wiener estimation with adaptive threshold selection for audio denoising,” in *Proceedings of the 9th Sound and Music Computing Conference, Copenhagen, Denmark*, pp. 11–14, 2012.